Neural Mechanisms of Early Motor Control in the Vocal Behavior of Juvenile Songbirds

by

Dmitriy Aronov

B.S., Applied Mathematics
Columbia University, 2005

Submitted to the Department of Brain and Cognitive Sciences
in partial fulfillment of the requirements for the degree of

DOCTOR OF PHILOSOPHY IN NEUROSCIENCE
at the
Massachusetts Institute of Technology

September 2010

Signature of Author: _____
Department of Brain and Cognitive Sciences
June 8, 2010

Certified by: _____
Michale S. Fee
Professor of Neuroscience
Thesis Supervisor

Accepted by: _____
Earl K. Miller
Picower Professor of Neuroscience
Chairman, Committee for Graduate Students

Neural Mechanisms of Early Motor Control in the Vocal Behavior of Juvenile Songbirds

by
Dmitriy Aronov

Submitted to the Department of Brain and Cognitive Sciences on June 8, 2010 in partial fulfillment of the requirements for the degree of Doctor of Philosophy in Neuroscience.

Abstract

An infant reaches out for her new toy, struggling day after day to simply grasp her fingers around it. A few years later, she hits a tennis serve, perfect in the timing of its intricately choreographed movements. How does a young brain learn to use the muscles it controls, to properly coordinate motor gestures into complex behavioral sequences? To a surprising extent, for many advanced vertebrate behaviors this knowledge is neither innately programmed nor acquired via deterministic developmental rules, but must be learned through trial-and-error exploration. This thesis is an investigation of the neural mechanisms that underlie the production and maturation of one exploratory behavior – the babbling, or subsong, of a juvenile zebra finch.

Using lesions and inactivations of brain areas in the song system, I identified neural circuits involved in the production of subsong. Remarkably, subsong did not require the high vocal center (HVC) – a premotor structure long known as the key region for controlling singing in adult birds – but did require the lateral magnocellular nucleus of the nidopallium (LMAN) – the output region of basal ganglia-forebrain circuitry previously considered a modulatory area. Recordings in LMAN during subsong revealed premotor activity related to the vocal output on a fast timescale. These results show, for the first time, the existence of a specialized circuit for driving exploratory motor control, distinct from the one that produces the adult behavior.

The existence of two neural pathways for singing has raised the question of how motor control is transferred from one pathway to another and, in particular, how the control of song timing develops in these pathways. I found that early singing can be decomposed into mechanistically distinct "modes" of syllable and silent gap timing – randomly-timed modes that are LMAN-dependent and developmentally-acquired, consistently-timed modes that are HVC-dependent. Combining acoustic analysis with respiratory measurements, I found that the consistently-timed mode in gap durations is formed by brief inspiratory pressure pulses, indicating an early involvement of HVC in coordinating singing with respiration. Using mild localized cooling – a manipulation that slows down biophysical processes in a targeted brain area – I found that the circuit dynamics intrinsic to HVC and LMAN are actively involved in controlling the timescales of distinct behavioral modes.

In summary, this work demonstrates the existence of two motor circuits in the song system. These circuits are specialized for the generation of distinct types of neural dynamics – random exploratory dynamics, which are dominant early in life, and stereotyped sequential dynamics, which become dominant during development. Characterization of behaviorally-relevant dynamics produced by neural circuits may be a general framework for understanding motor control and learning.

Thesis supervisor: Michale S. Fee
Title: Professor of Neuroscience

Table of contents

Acknowledgements

Asking Michale Fee for a position in his lab five years ago was a no-brainer – I was attracted there by the amazing techniques I heard so much about. Not long after joining, however, I realized that these techniques are nothing but little engineering tricks that are there to serve a greater purpose. What Michale really taught me is his relentless approach to posing the most important questions he can find and truly dissecting them – first logically, then experimentally. His focus, confidence, and self-imposed high standards have left me humbled, but at the same time incredibly refreshed and optimistic about figuring out the next behavior – whatever it may be – and really enjoying the process. More than anything else, I will miss our enthusiastic multi-hour discussions, which have challenged and reshaped my thinking on a daily basis.

Three lab members contributed directly to the work presented in this thesis. Aaron Andalman, the first grad student in the lab, has set an incredibly high bar that I've been trying oh so hard to live up to. He is a wonderful peer and an equally wonderful teacher – much of what I know these days, I know directly from him. We collaborated on some early LMAN recordings, as well as on the development of the reverse microdialysis method presented in this thesis. Lena Veit put up a heroic fight during her few months in the lab, setting up and running the dauntingly difficult pressure recordings in young birds. I am impressed and proud of what she's done, but more importantly thankful for the energy and fun she brought to this project. Finally, Jesse Goldberg – my colleague for almost a decade – is a mentor whose real contribution to this work is immeasurably beyond his recordings that I used for my analysis of LMAN inactivations. Few people are

as insightful, knowledgeable, and engaging as Jesse, and I will always cherish the years when I could reach out to him for advice.

Each of the following people deserves pages of thanks, but I resort here to a brief list. These former and current lab members have created an enjoyable, stimulating environment, and I cannot envision the same work being done with any other group of people: Natalia Denisenko, Jacob Foerster, Tim Gardner, Ricardo Gonzales, Alexay Kozhevnikov, Liora Las, Michael Long, Tatsuo Okubo, Bence Ölvezcky, Daniel Rubin, Benjamin Scott and Michael Stetner. I am also thankful to my thesis committee members for devoting their time to my work and for giving me great advice: Matthew Wilson, Christopher Moore, and my external reader, Ofer Tchernichovski – a pioneer in the field whose work has inspired a lot of what I've done.

In the last four years, I've been fortunate to be part of the Hertz Foundation and its remarkable group of fellows. In particular, I am grateful to Raymond Sidney, who personally sponsored my Hertz fellowship in honor of his own mentor – MIT computer science professor Silvio Micali.

Finally, I cannot possibly do justice to my family and friends on paper. Without their support and enthusiasm, any of this is unimaginable.

Chapter 1

Introduction

Exploratory behavior is a defining feature of vertebrate motor learning. The young of many species express immature versions of their future behavioral programs, incessantly practicing and refining them in pursuit of a repertoire that will eventually determine their survival and reproductive success. What are the neural mechanisms that produce these exploratory behaviors, and what developmental changes in the brain underlie their transition to adult motor control? I attempt to address these questions using a specific behavior – the babbling, or subsong, of a juvenile zebra finch. In the present introductory chapter, I describe this behavior in the context of exploratory learning and outline some specific goals for understanding how early singing is generated by the forebrain song system.

Exploratory behavior

Exploration is ubiquitous in motor systems

Simple behaviors commonly consist of several movements that are sequentially organized in time. Such actions are often produced by innately prewired circuits of neurons. Among the best-studied examples are central pattern generators (CPGs) in invertebrates, which produce behaviors like swimming in leeches, flight in locusts, and singing in grasshoppers (Stent et al. 1978; Wilson 1961; Ronacher 1989). Vertebrates too are born with repertoires of simple, but relatively mature behaviors that are necessary for immediate survival, such as breathing, feeding, and crying (Forssberg 1999).

Somewhat counterintuitively, the more complex vertebrate behaviors are usually neither innate nor built by rule-based deterministic processes. Rather, the ability to produce these behaviors is obtained during development through exploration. In humans

and other mammals, early exploratory behavior begins in the prenatal stage and persists after birth, involving spontaneous muscle twitches and full body movements, called "general movements" (Prechtl 1997; Forssberg 1999; Robinson et al. 2000). Such motor activity has been shown to activate sensory regions of the central nervous system – a process thought to facilitate the self-organization of spinal reflex circuits and cortical somatosensory maps (Petersson et al. 2003; Khazipov et al. 2004; Milh et al. 2007). Effectively, these early behaviors enable the brain to establish the relationship between movement and feedback from the somatosensory periphery, providing basic information about the shape and mechanical properties of the body it is starting to control.

At later developmental stages, exploratory movements begin to resemble particular species-specific forms of adult behavior. Familiar examples include infant stepping – variable leg movements that predate walking and running (Forssberg 1999; Yang et al. 1998). Similarly, primitive grasp-like "hand babbling" gestures develop into the precise coordination of hands and digits (Wallace & Whishaw 2003), early torso movements give rise to adult posture control (Hadders-Algra et al. 1996), and vocal babbling represents the first step in language acquisition (Oller et al. 1976; Doupe & Kuhl 1999). Higher-level exploratory behavior is often referred to as "play." By playing, young birds and mammals explore motor patterns that resemble complex locomotion, hunting (or predator evasion), fighting, and parenting (Fagen 1981; Bekoff & Byers 1998). In humans, the concept of exploratory play can be extended to cognitive processes as well and involves incessant conceptual experimentation often referred to as childhood creativity.

Exploration is the hallmark of reinforcement learning

As clearly evidenced by humans and other large mammals, exploratory behaviors can consume long periods of life and are often produced at great energetic costs to the animal. These behaviors frequently expose the engaged individual to danger, but unlike many adult actions, do not necessarily target an immediate external reward (Bekoff & Byers 1998). Is there an advantage to producing exploratory behaviors that explains their ubiquity in developing motor systems?

An answer may lie in the fact that variable, exploratory motor outputs are a necessary component of a learning algorithm known as reinforcement, or trial-and-error, learning (Sutton & Barto 1998; Doya & Sejnowski 1995; Seung 2003). Reinforcement learning requires the motor system to produce a range of commands, which on each rendition generate a different output. A second mechanism then judges these outputs, producing an evaluation ("error") signal that is relayed to the motor system. Through some corrective plasticity mechanism, this signal rewards motor programs that produced beneficial outputs, leading to their strengthening, and punishes erroneous motor programs, eventually eliminating them. Clearly, exploration is a critical component of this process – without it, the motor system does not produce variable fluctuations, some of which may incidentally be improvements to the motor output.

Reinforcement learning is a solution to two problems that exist in other motor learning strategies. First of all, this algorithm does not require the daunting task of determining which of the many neurons or synapses in a premotor structure were responsible for a particular error in the motor output and specifically correcting them (Seung 2003). Rather, the full behavior is evaluated, and a global reward or punishment

signal affecting the entire system is implemented. Secondly, this strategy allows motor learning to be adaptable, eventually settling on an optimal solution in any given set of circumstances. Innate construction of a motor circuit, on the other hand, endows every individual with the same collection of motor abilities and is generally inflexible

Variable motor behaviors are also produced by mature animals

Although I generally focus on exploratory learning in juvenile animals, it is important to note that the production of stochastic, variable behaviors is not unique to the early stages of developmental learning. Such actions, for instance, are also produced by adult animals following damage to the nervous system or to the peripheral organs, enabling them to relearn some aspects of motor control (Nudo et al. 1996; Thompson & Johnson 2007; Williams & McKibben 1992). Complex exploratory motor behaviors are exhibited by individuals that are faced with a novel task or with changes to the environment (Whishaw et al. 1999; Fonio et al. 2009). These examples illustrate that exploration is not exclusively a feature of immature motor circuits, but may be a purposeful behavior that enables adaptive motor control throughout life.

Furthermore, variability is often introduced to mature behaviors for reasons unrelated to motor learning. Small prey animals, for instance, flee predators in highly erratic, unpredictable paths that maximize their chances of escaping (Humphries & Driver 1970). Another example is found across many animal species in random foraging behaviors, which enable individuals and populations to discover new sources of food (Sokolowski 2010). On a more general level, stochastic behaviors generate adaptive unpredictability – a strategy that defends an individual against competitors and is

considered by some evolutionary ethologists to be the root of creative intelligence (Miller 1997; Wilson 1999).

Neural mechanisms of exploratory behavior

Motor systems produce two distinct forms of activity

The presence of exploratory learning implies that motor systems must be capable of producing two distinct forms of activity at different developmental stages. Early behavior is characterized by highly variable, temporally uncoordinated motor gestures. Mature behaviors, on the other hand, are often characterized by a high degree of stereotypy from one rendition to the next and a strong level of coordination – the production of movements at consistent relative times and in a precise order. How do motor systems achieve this dual role, and what mechanisms underlie their transformation from the juvenile to the adult forms of behavior?

A common presumption is that the transition from variable to stereotyped behavior occurs within a given brain area. In this view, a premotor brain region (or small set of regions) contains a great variety of epigenetically prestructured motor programs, sometimes referred to as "neuronal groups" (Edelman 1987; Sporns & Edelman 1993; Marler 1997; Forssberg 1999; Hadders-Algra 2000) Through the process of activity-dependent selection (essentially reinforcement learning), some of these programs are eliminated from the repertoire, while the others are retained.[1] The key feature of this model is that the biophysical processes that produce exploration are essentially immature versions of the processes that produce the behavior later in life.

[1] The original formulation of the Neuronal Group Selection Theory does not require innate motor programs to be localized to same circuits that later produce mature behaviors. Such interpteration of the theory, however, is common in the literature.

An alternative model is that there exist neural circuits specialized for the production of exploratory behaviors, and that the biophysical processes producing variable behavior are distinct from the ones that produce stereotyped behavior. Such separation of the circuit learning the behavior from the variability-producing circuit could, in principle, simplify computation by providing the motor system with independent control of the two processes. Independent control could in turn allow the system to target exploration to specific portions of the behavior, to modulate the amount of variability, and to retain exploratory abilities in adulthood, even after the learning stage is complete (Fiete et al. 2007).

Neural mechanisms of early behavior are poorly understood

Studies of motor control often concentrate on mature, well-trained animals; very little is known about exploratory behaviors in the brain. Various regions of the mammalian motor system, including the motor cortex, basal ganglia, and the thalamus have been implicated in the production of early movements (Robinson et al. 2000; Forssberg 1999; Eyre et al. 2000; Prechtl 1997). In fact, abnormalities of spontaneous body movements and behavioral variability in infants are sometimes used for early diagnosis of damage to these areas in conditions like cerebral palsy (Prechtl 2001; Hadders-Algra 2008). Yet, specific neural circuits and their roles in the production of exploratory behaviors have not been identified.

The song system: a model motor control circuit

Vocal babbling: a model of exploratory learning

Vocal behaviors like speech and singing are among the most remarkable examples of motor control, requiring a precise coordination of many muscles that comprise the vocal apparatus and the respiratory system (Levelt 1993; Goller & Cooper 2004). Species in several mammalian and avian families learn their vocalizations.[2] Paralleling other motor learning processes described above, vocal learning begins with the production of variable *babbling* vocalizations (Oller et al. 1976; Doupe & Kuhl 1999). Other than in human infants, babbling has been described in primates like marmosets and tamarins (Elowson et al. 1998; Snowdon 2001), in songbirds and parrots (Marler 1970; Liu et al. 2009; Pepperberg et al. 2008), in dolphins (Reiss & McCowan 1993), and in bats (Knörnschild et al. 2006). In most of these cases, babbling appears to be used primarily for practice rather than communication: it resembles conspecific adult vocalizations, but is generally quiet and produced with little or no relation to the animal's social context, including in isolation. For experimental studies, babbling is an excellent model of exploratory motor control in part because, compared to other behaviors, it is relatively easy to record and quantify.

Song development in zebra finches

Early in life, a male zebra finch listens to the song of his adult tutor, forming an auditory memory ("template") that he will later imitate (Immelmann 1969; Marler 1970). In zebra finches, as in other songbirds, babbling is called *subsong*. Subsong production begins at an age of about 30 days-post-hatch (dph) and consists of sequentially generated

[2] The term "vocal learner" usually refers to animals that not only develop their vocalizations during a learning process, but immitate sounds they hear. Few families of animals fit this definition, including only humans, songbirds, parrots, hummingbirds, as well as some cetaceans and bats (Jarvis 2004). Ability to immitate, however, is not required for the processes described here.

bursts of sound (syllables) separated by silent gaps. At this stage, syllables are quiet and highly variable in both duration and acoustic structure (Tchernichovski et al. 2001; Tchernichovski et al. 2004). Juvenile birds often produce hundreds to thousands of such sounds every day, even in complete social isolation.

At about 40-50 dph, subsong gradually transitions to the next stage, called the *plastic-song* stage. During this period, singing begins to exhibit some repeated acoustic structure identifiable across syllable renditions, although syllables in early plastic song remain highly variable (Tchernichovski et al. 2004; Ölveczky et al. 2005). Plastic song is also characterized by the emergence of temporal structure, evident in consistently repeated syllable durations and the appearance of rhythmicity in songs (Tchernichovski et al. 2004; Liu et al. 2004; Saar & Mitra 2008). For roughly the next month, temporal and acoustic features of plastic songs are gradually refined, eventually converging onto the single adult song that the bird will produce for the rest of his life.

Adult zebra finch songs are characterized by a hierarchical organization of sounds in time (Williams 2004). During a typical song bout, a bird produces several sequences of sound, called motifs, in rapid succession. Each motif is typically on the order of ~1 s long and consists of several distinct syllables, separated by gaps and delivered in a precise temporal order.[3] Syllables are on the order of ~100 ms long and, in turn, can consist of shorter, acoustically distinct notes. Slightly distinct versions of the same adult song are produced in two social contexts. Directed songs are produced for mating purposes in the presence of another zebra finch; undirected songs are more variable and are typically produced in isolation (Zann 1996; Kao & Brainard 2006).

[3] In some adult zebra finches, but more commonly in juveniles and in other species, the syntax is flexible (Ölveczky et al. 2005; Okanoya 2004). Syllables can be stuttered, omitted, and reordered. These cases validate the treatment of syllables as distinct behavioral modules.

Anatomy of the song system

The neuroanatomy of singing has been fairly well-characterized since the original discovery of the forebrain song system (Nottebohm et al. 1976). At least two reasons make this system advantageous for the study of motor control and learning mechanisms. One reason is that many song nuclei are highly specialized and anatomically segregated from the surrounding structures (Nottebohm et al. 1976). This property simplifies their targeting and often implies the exclusive involvement of their motor function in song production, rather than in a range of other behaviors. Another reason is that, in spite of this specialization, the song system parallels the general anatomical organization of other vertebrate motor systems, including those involved in mammalian motor control and learning (Reiner et al. 2004; Feenders et al. 2008). Many experimental results obtained in the song system are therefore likely to be generalizable.

Major components of the song system are located in the pallium – a large telencephalic structure that contains the cerebral cortex in mammals (Fig. 1; (Reiner et al. 2004)). Unlike the cerebral cortex, the avian pallium consists of distinct nuclei rather than laminae. However, numerous molecular, anatomical, and functional studies suggest that these brain areas are, in fact, homologous. "Cortical" structures in the song system include nuclei RA, HVC, and LMAN (see the legend of Fig. 1 for abbreviations; (Nottebohm et al. 1976; Bottjer et al. 1984)). Both HVC and LMAN send major glutamatergic inputs to RA (Mooney 1992).

RA is an output nucleus of the forebrain song system and can be considered similar to layer 5 of the mammalian motor cortex. Descending projections from RA

innervate syringeal motor neurons in nucleus nXIIts. RA also projects to a thalamic area DLM (Vates et al. 1997) and to several vocal and respiratory areas in the brainstem (Wild 2004). DLM projects to LMAN, completing a "thalamocortical" loop. Some of the brainstem areas send feedback projections to HVC, but via a different thalamic nucleus, Uva, completing another loop (Ashmore et al. 2008).

In addition to the cortical and thalamic regions, the forebrain song system includes area X, a basal-ganglia structure. Recent studies indicate that area X contains both striatal and pallidal components of the basal ganglia, including cell types nearly identical to those in the mammalian structures (Farries & Perkel 2002; Farries et al. 2005; Goldberg et al. 2010; Goldberg & Fee 2010). Similarly to the mammalian basal ganglia, area X receives descending cortical inputs, from HVC and LMAN, and forms a basal ganglia-thalamocortical loop via its projection to DLM (Perkel et al. 2002).

In spite of the mammalian-like anatomical organization, the song system has been traditionally divided into two pathways: the motor pathway, consisting of HVC, RA, and downstream brainstem areas, and the anterior forebrain pathway (AFP), consisting of area X, DLM, and LMAN. Below, I introduce the known functional roles of these two pathways.

Motor pathway produces stereotyped, sequential activity

Lesions of HVC and RA are highly disruptive to normal adult singing, suggesting that these areas form a critical circuit for song production (Nottebohm et al. 1976; Simpson & Vicario 1990). Single-unit recordings in these regions are supportive of this conclusion, showing stereotyped sequences of activity that are precisely time-locked to

the singing behavior of an adult song (Chi & Margoliash 2001; Leonardo & Fee 2005; Hahnloser et al. 2002). Whereas each RA neuron fires several high-frequency bursts of action potentials distributed throughout a motif, each RA-projecting neuron in HVC fires a single burst per motif. These activity patterns suggest a scheme in which HVC outputs encode time relative to motif onset. The population of HVC neurons active at a particular point in time activates a population of downstream RA neurons, which encode an appropriate motor output (Fee et al. 2004). Models of song learning suggest that the ability to produce a particular stereotyped acoustic sequence can, in part, be achieved by learning the strengths of HVC-to-RA synapses (Doya & Sejnowski 1995; Fiete et al. 2007).

Recent experiments show that mildly cooling HVC results in uniform temporal stretching of the adult song, whereas cooling RA has no effect on song timing (Long & Fee 2008). Because cooling slows down many biophysical processes in the targeted brain region, these data suggest that the dynamics responsible for song timing are intrinsic to the circuitry within HVC. Given the pattern of activity in RA-projecting neurons, these results are suggestive of a chain-like organization in HVC. Specifically, HVC neurons could be organized into functional nodes, such that neurons in a given node send strong excitatory projections almost exclusively to neurons in another node. Once triggered, activity in HVC would propagate through this "synfire chain," successively activating each node once during the song (Fee et al. 2004; Jin et al. 2007; Abeles 1991).

AFP generates variability and learning-related signals

Lesions of nuclei in the AFP have little effect on the production of mature adult songs. However, birds that receive such lesions as juveniles do not learn to imitate their tutors and produce highly abnormal songs in adulthood (Bottjer et al. 1984; Scharff & Nottebohm 1991). These results have lead to a hypothesis that the AFP is a "learning circuit," which introduces modulatory or instructive signals to the motor pathway that enable normal learning-related plasticity to occur (Doya & Sejnowski 1995; Troyer & Bottjer 2001).

Recent studies have shown an additional, premotor role of the AFP in song production. First, stimulation of LMAN – the output nucleus of the AFP – during singing produces an immediate, transient change in the vocal output, suggesting an ability of the AFP to influence singing in real time (Kao et al. 2005). Second, pharmacological inactivation of LMAN causes an immediate, reversible reduction of song variability in both juvenile and adult birds (Kao et al. 2005; Ölveczky et al. 2005; Kao & Brainard 2006). These results suggest that AFP outputs are not simply modulatory, but are actively involved in the generation of variable fluctuations in the motor output. Further experiments have shown that LMAN-dependent variability is not fully random, but carries a corrective signal, biasing the motor pathway to avoid vocal errors during learning (Andalman & Fee 2009).

Characterizing the dynamics generated by motor circuits

Computational and systems neuroscience has traditionally focused on characterizing stimulus-evoked activity in neural circuits. However, much of the activity in the brain is generated by the biophysical dynamics intrinsic to these circuits. Examples

include various types of oscillation (Buzsáki 2006), persistent activity (Goldman-Rakic 1995; Major & Tank 2004), and neuronal sequences (Abeles 1991; Hahnloser et al. 2002; Pastalkova et al. 2008). Theoretical studies have also suggested chaotic network dynamics as a basis for the production of stochastic neural activity (van Vreeswijk & Sompolinsky 1998; Vogels et al. 2005; Wilson 1999). Functionally, intrinsic dynamics are thought to underlie a variety of critical internal brain functions like attention, working memory, and the production of centrally-controlled motor patterns. How are these forms of activity generated, and what is their influence on behavior?

Although internally-shaped neural activity is prominent in many parts of the brain, the underlying biophysical dynamics are not readily observable, making these questions hard to address. In some cases, brain regions (Stewart & Fox 1990; Long & Fee 2008), cell types (Cardin et al. 2009; Bonifazi et al. 2009), or small groups of neurons (Stent et al. 1978; Marder & Bucher 2007) have been implicated in particular forms of network dynamics. However, generally, sources of dynamics are poorly understood, especially for activity patterns or behaviors that involve several brain regions or multiple cell types. Even less is known about the ways neural dynamics may be modified in the process of development, although changes in synaptic organization and single-neuron properties have been identified as possible mechanisms in some individual examples (Crépel et al. 2007).

Studies of neural dynamics often focus on understanding the role they play in shaping stimulus-evoked responses in sensory regions (Kenet et al. 2003). Motor systems, however, are possibly more amenable to study because the dynamics that they exhibit directly influence the behavioral output. Dynamics in motor systems, in fact, have

been precisely localized for some simple, oscillatory invertebrate behaviors (Stent et al. 1978; Marder & Bucher 2007). The zebra finch song system is an ideal model of the more complex dynamics because the behavior it produces is precisely timed, hierarchically-organized, developmentally learned, and involves multiple interconnected brain regions. As mentioned above, the neural dynamics of song production have been localized for mature, adult singing (Long & Fee 2008). Whether, and how, these dynamics change in the process of exploratory learning is an open question.

Organization of the following chapters

Most studies of the song system have addressed the issues of motor control in the late plastic and adult developmental stages. Almost no work exists on the mechanisms of early song production, in the subsong and early plastic-song phases. One reason is that these behaviors themselves are poorly understood, with only some studies beginning to lay out a quantitative framework for describing them (Tchernichovski et al. 2001; Tchernichovski et al. 2004; Saar & Mitra 2008). Uncovering the neural mechanisms of early singing, however, is a crucial step toward understanding how the brain generates exploration.

Chapter 2 is a published article that makes the first requisite step toward understanding the mechanisms of subsong production by using lesions, inactivations, and neural recordings to determine which brain areas are involved in this behavior.

Chapter 3 provides a detailed quantitative description of early song timing and the underlying respiratory patterns. By uncovering mechanistically distinct timescales in early singing, this chapter establishes a new vocabulary of terms that can be used to describe and quantify the behavior.

Chapter 4 uses lesions and cooling to localize circuit dynamics responsible for the generation of various song timescales discovered and described in the previous chapter.

Chapter 5 combines all results into a coherent model of early song production. It discusses the relevance of this model for the general understanding of circuit dynamics, as well as its implications for the study of exploratory behaviors in the brain.

Appendix A describes the theoretical design and the construction of a device for local brain cooling. This device is a general tool for analyzing the dynamics of brain circuits with temperature.

Figure 1. Major brain areas and pathways of the zebra finch song system. (a) The motor pathway consists of pallial nuclei HVC and RA, as well as downstream brainstem motor nuclei. A feedback projection exists via a thalamic nucleus Uva. (b) The anterior motor pathway (AFP) consists of area X, DLM, and LMAN, forming a basal ganglia-thalamocortical loop. Area X (the basal ganglia) receives descending inputs from HVC. RA receives inputs from the pallial nucleus LMAN and sends a descending "cortico-thalamic" projection to DLM.

Abbreviations are as follows. HVC: high vocal center; RA: robust nucleus of the arcopallium; Uva: nucleus uvaeformis; DM: dorsomedial nucleus; nXIIts: tracheosyringeal portion of the hypoglossal nucleus; LMAN: lateral magnocellular nucleus of the nidopallium; DLM: dorsolateral nucleus of the medial thalamus.

A

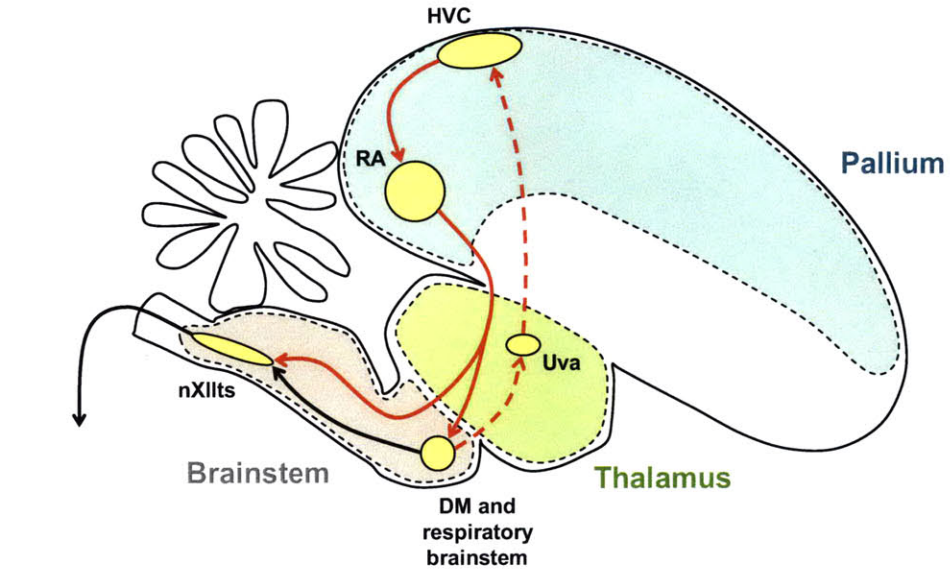

Motor pathway
Feedback connections
Brainstem connections

B

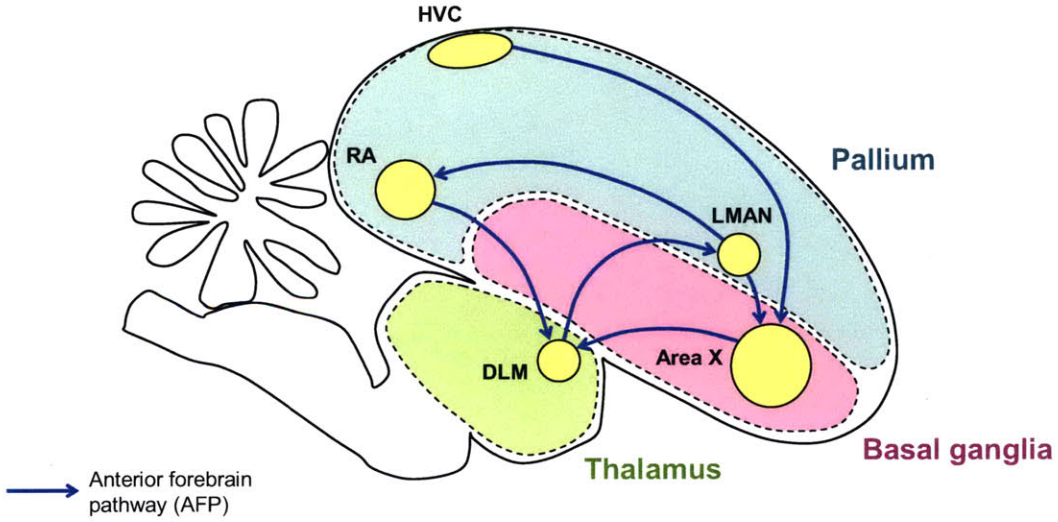

Anterior forebrain
pathway (AFP)

Chapter 2

A specialized forebrain circuit for vocal babbling in the juvenile songbird

This chapter was previously published as:

Aronov D., Andalman A.S., and Fee M.S. (2008) A specialized circuit for vocal babbling in the juvenile songbird. *Science* 320(5876): 630-4.

Young animals engage in variable exploratory behaviors essential for the development of neural circuitry and adult motor control, yet the neural basis of these behaviors is largely unknown. Juvenile songbirds produce subsong – a succession of primitive vocalizations akin to human babbling. We report that subsong production in zebra finches does not require HVC (high vocal center), a key premotor area for singing in adult birds, but does require LMAN (lateral magnocellular nucleus of the nidopallium), a forebrain nucleus involved in learning but not adult singing. During babbling, neurons in LMAN exhibited premotor correlations to vocal output on a fast timescale. Thus, juvenile singing is driven by a circuit distinct from that which produces the adult behavior – a separation possibly general to other developing motor systems.

How does a young brain learn to use the muscles it controls and the sensory organs by which it perceives the world? To a surprising extent, this knowledge is not built in by deterministic developmental rules, but must be obtained through exploration. For instance, the relationship of somatosensory periphery and movement is revealed to the developing brain by spontaneous muscle twitches, which facilitate the self-organization of spinal reflex circuits (Petersson et al. 2003) and cortical somatosensory maps (Khazipov et al. 2004; Milh et al. 2007). At a higher level, juvenile animals learn the causality of actions and the effects of these actions by ubiquitous and generally variable behaviors, such as infant stepping, grasp-like "hand babbling" movements, early vocalizations, and play (Wallace & Whishaw 2003; Robinson et al. 2000; Doupe & Kuhl 1999; Imada et al. 2006; Fagen 1981).

How are these exploratory juvenile behaviors generated? Are they produced by

the same brain areas responsible for corresponding adult behaviors later in life, or are there specialized brain regions involved? Forebrain areas, including the motor cortex and the basal ganglia have been implicated in the production of normal infant movements, as well as their abnormalities (Robinson et al. 2000; Forssberg 1999; Eyre et al. 2000; Prechtl 1997). Yet, the specific forebrain circuits for infant motor control remain to be identified.

Babbling is an early motor behavior produced by juveniles of vocal mammals and birds (Doupe & Kuhl 1999; Marler 1970; Elowson et al. 1998; Knörnschild et al. 2006; Reiss & McCowan 1993). In zebra finches, babbling, called subsong, occurs roughly from ages 30 to 45 days-post-hatch (dph). Plastic song follows, with the gradual appearance of distinct and identifiable, but variable, vocal elements (syllables). By 80-90 dph, plastic song is gradually transformed into highly complex, stereotyped motifs – sequences of syllables that comprise adult song. The premotor circuit for adult song production consists of HVC, RA, and brainstem motor nuclei (summarized in Fig. 1a). This "motor pathway" is crucial for generating stereotyped, learned vocalizations (Nottebohm et al. 1976; Simpson & Vicario 1990) and exhibits firing that is precisely time-locked to the song output (Yu & Margoliash 1996; Chi & Margoliash 2001; Hahnloser et al. 2002; Leonardo & Fee 2005).

Another circuit, the anterior forebrain pathway (AFP), is homologous to basal ganglia thalamocortical loops in mammals and projects to RA through a forebrain nucleus LMAN (Bottjer et al. 1989; Farries & Perkel 2002). Although LMAN is not required for singing in adult birds, it is necessary for normal song learning in juveniles (Bottjer et al. 1984; Scharff & Nottebohm 1991) and plays a role in modulating song

variability in adult and juvenile birds (Kao et al. 2005; Ölveczky et al. 2005). These and other studies have suggested a view that the motor pathway drives singing, whereas outputs of the AFP modulate or instruct the motor pathway during learning (Doya & Sejnowski 1995; Troyer & Bottjer 2001).

Subsong persists in the absence of HVC

Here we ask whether primitive subsong vocalizations result from an immature form of the adult motor pathway, or whether they are driven by other premotor circuits. Given the importance of HVC for mature singing (Nottebohm et al. 1976; Hahnloser et al. 2002; Thompson & Johnson 2007), we sought to characterize its involvement early in development. In 9 subsong-producing juvenile birds (ages 33-44 dph), we eliminated HVC bilaterally, either by electrolytic lesions or by pharmacological inactivation (see Supplementary Material). In 3 additional birds, we left HVC intact, but specifically eliminated its projection to RA by bilateral transection of the HVC-to-RA fiber tract. Following these manipulations, all birds continued producing largely unaffected subsong (Fig. 1a; Fig. S3).

Surprisingly, older birds – those in the plastic song stage (45-73 dph, n=12) and adults (n=5, undirected singing) – also sang following bilateral HVC elimination (but see Supporting Material). These birds lost structure and stereotypy in their songs, reverting to the production of subsong-like vocalizations. Following pharmacological inactivation of HVC, this reversion to subsong-like vocalizations was fast (within 20 min) and reversible (Fig. S4), suggesting that the effect is not due to long-term changes in neural circuitry, but rather occurs immediately as a result of the loss of spiking activity in HVC. At all

ages, singing in the absence of HVC was produced at normal rates (Fig. 3) and followed an ordinary circadian rhythm, with more songs produced in the morning than in later parts of the day (data not shown).

Singing without HVC is highly similar to normal subsong

We asked whether the sounds produced in the absence of HVC are indeed similar to subsong. We characterized acoustic properties of songs by measuring spectral features shown to be effective for quantifying developmental trends in zebra finches (Tchernichovski et al. 2000; Derégnaucourt et al. 2005). Distributions of these features before and after HVC elimination were highly similar for subsong-producing birds (see Supporting Material). An additional feature of normal subsong is the absence of repeatable acoustic elements of a stereotyped length. This is evident in a wide, unimodal distribution of syllable durations for subsong-producing birds (n=9 birds younger than 45 dph, Fig. 2a,b). Following HVC elimination, these distributions were unchanged (see Supporting Material). In contrast, plastic and adult songs contain distinct syllables that form multiple narrow peaks in the distributions of durations. Following HVC elimination in older birds, all distinct syllables were lost, resulting in unimodal distributions similar to those of subsong (n=25 birds; Supporting Material).

Furthermore, subsong is characterized by a lack of sequential stereotypy, which appears later in plastic and adult songs. We quantified stereotypy by measuring the peak of the spectral cross-correlation between different song renditions (Fig. 2c; see Supplementary Material). In control conditions, stereotypy was higher for older birds (Fig. 2d; $p<0.0001$ for non-zero slope of the linear regression of stereotypy and age).

However, independently of age, stereotypy was reduced to the level of subsong following HVC elimination (Wilcoxon $p>0.1$ for the difference from normal subsong). In summary, analyses of acoustic structure indicate that, by a wide range of measurements, singing in the absence of HVC is highly similar to normal subsong.

Subsong requires activity in RA and LMAN

If subsong persists in the absence of HVC, what neural circuits are engaged in its production? One possibility is that subsong does not require the forebrain system and is entirely produced by midbrain or brainstem circuitry, even in the absence of RA. A second possibility is that subsong is driven by circuitry intrinsic to RA, even in the absence of HVC and LMAN. The third possibility is that subsong is driven by, or requires, inputs from LMAN to RA. We tested these hypotheses by lesions and inactivations of RA and LMAN.

RA lesions entirely blocked singing in juvenile birds (n=5, 39-73 dph), indicating that subsong-like vocalizations require descending inputs from the forebrain (Fig. 3). Similarly, song production was abolished by lesions of HVC and subsequent inactivation of LMAN (n=12 experiments in 5 birds, 51-75 dph), indicating that RA circuitry, without its afferent inputs, is not sufficient to generate singing. We further tested the necessity of LMAN inputs to RA by inactivating LMAN in juvenile birds. LMAN inactivation entirely abolished subsong production in all birds younger than 45 dph (n=6 experiments in 4 birds). However, in agreement with previous studies, LMAN inactivation did not block singing in most older birds (6/7 experiments in 5 birds, 45-67 dph), although it produced a dramatic reduction in song variability (Kao et al. 2005; Ölveczky et al. 2005).

Together, these results indicate that RA and its inputs from LMAN are necessary for subsong production.

LMAN neurons exhibit premotor activity during subsong

An intriguing possibility suggested by the above results is that LMAN drives subsong production, i.e., that it generates patterns of spiking activity that control the acoustic structure of subsong on a short (10 ms) timescale. To test this prediction directly, we recorded from single RA-projecting LMAN neurons during subsong production in intact birds (n=15 neurons in 3 birds, 38-45 dph; see Supplementary Material) and in birds with bilateral HVC lesions (n=16 neurons in 2 birds, lesioned at 38 and 50 dph). To quantify premotor activity, we examined firing in a short window preceding each syllable boundary (onset or offset). First, we only considered syllable boundaries separated from other onsets or offsets by relatively long (>150 ms) periods to eliminate the possible confound of neighboring syllables on the firing pattern. There was a significant increase in firing prior to syllable onsets in 12 of 31 neurons (16.1±1.6 Hz in a 50-ms window preceding syllable onset compared to 8.6±0.6 Hz in a 100-ms baseline period preceding this window; $p<0.05$; e.g. neuron 3, Fig. 4a,b; see Supplementary Material). Similarly, syllable offsets were preceded by a significant increase in firing in 5 of 31 neurons (21.2±3.4 Hz prior to syllable offset compared to baseline 15.5±1.3 Hz; $p<0.05$; e.g. neuron 14, Fig 4c,d). Interestingly, similar neuronal firing patterns related to onsets and offsets of behavioral sequences have been observed in other basal-ganglia-related circuits (Fujii & Graybiel 2003).

In the above analysis, we only considered syllable boundaries separated by long

(>150 ms) periods of time to isolate syllable onset- and offset-related changes in firing. However, the firing of some LMAN neurons also correlated with more rapid changes in song structure. For instance, neuron 12 (Fig. 4g,f) exhibited increased firing prior to syllables that followed short (10-150 ms), rather than long intervals and a reduction in firing during silent periods between syllables. Over all, 7 neurons showed a premotor increase in activity prior to syllables separated by short intervals ($p<0.05$ for the comparison of a 30-ms window preceding a syllable with 30 ms of baseline). This suggests that some LMAN neurons may have a premotor relation to subsong structure at the level of individual syllables.

In neurons that exhibited a significant increase in firing prior to syllable onsets (n=18), high-frequency bursts of spikes (>100 Hz) preceded 13.2±1.4% of syllables. The most likely timing of a burst onset was 17.2±3.1 ms prior to syllable onset. Such latency is, in fact, anticipated for premotor activity in LMAN, given the 10-15 ms latency reported for vocal perturbation following electrical stimulation in RA (Fee et al. 2004), and the 2-5 ms antidromic latency we found in LMAN neurons (see Supplementary Material). Importantly, although the exact relationship of firing to song varied across cells, 20 of 31 (65%) neurons we recorded showed some type of premotor correlation to the vocal output. Premotor firing in LMAN did not require activity within HVC; 8 of 16 neurons exhibited significant correlations to song structure in HVC-lesioned birds (Fig. S5).

Discussion

Our data indicate that LMAN, and possibly other components of the AFP,

comprise an essential premotor circuit for the production of early babbling. On the other hand, we show that the classical premotor nucleus HVC (Nottebohm et al. 1976), is not necessary for the generation of subsong. We therefore propose that two premotor pathways in the songbird function to produce vocalizations at different stages of development. In young juveniles, the AFP generates poorly structured subsong, whereas in adult birds, the classical HVC-motor pathway generates highly stereotyped motor sequences. These pathways interact in the intermediate plastic song stage (Ölveczky et al. 2005) to generate the partially structured but variable vocalizations upon which vocal learning operates.

The transfer of functional dominance from one pathway to another during vocal learning elegantly parallels their anatomical development. HVC does not reach its adult size until the late plastic song stage (Alvarez-Buylla et al. 1992) and establishes functional synapses in RA later than LMAN (Mooney 1992; Mooney & Rao 1994). Song maturation and the decrease in vocal variability have thus been attributed to the strengthening of inputs from HVC and the concurrent weakening of inputs from LMAN (Herrmann & Arnold 1991; Akutagawa & Konishi 1994; Kittelberger & Mooney 1999; Stark & Perkel 1999). Curiously, although HVC neurons form synapses in RA at around the onset of singing (30-35 dph (Mooney 1992)), our results show that they do not significantly contribute to song production in its earliest stage. It is therefore possible that the HVC-to-RA pathway is active during early subsong, but is not yet functionally strong enough to drive singing by itself or influence vocalizations in a detectable way.

Identifying forebrain circuits involved in the production of juvenile movements is a requisite step toward understanding the mechanisms by which sensorimotor learning

takes place. Several models of developmental learning suggest that early motor behaviors originate in the same circuits that later produce adult behavior. In this view, known as neuronal group selection theory, an initially large number of motor patterns undergo a selection process through competition, gradually eliminating circuits that produce undesirable behaviors (Forssberg 1999; Edelman 1987; Sporns & Edelman 1993; Marler 1997; Hadders-Algra 2000). Our findings, however, suggest a rather different model, in which distinct specialized circuits are dedicated to the generation of highly variable juvenile behavior. We speculate that similar circuits for the production of infant behavior may be a general feature of developmental learning in the vertebrate brain.

Supplementary material: materials and methods

Sound recordings

Subjects were juvenile and adult male zebra finches of various ages (>30 dph). Birds were obtained from the Massachusetts Institute of Technology breeding facility. Animal care and experiments were carried out in accordance with the National Institute of Health guidelines and approved by the local Institutional Animal Care and Use Committee. Birds were placed in custom-made sound isolation chambers and vocalizations were recorded either with Sound Analysis Pro (Tchernichovski et al. 2000) or custom-written software. Thresholds used for triggering sound recordings were substantially lower than those commonly used (1000 ms "minimum peak record duration" with a minimum of 5 "peaks crossing the threshold" in Sound Analysis Pro) in order to ensure recording of all quiet subsong vocalizations. Our settings were sufficient for capturing sounds as quiet as "tet" calls and feather ruffles. To estimate frequencies of songs and calls, we segmented an entire day of recordings into 1-sec segments. We then estimated the numbers of these segments containing calls and songs by manually browsing through a random subsample of 1000 of these segments and directly counting the numbers of vocalizations. In 4 adult birds, we also recorded directed vocalizations by presenting a female bird in a separate cage (see Analysis of Acoustic Features).

Surgery and lesions

Prior to surgery, birds were anesthetized with 1-2% isofluorane in oxygen and placed in a stereotaxic apparatus. Craniotomies were made bilaterally above RA, HVC, or LMAN. RA was identified with a carbon fiber electrode (0.4-0.8 MΩ; Kation

Scientific) by the presence of characteristic spontaneous activity. To localize HVC or LMAN, a bipolar stainless steel stimulating electrode was implanted in RA. Current pulses (200 μs at 1 Hz, 50-200 μA) were then delivered with the electrode and HVC or LMAN were localized by the presence of short-latency (2-5 ms) antidromic responses. Lesions in HVC or RA were made with a platinum-iridium electrode (Micro Probe; 100 μA current for 60 s). A 3-dimensional lattice of 6-10 lesions spaced at 250 μm was made in each hemisphere for complete bilateral lesions. Birds were returned to sound isolation chambers, and vocalizations were recorded for at least 10 days following surgery.

In some animals (n=5), a retrograde tracer was injected into RA during the same surgery (20-30 nl of alexa-conjugated dextran or cholera toxin subunit β, Invitrogen). After the experiment, the animal was sacrificed and perfused with 3-4% paraformaldehyde. The brain was extracted and sliced parasagittally for histological examination. We confirmed completeness of HVC lesions by observing the absence of retrogradely-labeled cells in HVC, but the presence of labeling in LMAN (Fig. 1c).

Pharmacological inactivation

For pharmacological inactivation of HVC or LMAN, we devised probes to perform reverse microdialysis without physically restraining the birds (Fig. S4). Probes consisted of a reservoir (cap of a 23-gage hypodermic needle) connected by a polyimide tube to a concentrically attached 500-μm-long tube of dialysis membrane (Spectra/Por). In this design, a pharmacological agent could diffuse freely from the reservoir down the tube and across the dialysis membrane. The length of the polyimide tube was chosen to reach the region of interest from the brain surface. A smaller polyimide tube was inserted

into the dialysis tube and used as flush outlet. All attachment points, as well as the end of the dialysis tube, were sealed with bio-compatible epoxy (Epo-Tek).

Probes were implanted bilaterally into HVC or LMAN and attached to the skull using dental acrylic. In 3 birds, we recorded spontaneous activity in the vicinity of the dialysis probe under anesthesia to calibrate drug concentrations necessary for inactivation of a correctly-sized brain region (Fig. S4). We found that, for complete inactivations of HVC or LMAN, concentrations of muscimol or TTX (Sigma) in the reservoir of the probe needed to be ~500 times higher than those used for direct injections (Ölveczky et al. 2005). For inactivation in freely-behaving birds, animals were briefly placed in a small foam restraint and drug (0.016 mg/ml TTX or 1.5 mg/ml muscimol) was applied to the reservoir. For washout, the drug was flushed out of the reservoir and substituted with phosphate-buffered saline (PBS).

Fiber tract transections

We performed bilateral transections of the HVC-to-RA fiber tract by making 3 incisions with an ophthalmic knife (Sharpoint) at fixed stereotaxic coordinates (~500 μm posterior to HVC, between 1.5 and 3.5 mm lateral, 2.5 mm maximum depth). In the same surgery, we injected a retrograde tracer (see above) into RA, as well as a tracer of a different wavelength into area X (40 nl). In these birds, we confirmed completeness of the transections by observing retrograde labeling of X-projectors, but not RA-projectors in HVC, while observing both tracers in LMAN (Fig. S3).

Electrophysiology

Recordings in LMAN were carried out using a motorized microdrive described previously (Fee & Leonardo 2001). A stimulating electrode was implanted in RA and cells were isolated by searching for spontaneous or antidromically evoked activity. The signal-to-noise ratio was typically 5-15:1. Putative RA-projecting neurons exhibited short-latency (<5 ms) responses to antidromic stimulation with a jitter of less than 100 μs. Of the 31 antidromically identified neurons that were recorded during singing, 27 were further confirmed as RA-projecting by collision tests (Hahnloser et al. 2002). Each neuron was recorded during the singing of multiple subsong bouts (14-681 bouts, average 138).

Data analysis

All data analyses were performed with custom-written software in Matlab and Sound Analysis Pro for Matlab (SAM).

Song analysis

For syllable segmentation in each recording, we calculated a sound threshold as the Fisher discriminant of two Gaussian modes (corresponding to noise and sound) fit to the values of log-amplitude. We detected crossings of this threshold and defined sound onsets and offsets as the closest points to these crossings where amplitude deviated from noise by 2 standard deviations. Sounds separated by <7 ms of silence were merged into a single syllable, and segments of sound <7 ms long were eliminated. Bout were defined as sequences of syllables separated by at least 500 ms. Song and call rates were quantified on the full day immediately preceding each surgery and on the first full day of singing

following each surgery. For experiments that abolished singing, call rates were quantified on the second day after surgery.

To quantify the level of stereotypy, 10 bouts were randomly selected from the data. We only considered bouts that were at least 2 s long, in order to include at least 2 song motifs for adults and late plastic-song birds. For each pair of bouts, a correlation matrix was calculated by computing the correlation of power spectra (between 850 Hz and 8.5 kHz) for each pair of points in time (1-ms spectrogram windows). We then measured the maximum value of the lag correlation function, excluding points within 1 s from either end of the function. The resulting values were averaged across the 45 (10x9/2) comparisons. For regression analysis of stereotypy and age (Fig. 2d), we assigned all adults the age of 90 dph.

Spectral features (see Analysis of Acoustic Features) were measured on each time slice of the spectrogram (1 ms long window). We measured these features on time slices occurring during syllables randomly selected from the data. At least 100,000 time slices were included in the distributions of features (Fig. 3e).

Analysis of neuronal recording

For analysis of neuronal recording, instantaneous firing rates (IFRs) were calculated as inverses of inter-spike intervals. Bursts were defined as events with IFR exceeding 100 Hz. For assessment of premotor activity, average firing rates were quantified in a test window and a baseline window (see text). The ratio of the test rate to the baseline was measured. For each neuron, we asked whether this ratio was significantly above chance level. To evaluate this, we created 1000 surrogate datasets in

which syllables and intervals were randomly rearranged within a song bout. The start of the bout was also jittered by a Gaussian-distributed value with standard deviation equal to the average syllable length. P-value was calculated as the fraction of the surrogate datasets for which the ratio of the test firing rate to the baseline was above the ratio for the real dataset.

Supplementary material: analysis of acoustic features

Our results show that zebra finches produce singing highly similar to subsong following bilateral lesions or inactivations of HVC. Here, we quantify these similarities by comparing singing before and after HVC elimination using an array of acoustic features. These features have proven to be effective for quantifying developmental trends in zebra finches and are widely used for quantifying song similarities and differences across experimental conditions (Tchernichovski et al. 2000; Derégnaucourt et al. 2005). Details concerning the calculation of these features have been described previously (Tchernichovski et al. 2000; Derégnaucourt et al. 2005). Here, we provide a brief description of each one, along with the quantification of our data.

In the first section, we focus on the songs of subsong-producing birds (<45 dph) before and after HVC elimination. In the second section, we analyze developmental changes in singing and the effects of HVC elimination on the songs of older birds.

HVC elimination in subsong-producing birds (<45 dph)

Weiner entropy

Weiner entropy measures the width and uniformity of the power spectrum. Broadband noise has high entropy values, whereas pure tones and harmonic sounds have low entropy values. HVC elimination had no effect on the entropy of subsong. Distributions of this feature before and after HVC elimination were nearly identical (Fig. S1a), with no significant differences in either entropy mean (Wilcoxon p=0.67) or variance (p=0.67).

Pitch goodness

Pitch goodness quantifies the periodicity of the spectrum of a particular sound. Thus, harmonic sounds have high values of pitch goodness, whereas broadband noise and pure tones have low values of pitch goodness. HVC elimination had no effect on the pitch goodness of subsong (Fig. S1b). There were no differences between the means (Wilcoxon $p=0.60$) or variances ($p=0.22$) of this measure.

Relative amplitude

Amplitude measures the power of sound across all frequencies. Since power in our recordings is un-scaled, we measured amplitude relative to the baseline noise level in the sound isolation chamber separately for each recording. Amplitude was not affected by HVC elimination (Fig. S1c) and exhibited no significant differences of means (Wilcoxon $p=0.14$) or variances ($p=0.06$) between the two conditions.

Frequency modulation

Frequency modulation (FM) is the angular component of squared time and frequency derivatives of sound. Sounds whose frequency is not changing in time have FM values close to 0 degrees. Sounds with rapidly changing frequency have values closer to 90 degrees. Frequency modulation was not affected by HVC elimination (Fig. S1d) and had no significant differences of means (Wilcoxon $p=1$) or variances ($p=1$) between the two conditions.

Pitch

We estimate pitch of sounds using a method adapted for zebra finch songs. At each point in time, we measure harmonic pitch, i.e., the fundamental frequency of sound. Whereas this measure is well-defined for harmonic sounds, it is not appropriate for pure tones or broadband noises. Therefore, for sounds that have high values of Weiner entropy (>-3) or low values of pitch goodness (<100) we consider pitch to be the average frequency of sound (i.e., the center of spectrum gravity in the frequency domain) instead.

Pitch is the only feature that was affected by HVC elimination in subsong-producing birds (Fig. S1d). Following HVC elimination, average pitch was reduced to 85.1±2.1% of control across the 9 birds younger than 45 dph (Wilcoxon $p<0.001$). Although this reduction was significant, pitch in the absence of HVC was well within the range of normal subsong. In fact, compared to the control pitch, average pitch following HVC elimination was shifted at most by 0.28 standard deviations (0.18±0.03 on average).

Could direct inputs from HVC to RA influence subsong pitch? We analyzed pitch distributions before and after bilateral transections of the HVC-to-RA fiber tract in subsong-producing birds (Fig. S3). Pitch was not affected by these transection (99.5±1.4% of control across 3 birds). Thus, direct inputs to RA via the HVC-motor pathway appear to have no influence on this feature. A possible explanation of this result is that pitch is affected by inputs from HVC to the AFP in subsong-producing birds.

Syllable duration

Distributions of syllable durations are shown in Fig. 2b. In subsong-producing birds, HVC elimination had no effect on syllable duration (113±7 ms in control songs,

115±10 ms in the absence of HVC, p=0.86). Similarly, there was no effect on the variance of syllable durations (p=0.80).

Bout duration

We defined bouts as sequences of syllables separated by more than 500 ms of silence. HVC elimination had no effect on bout duration (2.57±0.21 s in control, 2.13±0.22 s in the absence of HVC, p=0.22).

In summary, singing following HVC elimination in birds younger than 45 dph is highly similar to normal subsong by all measures. The only significant difference (reduction in pitch) cannot be explained by disruption of the HVC-to-RA motor pathway. Thus, HVC inputs to RA appear to have no detectable behavioral contribution to the production of subsong.

HVC elimination in plastic-song and adult birds

Following complete bilateral HVC elimination, birds in the plastic-song stage (n=12, 45-73 dph) and adults (n=5) produced subsong-like vocalizations. To our knowledge, this is the first report of singing following bilateral HVC lesions. These songs were produced only in social isolation (undirected singing). When adult birds were presented with a female, a condition that would normally elicit directed singing, lesioned birds did not sing, although they otherwise exhibited normal approach behavior. This result is consistent with earlier studies (Nottebohm et al. 1976; Simpson & Vicario 1990) that reported an absence of directed singing following bilateral HVC lesions in the canary

and the zebra finch. Regression of song structure similar to that we observe has been reported following partial HVC lesions in the zebra finch (Thompson & Johnson 2007). In addition, left HVC lesions in the canary produced a similar regression (Nottebohm et al. 1976; Nottebohm 1976). Given the left-hemispheric dominance of singing in the canary, these unilateral lesions may be functionally equivalent to bilateral lesions in the zebra finch.

Singing by plastic-song and adult birds following bilateral HVC elimination was similar to normal subsong. Fig. S2 shows the averages and variances of acoustic features before and after HVC elimination for birds in various age groups. Weiner entropy, pitch goodness, amplitude, and pitch exhibited significant developmental changes ($p<0.05$ for linear regression of means and variances with age across birds, consistent with (Derégnaucourt et al. 2005)). Following HVC elimination, the means and variances of these features changed dramatically, in all cases acquiring values more similar to those of normal subsong.

In addition to pitch (see above), two features of plastic and adults songs in the absence of HVC were different from normal subsong: syllable durations and the variance of the entropy distribution.

Syllable durations

Compared to normal subsong, average syllables were shorter following HVC elimination in birds older than 45 dph (85±5 ms for plastic-song birds and 79±9 ms for adults, compared to 113+/7 ms for subsong; $p<0.05$ in both cases; Fig. 2b). Though shorter on average, syllables produced by these birds were within the range of normal

subsong; on the syllable duration distribution of any subsong-producing bird, average durations of all birds without HVC were within 0.6 standard deviations from the mean.

Entropy

Although average entropy values were not affected by HVC elimination, the variances of entropy distributions were lower for plastic-song and adult birds after HVC elimination compared to normal subsong (0.35±0.05 in both cases, compared to 0.56±0.04 for normal subsong, $p<0.02$). This indicates a greater variation in the quality of sounds produced during normal subsong. Notably, this difference between normal subsong and songs of birds in the absence of HVC is small compared to the developmental change (factor of 2.43 increase in entropy variance from subsong to adult song).

In summary, singing by plastic-song and adult birds in the absence of HVC is similar by many measures to normal subsong, but exhibits some significant differences. Since we show that LMAN is required for singing in the absence of HVC, these differences could be due to developmental changes in LMAN circuitry or its connections to RA. Alternatively, they could result from changes in any other nuclei upstream or downstream of LMAN, or even from developmental changes in the peripheral vocal organ.

Figure 1. Subsong production does not require HVC. (a) Results of bilateral HVC elimination (by lesion or pharmacological inactivation). Top: major connections of the song system with and without HVC; red: motor pathway, blue: anterior forebrain pathway (AFP). Left panel: sonograms of three birds at different ages. Right panel: sonograms of the same birds in the absence of HVC. Frequency ranges from 500 Hz to 7.5 kHz. Color scale (from black to red) spans a power range of 8 dB. (b) Histological verification of HVC lesions. Left: Inverted dark-field image of a parasagittal section of a normal zebra finch brain (50 dph). Red: retrograde fluorescence labeling of neurons in HVC following tracer (alexa-conjugated cholera toxin subunit β) injection into RA. Inset: retrograde labeling of neurons in LMAN from the same injection. Right: Brain sections of the plastic-song bird shown in (a). Scale bars: 500 μm.

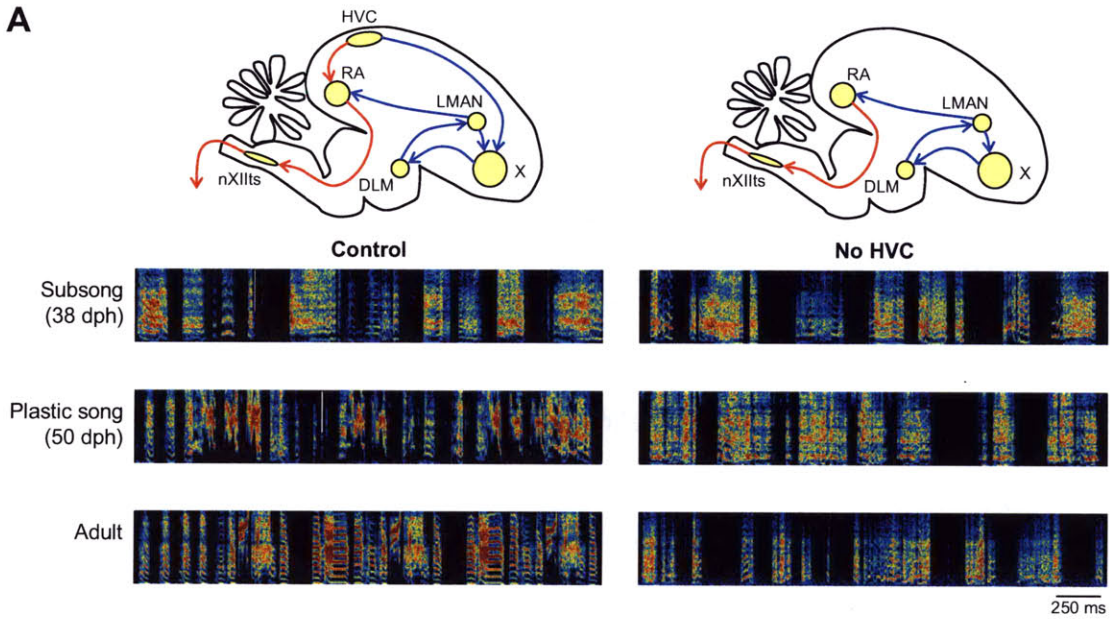
A
HVC
RA
LMAN
nXIIts
DLM
X
Control
No HVC
Subsong
(38 dph)
Plastic song
(50 dph)
Adult
250 ms

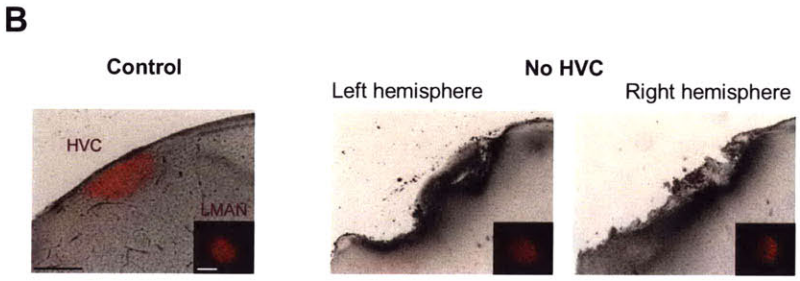
B
Control
No HVC
Left hemisphere
Right hemisphere
HVC
LMAN

Figure 2. Singing in the absence of HVC is highly similar to normal subsong. (a) Distributions of syllable durations for three birds of various ages (blue) and distributions for the same birds in the absence of HVC (red). (b) Average syllable duration distributions for normal subsong-producing birds (blue) and birds of different ages in the absence of HVC. (b) Sample spectral correlation matrices for a pair of songs produced by an adult bird (left) and by the same bird after HVC lesion (right). Averaging the matrix along its diagonals reveals strong correlation peaks in control (pre-lesion) condition, but not after HVC lesion. (b) Maximum values of the spectral correlation, averaged across all pairwise comparisons of 10 song bouts, for birds in control conditions and in the absence of HVC. Dashed lines: linear regression; error bars: standard errors across pairs of bouts.

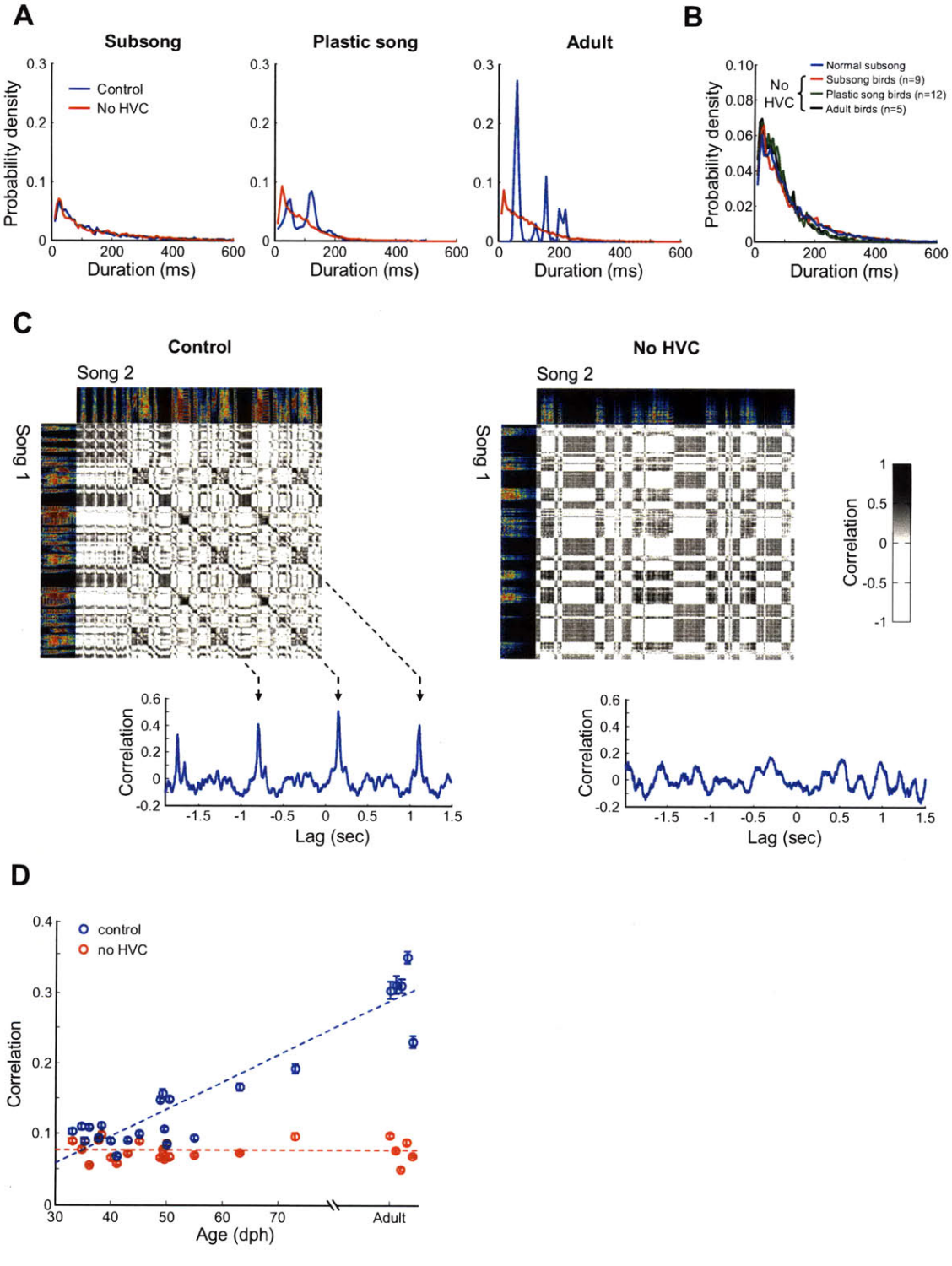
A
Subsong
Plastic song
Adult
Control
No HVC
Probability density
Duration (ms)
B
Normal subsong
Subsong birds (n=9)
Plastic song birds (n=12)
Adult birds (n=5)
No HVC
C
Control
No HVC
Song 2
Song 1
Correlation
Lag (sec)
D
control
no HVC
Correlation
Age (dph)
Adult

Figure 3. Subsong production requires LMAN and RA. Average rates of song and call production in all lesion and inactivation experiments. To measure rates, a full day of recording was partitioned into 1-sec segments, and the numbers of segments containing calls or songs were estimated. In cases where age is unspecified, data from all birds is pooled together. Note that for subsong-producing birds (<45 dph), the average rate of singing was not affected by HVC elimination (Wilcoxon $p>0.5$). Top: For each condition, the fraction of experiments in which any amount of singing occurred. Error bars: s.e.m. values across birds. In experiments that abolished singing, silencing was specific to songs and did not affect the frequency of call vocalizations that are known not to require the song system (Simpson & Vicario 1990).

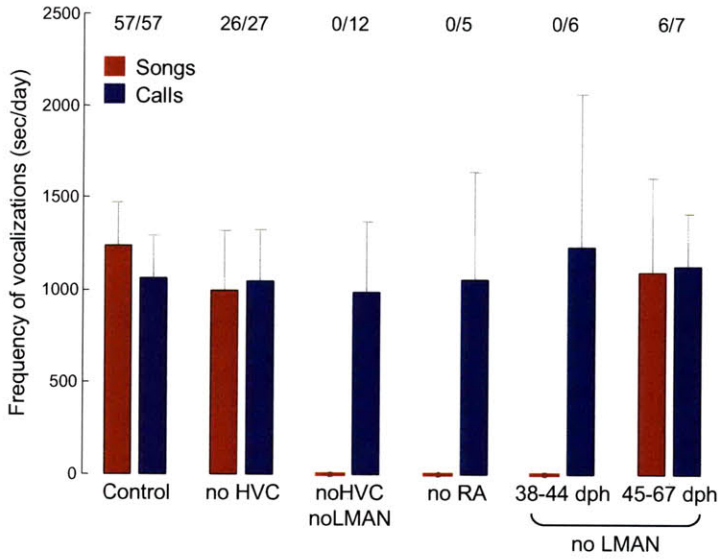
2500
2000
1500
1000
500
0
Frequency of vocalizations (sec/day)
57/57
26/27
0/12
0/5
0/6
6/7
Songs
Calls
Control
no HVC
noHVC
noLMAN
no RA
38-44 dph
45-67 dph
no LMAN

Figure 4. LMAN exhibits premotor activity during subsong. (a) Activity of an RA-projecting LMAN neuron during subsong production. Blue segments indicate individual syllables. Instantaneous firing rate exhibits peaks prior to syllable onsets. (b) Examples of spiking activity (red) prior to onset sound amplitude (black) for neuron 3. Asterisk indicates a matching example with (a). Histogram: average firing rate across all syllable onsets for neuron 3. Blue trace: average sound amplitude. Average includes only those syllables that were preceded by long (>150 ms) periods of silence. (c-d) Activity of a neuron that exhibited peaks in firing prior to syllable offsets. Plotted as in (a-b). Averages in (d) include only long (>150 ms) syllables that were followed by long (>150 ms) periods of silence in order to isolate offset-related changes in firing from onset-related changes. (e) Activity of a neuron that exhibited firing prior to syllable onsets following short (<150 ms) intervals. Plotted as in (a). Bottom: Spiking activity (red) occurring prior to syllable onsets for neuron 12. (f) Averages of firing rate and sound amplitude for neuron 12, separately for syllables that followed short (10-150 ms) and long (>150 ms) intervals. Plotted as in (b). (g) Syllable onset-centered spike raster for neuron 12. Raster is sorted according to the length of the interval that preceded the syllables; dashed lines indicate interval boundaries. Blue marks: spikes that occurred in high-frequency (>100 Hz) bursts. Grey marks: spikes that occurred outside of bursts.

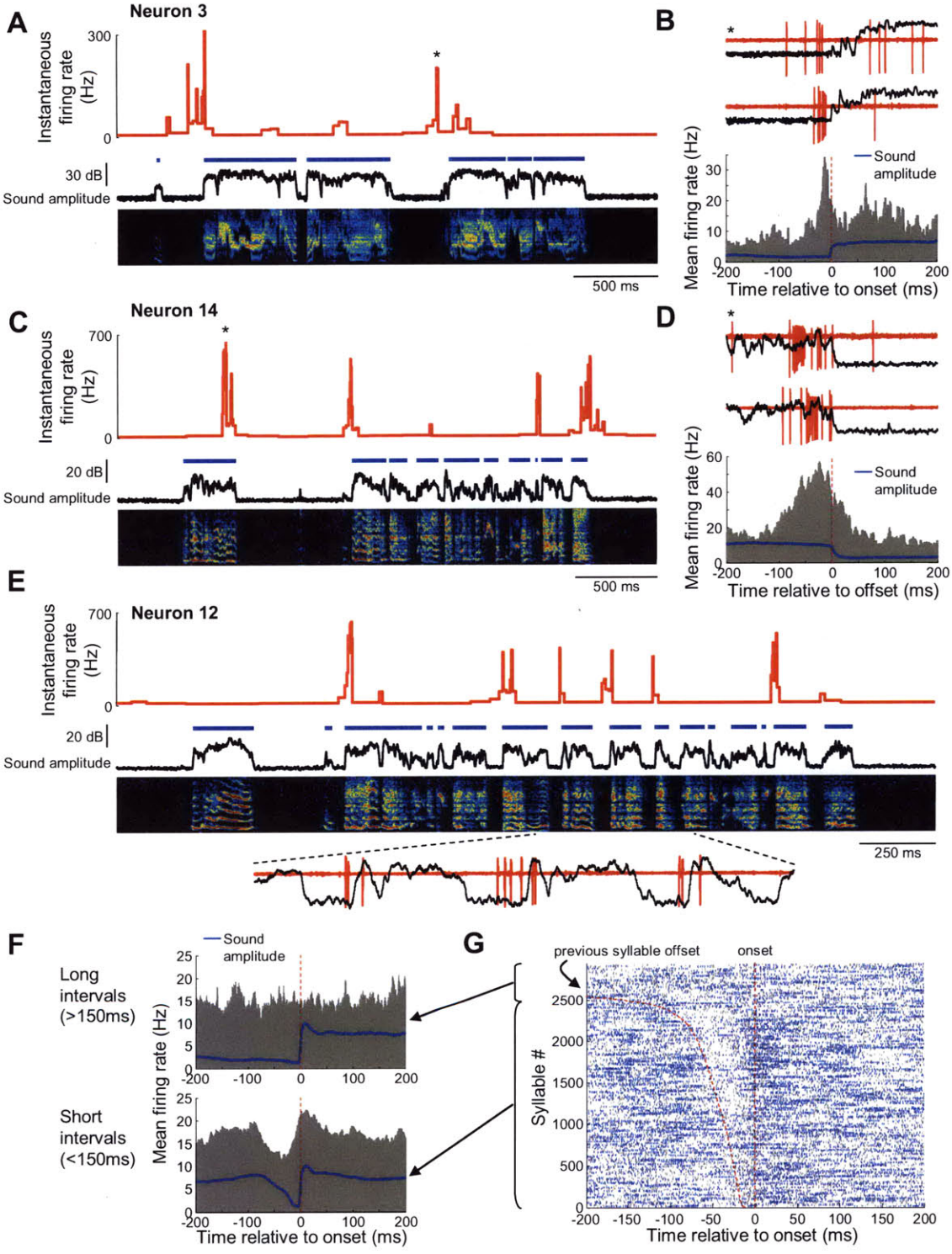
A
Neuron 3
Instantaneous firing rate (Hz)
300
0
30 dB
Sound amplitude
500 ms
B
Mean firing rate (Hz)
Sound amplitude
Time relative to onset (ms)
C
Neuron 14
700
20 dB
D
Time relative to offset (ms)
E
Neuron 12
250 ms
F
Long intervals (>150ms)
Short intervals (<150ms)
G
previous syllable offset
onset
Syllable #

Figure S1. Singing in the absence of HVC is highly similar to normal subsong. (a-e) Average distributions of acoustic features (see text) before and after elimination of HVC across 9 birds under the age of 45 dph. Signal used for amplitude measurements in (c) was recorded from a microphone clipped to the side of a 30x25x20 cm cage.

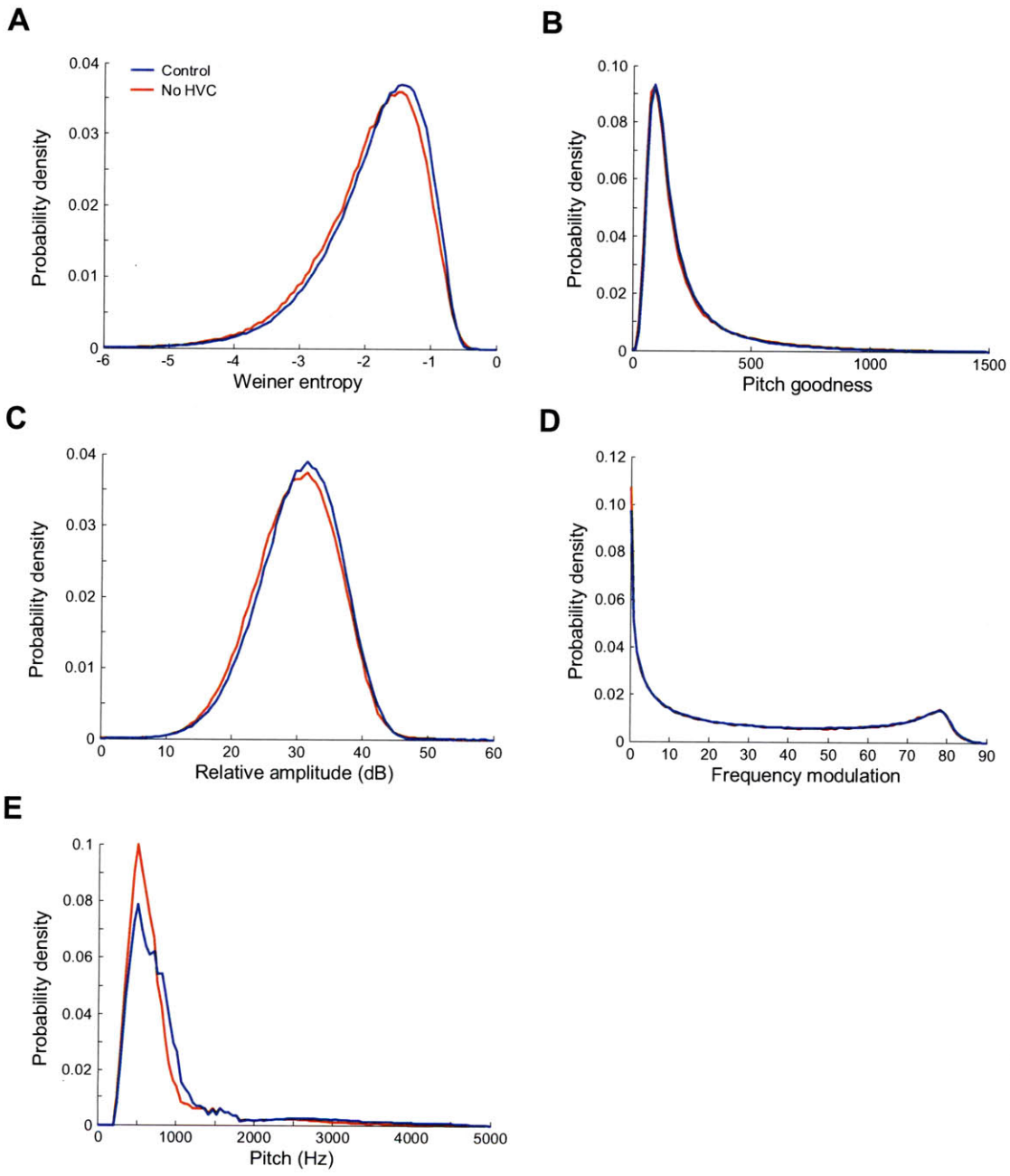
A
Control
No HVC
Probability density
Weiner entropy
B
Probability density
Pitch goodness
C
Probability density
Relative amplitude (dB)
D
Probability density
Frequency modulation
E
Probability density
Pitch (Hz)

Figure S2. Quantification of acoustic features (see text) before and after HVC elimination for three age groups: subsong-producing birds (33-44 dph), plastic-song birds (45-73 dph), and adults. (a-e) Means and variances of acoustic features, averaged across all birds in each age group.

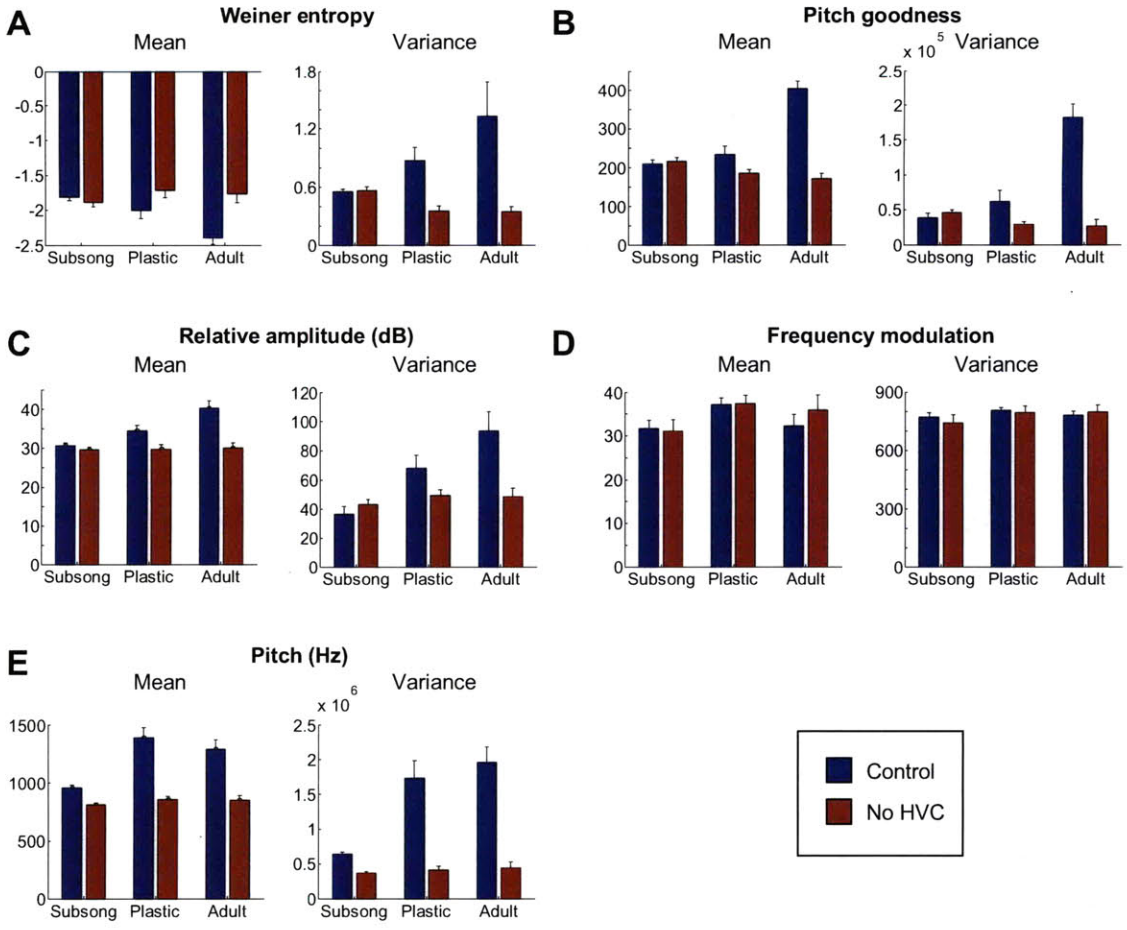
A
Weiner entropy
Mean
Variance
B
Pitch goodness
Mean
x 10^5
Variance
C
Relative amplitude (dB)
Mean
Variance
D
Frequency modulation
Mean
Variance
E
Pitch (Hz)
Mean
x 10^6
Variance
Subsong
Plastic
Adult
Control
No HVC

Figure S3. Singing following transection of the HVC-to-RA fiber tract is highly similar to normal subsong. (a) Sample sonograms of 3 birds in the subsong stage (left) and sample sonograms of the same birds following bilateral transection of the HVC-to-RA fiber tract (right). (b) Distributions of syllable durations for the 3 birds shown in (a) before and after transection. Distributions in the two conditions are almost entirely overlapping. (c) Parasagittal brain sections of Bird 1.8.6 shown in (a) and (b), illustrating the location and extent of the transections in the two hemispheres. (d) Fluorescence images for Bird 1.8.6 and an age-matched control bird. Retrograde labeling of neurons following tracer injection (alexa-conjugated dextran) into RA (red) is overlaid with retrograde labeling following injection into area X (blue). Both X- and RA-projecting neurons in HVC are labeled in the control bird, but only X-projectors are labeled in the bird that received transections. In both birds, both X- and RA-projecting neurons in LMAN are labeled.

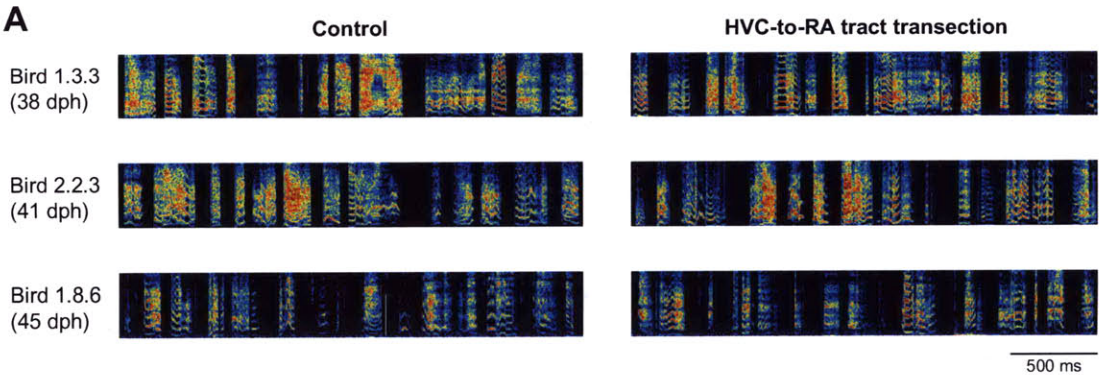
A
Control
HVC-to-RA tract transection
Bird 1.3.3
(38 dph)
Bird 2.2.3
(41 dph)
Bird 1.8.6
(45 dph)
500 ms

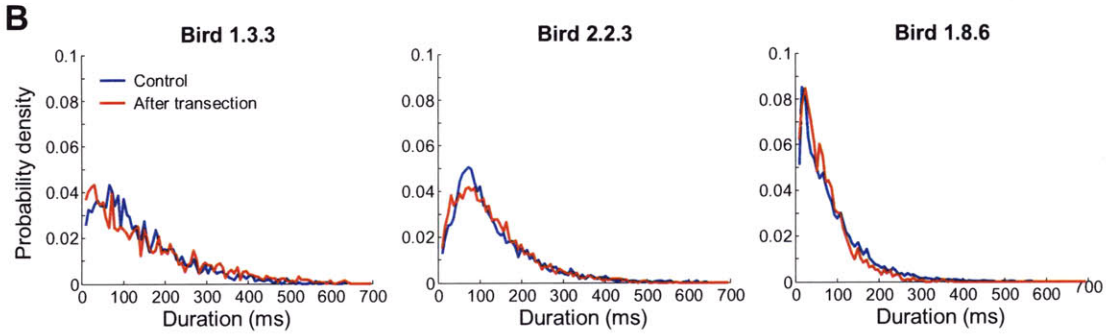
B
Bird 1.3.3
Bird 2.2.3
Bird 1.8.6
Control
After transection
Probability density
Duration (ms)

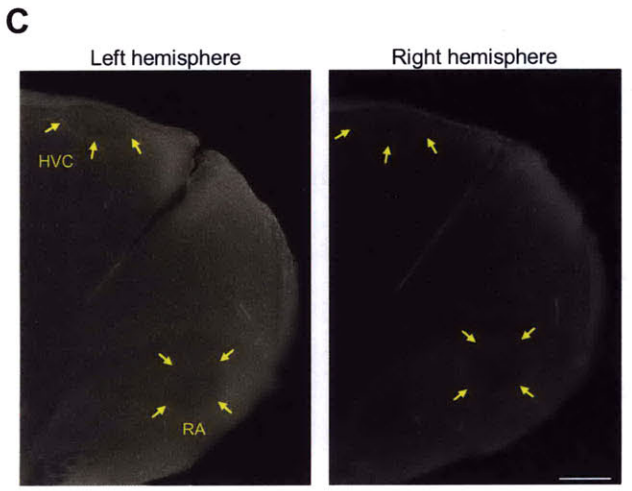
C
Left hemisphere
Right hemisphere
HVC
RA

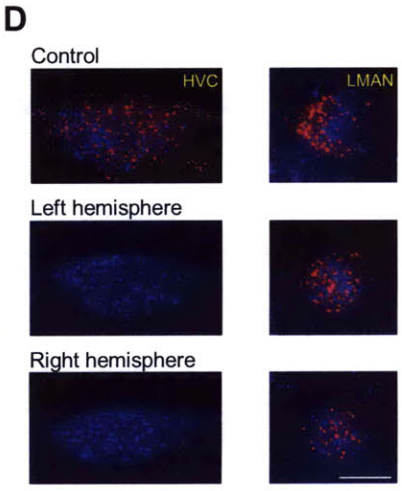
D
Control
HVC
LMAN
Left hemisphere
Right hemisphere

Figure S4. Bilateral inactivation of HVC in the singing bird. (a) Schematic diagram of an un-tethered reverse microdialysis probe for drug delivery to brain areas in a freely behaving zebra finch. Drug (muscimol or TTX) is placed in the reservoir, from which it freely diffuses along the inflow tube and across the semipermeable dialysis membrane. Outlet tube is used for drug washout. (b) Song production in a 50-day-old bird following bilateral inactivation of HVC with muscimol (1.5 mg/ml) and restoration of normal singing following washout. (c) Confirmation of HVC inactivation by the dialysis probe. Spontaneous activity under anesthesia was recorded at various distances from the probe following application of phosphate-buffered saline (PBS). Muscimol (1.5 mg/ml) was then placed in the probe (0 min) and activity was recorded at a fixed location 700 μm from the probe until 40 min. Spontaneous activity was abolished ~20 min after drug application. After 40 min, the lack of spontaneous activity was confirmed at locations up to 900 μm from the probe. Blockade of activity at these locations was confirmed again in a different recording session 8 hours after drug application. Drug was then washed out by replacement with PBS, and a normal level of spontaneous activity was recorded the following day (24 hrs).

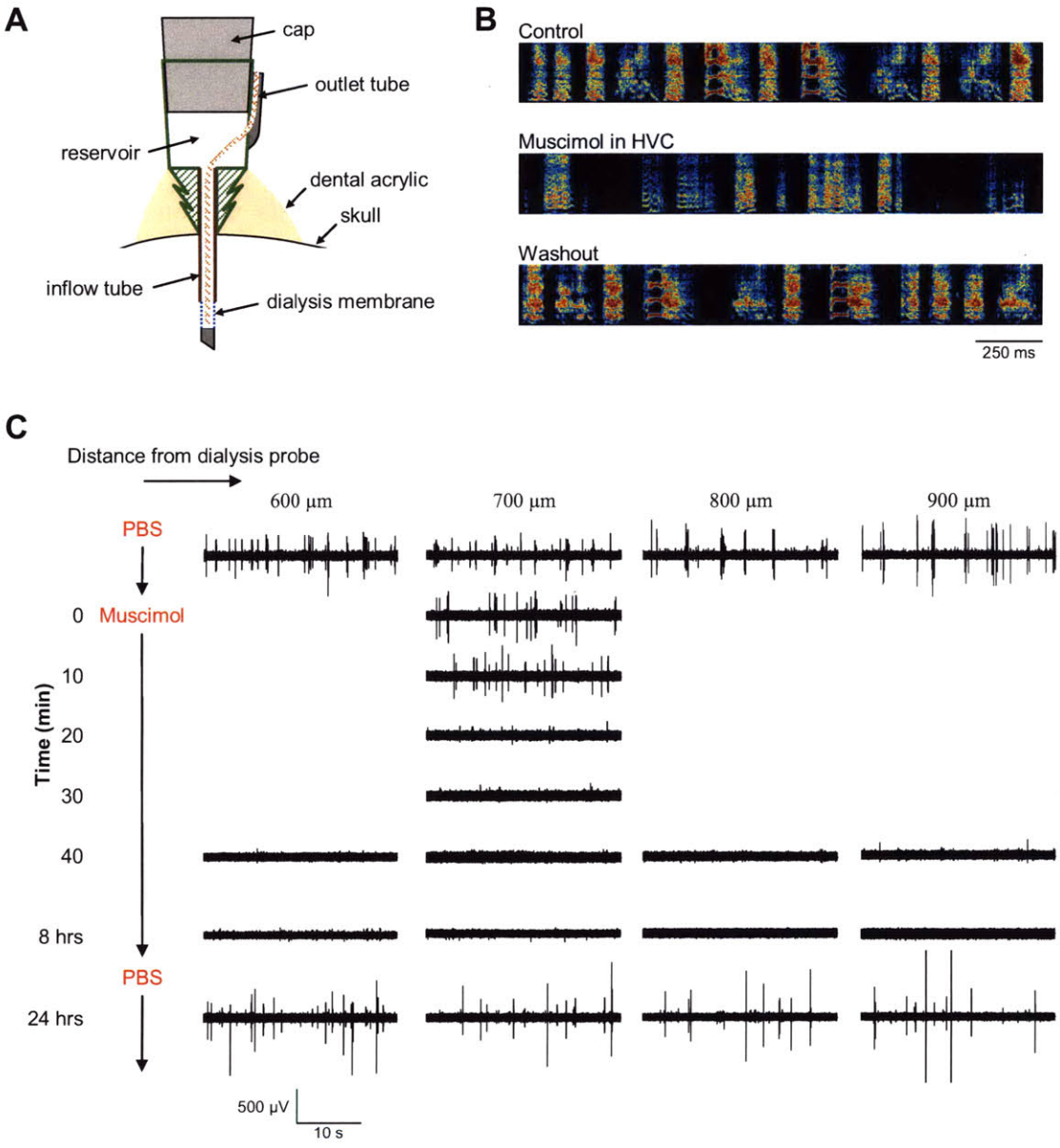
A
cap
outlet tube
reservoir
dental acrylic
skull
inflow tube
dialysis membrane
B
Control
Muscimol in HVC
Washout
250 ms
C
Distance from dialysis probe
600 µm
700 µm
800 µm
900 µm
PBS
0
Muscimol
10
20
30
40
8 hrs
PBS
24 hrs
Time (min)
500 µV
10 s

Figure S5. LMAN exhibits premotor activity during singing in birds with bilateral HVC lesions. (a) Activity of an RA-projecting LMAN neuron during two consecutive bouts of singing. Blue segments indicate individual syllables. The neuron exhibits increased firing prior to syllable onsets. (b) Activity of an RA-projecting LMAN neuron that exhibits increased firing prior to syllable offsets. Plotted as in (a). (c) Average firing rates across all syllable onsets for the neuron shown in (a) and across all syllable offsets for the neuron shown in (b).

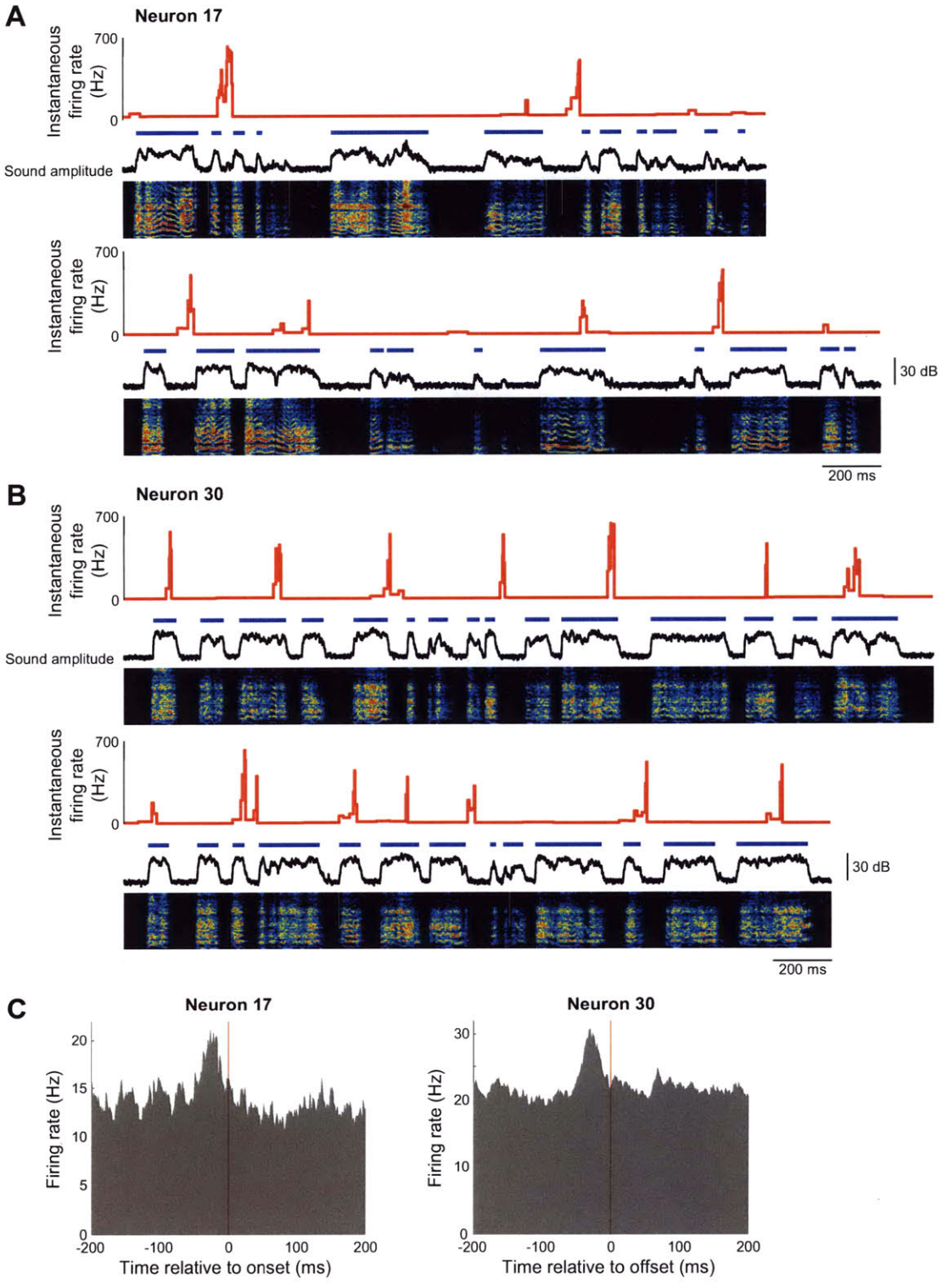
A
Neuron 17
Instantaneous firing rate (Hz)
700
0
Sound amplitude
30 dB
200 ms
B
Neuron 30
C
Neuron 17
Neuron 30
Firing rate (Hz)
Time relative to onset (ms)
Time relative to offset (ms)

Chapter 3

Quantitative description of timing in early song production

Song development, much like motor learning in general, is characterized by the gradual organization of actions into reliable temporal sequences. What are the biophysical mechanisms that underlie this development of timing? A requisite step in addressing this question is understanding the behavior itself on a detailed, quantitative level, and describing how it changes with development. The time-varying structure of an adult zebra finch song is well-described, as evidenced in part by the large number of features used to describe its temporal characteristics (e.g., bouts, motifs, syllables, etc). However, no equivalent set of features exists for specifically characterizing the temporal structure of songs early in development (although some important steps in that direction have been made; (Tchernichovski et al. 2001; Tchernichovski et al. 2004; Saar & Mitra 2008)). The goal of this chapter is to analyze the timing in early singing and to develop a vocabulary of terms useful for the quantification of this behavior.

Behavioral timescales of subsong

We first sought to characterize the temporal features of subsong production and to identify the critical timescales of this behavior. Fig. 1a illustrates a typical song bout of a 44 days-post-hatch (dph) juvenile bird. As does adult song (Glaze & Troyer 2006), early singing consists of distinct acoustic transitions between two modes (Fig. 1b) – segments of sound (syllables) and silent intervals between them (gaps). A crucial feature of this behavior, in contrast to adult singing, is the presence of broadly distributed timescales, of both the syllables and the gaps. For instance, it is not uncommon for the durations of syllables or gaps in a song to be different by more that an order of magnitude (e.g.

syllables 1-3 in Fig. 1a). We therefore began the characterization of song dynamics by describing the durations of these acoustic elements.

We recorded the songs of 61 birds between the ages of 33 and 59 dph (see Methods). In the youngest of these birds, syllable durations tended to form broad distributions (Fig. 1c). Short syllables (<50 ms) occurred with the highest probability density, but the distributions had long tails, often extending past 400 ms. Interestingly, the tails of distributions were well-fit by exponential functions, as illustrated by their linearity on a semi-logarithmic plot (Figs. 1d, S1). Most birds under the age of 40 dph produced syllables that were well-fit by exponential distributions (16 of 24 birds, see Methods for the goodness-of-fit statistic). This fraction of birds decreased with age over a short developmental period, such that none of the 15 birds older than 50 dph exhibited exponentially-distributed syllable durations (Fig. 1e). This deviation from an exponential fit is due to the appearance of consistently-timed syllables during the early plastic song phase (see Chapter 2, (Tchernichovski et al. 2004; Aronov et al. 2008), Fig. S1), which we shall address later. For the remainder of this chapter, we define "subsong" as the production of syllables whose durations do not strongly deviate from an exponential distribution.

An exponential distribution is indicative of a Poisson process, in which the probability of terminating a syllable is uniform it time and thus independent of when the syllable was initiated. The time constant of this exponential (which is equivalent to the average syllable duration, see Methods) is therefore a single timescale that characterizes the syllables of an individual bird. Across the population of subsong-producing birds, the

time constant was 87.4±3.7 ms (±s.e.m. here and elsewhere in the chapter unless stated otherwise; N=20 birds, Fig. 1f,g).

We next sought to characterize the timing of silent gaps in subsong. Because subsong appears to be a series of randomly-timed transitions between vocal and silent periods, we expected gap durations to be distributed similarly to those of syllables. Yet, surprisingly, gap duration distributions in subsong-producing birds were not uniformly decreasing, but typically exhibited a more complex structure, often including a secondary peak near 60 ms (Fig. 2a,b). Thus, even in young subsong birds with no stereotypy in syllable durations, gaps appear to exhibit some consistency in timing.

Even outside of the peak at ~60 ms, the distributions of gap durations, unlike those of syllable durations, were not well-described by a single exponential, as indicated by a comparison of short and long gaps. Specifically, distributions of short gaps (<~30 ms, see Methods) appeared to be approximately exponential (time constant of 30.0±3.7 ms, N=18 birds), as did the distributions of gaps between 100 and 200 ms (time constant 54.7±2.1 ms). These time constants were different ($p<0.001$, paired t-test), indicating a possible presence of two mechanistically distinct modes in gap durations. Furthermore, although gap distributions were well-described by an exponential function at long durations (100-200 ms), they strongly deviated from this exponential fit for gaps longer than ~300 ms (Fig. 2c).

What accounts for this complexity of gap timing? In particular, what causes gaps to be relatively precisely timed at ~60 ms durations, even in young birds with no equivalent precision in syllable timing? Because inspirations occur primarily during silent intervals (Franz & Goller 2002), we hypothesized that the distinct modes of gap timing

are related to different respiratory patterns during the gaps. To characterize these patterns, we recorded air sac pressure in 6 young juvenile birds (ages 39-50) during subsong production (see Methods). These recordings allowed us to identify periods of expiration (positive air sac pressure relative to atmospheric pressure) and inspiration (negative pressure).

Fig. 2d shows a typical air sac pressure recording during the production of three bouts of subsong. As described earlier in adult birds (Franz & Goller 2002), silent periods between bouts typically contained a periodic pressure fluctuation at 2-3 Hz corresponding to eupnic breathing. Similarly to adult song, subsong was accompanied by an increase in the amplitude of both expirations and inspirations. Syllables were almost always produced during periods of expiration (99.6±0.2% of all vocalized time points, N=8 birds). Gaps, however, were less homogenous in their respiratory patterns. On the basis of these patterns, we were able to identify roughly four "modes" of gaps production, described below.

Many of the gaps were non-inspiratory (mode-1 gaps, 32.4±2.7% in N=8 birds; Fig. 2e) – that is, air sac pressure stayed positive at all times between the two flanking syllables during these gaps. Although some of these gaps were up to ~100 ms long (e.g., bottom example in Fig. 2e), most were very brief (mean duration 31.2±2.0 ms). Conversely, most brief gaps were non-inspiratory (91.3±3.4% of all gaps <25 ms). Mode-1 gaps can be thought of as non-vocalized periods that break a single expiratory gesture into multiple syllables. In fact, individual expiratory pressure pulses in subsong contained 1.49±0.06 syllables, with some pulses containing as many as 8 syllables. The presence of

non-inspiratory gaps is unique to subsong; in adult zebra finches nearly every gap contains an inspiration (Franz & Goller 2002).

The remaining gaps were those that contained at least one inspiratory pressure pulse (IP). In order to exclude most gaps during which birds returned to eupnic breathing, we first consider gaps shorter than 300 ms. Gaps that were shorter than 300 ms and contained at least one IP comprised 55.2±2.8% of all gaps (Fig. 2f,g). IPs (i.e., periods of negative air sac pressure) were brief (average duration 50.6±3.0 ms) and appeared to be distinct events with rapid onsets and offsets. Many gaps containing an IP also included positive pressure regions. These silent non-inspiratory periods were on average 44.8±3.1 ms long and could occur prior to the IP, after the IP, or even between two IPs occurring in a single gap (e.g., the four examples in Fig. 2g). In order to easily refer to these events, we loosely define mode-2 gaps as those that contain a single IP that is immediately preceded and followed by syllables (Fig. 2f; we define mode-3 gaps as those that contain prolonged positive pressure regions in addition to at least one IP (Fig. 2g). The reasons for this distinction will be further clarified when we examine the neural mechanisms of gap generation.

Finally, 12.4±1.3% of all gaps were longer than 300 ms and generally contained eupnic breathing (mode-4 gaps, Fig. 2h). The shortest of these consisted of what appeared to be a single period of the breathing cycle. However, most mode-4 gaps were long periods of silence between subsong bouts (median duration 1.66±0.20 s, ±bootstrap standard error, but often tens of seconds long). Interestingly, long gaps followed a power-law duration distribution with a long tail extending to ~30 s (power-law exponent γ=-1.37±0.03 for gaps 300 ms – 30 s long; see Supplementary Material). In addition to

eupnic breathing, mode-4 gaps often contained deep, non-eupnic inspirations and non-vocalized expiratory pressure pulses (EPs). These events occurred only at the onsets and offsets of subsong bouts.

Our recordings suggest the following model for the generation of gaps in early singing. Mode-1 gaps were produced during expiratory pressure pulses and, similarly to syllables, exhibited a roughly exponential duration distribution (Fig. 2i). These gaps were the main component of the overall gap distribution at brief durations, forming an initial sharply-decreasing segment. In fact, the time constant of mode-1 gaps mentioned above (31.2±2.0 ms) was similar to the time constant of the gap duration distribution at brief durations (30.0±3.7 ms). Mode-2 gaps contained a consistently-timed IP, forming a peak in the gap duration distribution. The center of this peak (53.3±1.0 ms, see Methods) was indeed similar to the average IP duration (50.6±3.0 ms; Fig. 2j). Durations of mode-3 gaps were formed by a summation of an IP duration and the durations of non-vocalized expiratory pressure periods. Total durations of expiratory pressure periods in mode-3 gaps formed a roughly exponential distribution with a time constant of 47.8±4.7 ms (measured in the tail between 50-150 ms; Fig. 2k). Added to the duration of an IP, they formed a long tail in the overall distribution at gap durations >100 ms. Indeed, the time constant of an exponential fit to the distribution (54.7±2.1 ms at gaps 100-200 ms long) was similar to the timescale of these non-inspiratory periods. Finally, gaps >300 ms were primarily generated by transitions to the eupnic breathing state (mode-4 gaps). Due to the presence of these gaps, the overall gap distribution deviated from an exponential at long durations (roughly >300 ms).

In summary, the various components of gap duration distributions were formed by a diversity of the underlying respiratory patterns. In particular, the peaks in these distributions were associated with consistently-timed inspirations of a similar duration. Extraction of different modes from the overall gap distribution (see Supplementary Material for detailed analysis) allows one to quantify several aspects of respiratory timing, even without simultaneous air-sac pressure recordings.

Early development of song timing

We next sought to understand how the temporal structure of singing changes during the period of early development. Fig. 3a shows the songs of a typical bird recorded during the period of transition from subsong to early plastic song. Although the spectral changes of songs during this period were relatively subtle, the temporal changes were pronounced. At ~45 dph, birds began to produce syllables with consistently-timed durations ("proto-syllables"), which resulted in the appearance of one or more peaks in syllable duration distributions (Fig. 3a-c). Proto-syllables became more common over time, resulting in the growth of the size of these peaks. The peak in duration of these early syllables varied greatly across birds (50-174 ms; mean 93.8 ms, standard deviation 32.0 ms, N=48 syllable duration peaks in 40 birds; Fig. 3d, S1).

As discussed above, the peak in gap duration distributions corresponded to the inspiratory component of mode-2 and mode-3 gaps; we collectively refer to the consistently-timed gaps in this peak as "proto-gaps." As described above, this peak appeared earlier in development and was present in most birds prior to the appearance of a peak in syllable duration distributions. Proto-gaps also became more common during

development, primarily due to the increase in the incidence of mode-2 gaps (Figs. 2c, S2). In contrast to the peaks in syllable duration distributions, the peaks in gap duration distributions were at shorter durations and more narrowly distributed across birds (mean 53.3 ms, standard deviation 8.0 ms, N=59 birds; Fig. 3d).

In addition to introducing proto-syllables into their songs during the plastic song period, birds appeared to string these together with proto-gaps into long, rhythmic sequences. For example, the bird in Fig. 3e exhibited a peak in gap durations at ~60 ms and a peak in syllable durations at ~150 ms. Syllables with durations close to this peak occurred almost exclusively before and after the ~60 ms proto-gaps; they were rarely present before and after gaps <25 ms or >100 ms (Fig. 3f). To analyze this sequencing, we identified proto-syllables and proto-gaps as those syllables and gaps whose durations were within 20 ms of the corresponding peaks in the distributions. Across 23 plastic song-producing birds, 35.3±1.8% of syllables were identified as proto-syllables. Incidences of proto-syllables before and after proto-gaps were higher than this value (43.5±2.2% and 40.6±2.0% respectively; $p<0.05$ and $p<0.01$). Of all the gaps, 44.0±2.0% were identified as proto-gaps. Before and after proto-syllables, incidences of proto-gaps were also higher than this value (54.2±2.4% and 51.3±2.9% respectively; $p<0.05$ and $p<0.01$). These numbers indicate that song transitions in which a proto-syllable follows a proto-gap are 16% more likely than expected by chance; transitions from a proto-syllable to a proto-gap are 24% more likely. Proto-syllable/proto-gap sequences can account for the previously described early appearance of rhythm in song production (Saar & Mitra 2008).

In summary, early singing is characterized by the production of randomly-timed syllables and gaps, both of which form wide distributions of durations. During the subsong phase, birds initiate some level of consistency in gap timing by producing ~60 ms gaps that contain an inspiratory pressure pulse. During the period of early plastic song, these gaps become more common and are strung together with consistently-timed proto-syllables, which form peaks in syllable duration distributions. Rhythmic syllable/gap sequences gradually become the dominant component of the song, eventually forming the motifs of late plastic and adult singing (Liu et al. 2004; Tchernichovski et al. 2004).

Supplementary material: analysis of timescales in early singing

All data analyses were performed with custom-written software in Matlab.

Analysis of syllables

For syllable segmentation in each recording, we filtered sound between 1-4 kHz and calculated the log-amplitude. We smoothed the log-amplitude of sound with a 2.5-ms square window. In each recording, log-amplitudes were typically bimodally distributed. To estimate amplitude values at these modes (silent and vocalized modes), we fit a sum of two Gaussians to this distribution using expectation maximization (EM). We then defined an "upper threshold" as the Fisher discriminant of the two identified Gaussian modes, and a "lower threshold" as 2 standard deviations above the mean of all values below the upper threshold. We first listed all upper-threshold crossings of the log-amplitude trace. Initially, we defined syllable onsets as the positive-direction crossings and syllable offsets as the negative-direction crossings. We then looked at the log-amplitude trace in each gap between two successive syllables. If amplitude was always above the lower threshold in a gap, we merged the two flanking syllables into a single syllable. Otherwise, we extended the syllable onset to the latest preceding crossing of the lower threshold. Similarly, we extended the syllable offset to the earliest following crossing of the lower threshold. We then eliminated all identified syllables that were shorter than 7 ms. Finally, we merged all syllables separated by <7 ms of silence into single syllables. We manually examined all recordings to eliminate calls and cage noise from the data.

We analyzed syllable by fitting exponential functions to their syllable duration. Maximum-likelihood estimation (MLE) is typically used to fit an exponential distribution to data. On a finite interval (a, b), maximum-likelihood analysis yields the equation

$$\langle s_i \rangle_{a<s_i<b} = \tau' + a - \frac{(b-a)e^{-(b-a)/\tau'}}{1-e^{-(b-a)/\tau'}}$$

Here, the left side of the equation indicates the mean of all syllables with durations s_i between a and b, and τ' is a time constant of the exponential distribution that has the maximal probability of producing the observed data. We used the Matlab non-linear zero finding algorithm to solve the above equation for τ'.

First, we used this procedure to fit exponential distributions to all syllable durations between $a = 25$ ms and $b = 400$ ms. (Note that distributions were generally not exponential at very brief durations, usually forming a peak near 20 ms; this may be due to peripheral mechanical constraints on the production of brief sounds.) We then estimated the goodness-of-fit by measuring the maximum difference between the c.d.f.'s of the actual distribution and the exponential fit. For each bird, we normalized this measurement by multiplying this maximum difference by the square root of the number of syllables (Lilliefors 1969). Distributions that were well-fit by exponentials had small amounts of deviation (<2), whereas distributions that were different from exponentials due to the presence of peaks typically had deviation values >2. We therefore used 2 as the threshold for distinguishing subsong from plastic song.

To quantify peaks in plastic song, we fit an exponential to the long tail of the syllable duration distribution (200-400 ms). We then subtracted this exponential from the p.d.f. of the distribution, which was calculated in 1 ms-long bins (Fig. S1c,g). The residual peak was typically well-fit by a Gaussian. We therefore measured the size and

duration of the peak as the amplitude and center of the Gaussian fit, respectively. In 8 of 40 plastic song-producing birds, the single-Gaussian fit was relatively poor ($r^2<0.9$) because two peaks were present in the distributions. For these birds, we fit a sum of two Gaussians to the data instead. The total peak size was then calculated as the sum of the two individual amplitudes, and both center values were included in the analysis of syllable durations.

Analysis of gaps

Our results indicate that silent gaps between syllables in early singing are generated by a diversity of respiratory patterns: silent non-inspiratory periods (mode-1 gaps), inspiratory pressure pulses (IPs, mode-2 gaps), combinations of IPs with silent expiratory-pressure periods (mode-3 gaps), and eupnic breathing (mode-4 gaps). We sought to understand how these events contribute to the overall gap duration distribution and, conversely, to extract various respiratory timescales from the measured distribution. Such extraction allows one to understand the effects of various brain manipulations (e.g. lesions and cooling) on respiratory dynamics using the statistics of the song alone.

Because eupnic-breathing gaps tended to be long (>300 ms), we first concentrated on gaps shorter that 300 ms. We assumed that some fraction p_1 of these were mode-1 gaps (Fig. S2a). Since the durations of mode-1 gaps were approximately exponentially distributed (Fig. 2i), we wanted to estimate both p_1 and the time constant τ_1 of this exponential. Almost all brief gaps were mode-1 (see main text); accordingly, at brief durations (typically <30-40 ms), overall gap durations were not contaminated by other gaps modes and were also well-fit by an exponential. At longer durations, distribution

p.d.f.'s tended to increase and form a peak at ~60 ms. We identified the duration t_{min} at which p.d.f.'s began to increase by finding the minimum of a smoothed p.d.f. (1 ms bins, 20-ms square-window smoothing). (Because on some recording days in younger birds a minimum was not present, we excluded those days when determining t_{min}). We then fit an exponential distribution to all gaps shorter that were shorter $0.75t_{min}$ using the maximum-likelihood estimation procedure described above. This fit provided us with a value of τ_1 (time constant of the exponential) and p_1 (area under the exponential curve). Exponential fits for typical subsong- and plastic song-producing birds are shown in Figs. S2b,g.

The remaining fraction (1-p_1) of all gaps were mode-2 and mode-3 gaps. To estimate their distribution, we subtracted the mode-1 exponential fit described above from the overall gap distribution p.d.f. (calculated in 1 ms windows). The residual distributions (Fig. S2c,h) tended to exhibit a peak near 60 ms and were strongly asymmetric, with a long exponential tail >100 ms. We assumed that some fraction p_2 of these gaps were mode-2 gaps, while the remaining 1-p_2 were mode-3 gaps. Mode-2 gaps closely matched the durations of IPs, the durations of which exhibited approximately Gaussian distributions (Fig. 2j). Mode-3 gaps contained additional non-inspiratory components, the durations of which were approximately exponentially distributed (Fig. 2k). Thus, the duration of a mode-3 gap could be modeled as a sum of a Gaussian-distributed variable and an exponential-distributed variable, forming an ex-Gaussian distribution (Hohle 1965) To describe the combined distribution of mode-2 and mode-3 gaps we therefore needed four parameters: p_2, mean μ and standard deviation σ of the Gaussian, and time constant τ_2 of the exponential.

Time constant τ_2 could be estimated from the long tail of the distribution. The distribution was typically uncontaminated by the Gaussian at durations >100 ms. However, it deviated from the exponential at durations >200 ms due to the presence of mode-4 gaps (Fig. 2c). We thus estimated τ_2 by fitting an exponential to the p.d.f. between 100-200 ms (Fig. S2c,h). The remaining parameters (p_2, μ, and σ) were estimated using nonlinear optimization (Matlab curve fitting toolbox) to minimize the mean squared difference of the fit from the p.d.f. Typical fits are shown in Fig. S2d,i. A notable difference between subsong- and plastic-song producing birds is the value of p_2: the fraction of consistently-timed mode-2 gaps is increased with development.

A priori, mode-2 need not be a distinct mode of the distribution; these gaps can, in principle, be mode-3 gaps that have particularly brief durations of silent, positive-pressure periods. However, by fitting a general Gaussian/ex-Gaussian mixture to the data (Fig. S2d,i), we find that the extracted Gaussian component is often a sizable component of the mixture (Fig S2e,j). The amplitude of this component increases with development (Figs. 3c, S2j). Furthermore, the Gaussian component is eliminated by HVC lesions (see Chapter 4). These observations are consistent with mode-2 being a mechanistically-distinct component of gap duration distributions, rather than an extreme of mode-3. Note that the centers of Gaussian fits to these two modes can theoretically be different if produced by distinct mechanisms. However, we did not observe large differences in the inspiratory components of mode-2 and mode-3 gaps and thus fit these modes with the same parameters μ and σ.

As we mentioned above, gaps deviated from an exponential distribution at long durations (>250 ms) due to the presence of eupnic-breathing (mode-4) gaps. Because the

durations of mode-4 gaps spanned many orders of magnitude (up to tens of seconds or more), we analyzed their distributions on log-log scale plots (Fig. S3). Interestingly, gaps were distributed according to a power-law on a wide range of durations (300 ms – 30 s), as illustrated by the linearity of their distributions on these plots. Because mode-4 gaps were essentially intervals between song bouts, the power-law indicates a scale-invariant organization of singing times. That is, song bouts were not randomly-distributed in time, but tended to occur in clusters (e.g., Fig. 2b), which themselves clustered into longer singing periods, and so on. Deviation of the power-law at durations longer than 30 s indicates that gaps <30 s may be a component of the singing behavior, rather than returning to the non-singing behavioral state (see Chapter 5 for detailed discussion).

Methods

Sound recordings

Subjects were juvenile male zebra finches between 32 and 59 days-post-hatch (dph). Birds were obtained from the Massachusetts Institute of Technology breeding facility. Animal care and experiments were carried out in accordance with the National Institute of Health guidelines and approved by the local Institutional Animal Care and Use Committee. Birds were placed in custom-made sound isolation chambers and vocalizations were recorded with Sound Analysis Pro (Tchernichovski et al. 2000), which was configured to ensure triggering recordings on all quiet vocalizations of young birds (see Chapter 2; (Aronov et al. 2008)).

Air sac pressure recordings

Air sac pressure measurements during subsong production were performed using methods similar to those previously used on adult birds (Franz & Goller 2002; Goller & Cooper 2004). A device was constructed using a piezoresistive pressure transducer chip (Fujikura), to which a miniature connector (Omnetics) was attached. A small stainless steel tube was inserted into the pressure port of the transducer and sealed with Torr Seal. Pressure signals were amplified directly on the device using surface-mount electronics.

Prior to surgery, birds were anesthetized with 1-2% isofluorane in oxygen. A small hole was made in the posterior thoracic air sac and a silastic tube (o.d. 2 mm, length 7 mm) was inserted. The tube was sutured to the rib cage, and the insertion site was sealed with a silicone elastomer (KwikCast). The other end of the tube was attached to the steel tube on the pressure transducer. A wire inserted into a silastic tube (o.d. 0.9 mm,

length 16 mm) was placed subcutaneously on the bird's back, and the device was tied to this tube. After starting to sing following surgery birds were attached using a thin cable to custom-made mercury commutators. Sound and air sac pressure were digitized at 40 kHz and recorded simultaneously using custom-written software in Matlab.

Figure 1. Subsong exhibits exponential distributions of syllable durations. (a) Bottom: sonogram of a typical song produced by a 44-dph juvenile zebra finch. Segments above the sonogram indicate extents of detected syllables. Syllables marked by numbers 1-3 are widely different in durations, although they occur consecutively. Top trace: log-amplitude of the sound in the 1-4 kHz band. (b) Distribution of log-amplitude values for the example in (a). (c) Syllable duration distribution of the bird shown in (a), marking the durations of the same syllables. (d) Same distribution on a semi-logarithmic scale. Linearity on the latter scale is indicative of an exponential distribution. (e) Fraction of birds whose syllables are well-fit by exponential distributions (see Methods) for different age groups. Error bars: 95% confidence intervals for a binomial distribution. (f) Syllable duration distributions for all subsong-producing birds (grey lines) and the population average (red line). (g) Distribution of exponential time constants for all distributions shown in (f).

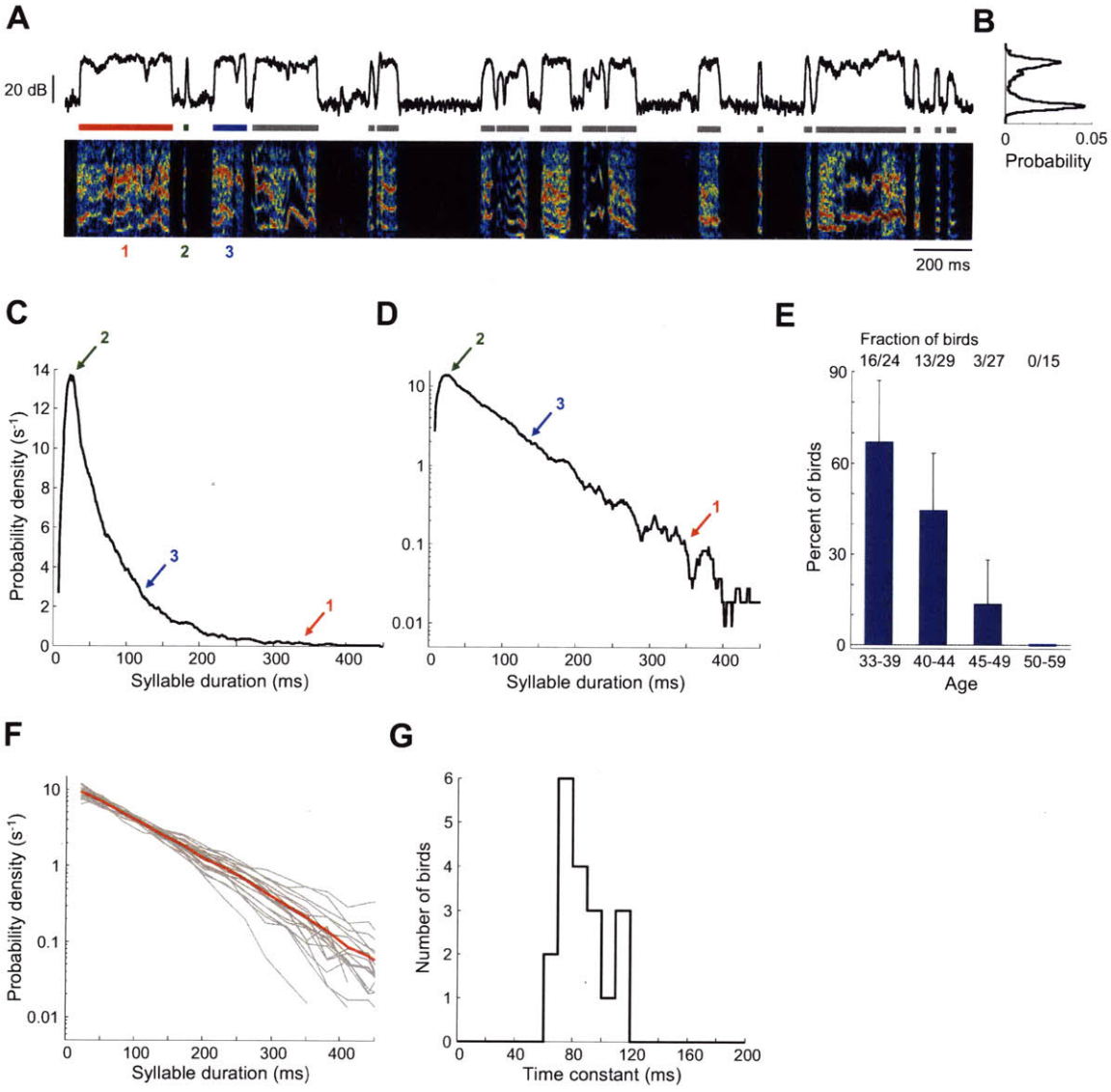
A
20 dB
1
2
3
200 ms
B
0
0.05
Probability
C
Probability density (s-1)
Syllable duration (ms)
D
Syllable duration (ms)
E
Fraction of birds
16/24
13/29
3/27
0/15
Percent of birds
33-39
40-44
45-49
50-59
Age
F
Probability density (s-1)
Syllable duration (ms)
G
Number of birds
Time constant (ms)

Figure 2. Silent gaps in subsong are shaped by a diversity of respiratory patterns. (a) Syllable duration distributions of a typical subsong-producing bird. (b) Gap duration distribution for the same bird. Although the syllable duration distribution is exponential, gap durations are more complex, exhibiting a brief mode (<40 ms), a secondary peak (40-100 ms), and a long tail (>100 ms). (c) Gap duration distribution on a semi-logarithmic scale. The long tail deviates from an exponential fit at 300-400 ms. (d) Top: Sample sonogram of the bird shown in (a-c), marking the gaps whose durations are shown in (a-c). Bottom: Simultaneous air sac pressure recording, showing expirations (positive pressure) and inspirations (negative pressure). (e) Examples of mode-1 gaps, defined by the lack on an inspiration. (f) Examples of mode-2 gaps, defined by a single inspiratory pressure pulse, IP. (g) Examples of mode-3 gaps, defined by the presence of at least one IP, as well as positive-pressure periods. (h) Examples of mode-4, defined by the presence of eupnic breathing. Some mode-4 gaps also contain non-eupnic IPs (1st, 2nd, and 4th examples) and non-eupnic silent positive-pressure periods (2nd and 4th examples). Examples in (e-h) are from the bird shown in (a-d); the top examples are from the trace in (d). (i) Gap duration distribution of a subsong bird overlaid with the distribution of mode-1 gaps. (j) Gap duration distribution overlaid with the distribution of IP durations (rescaled to match the peak height). (k) Gap duration distribution overlaid with the distribution of positive-pressure periods in mode-2 and 3 gaps (shifted by the mean IP duration).

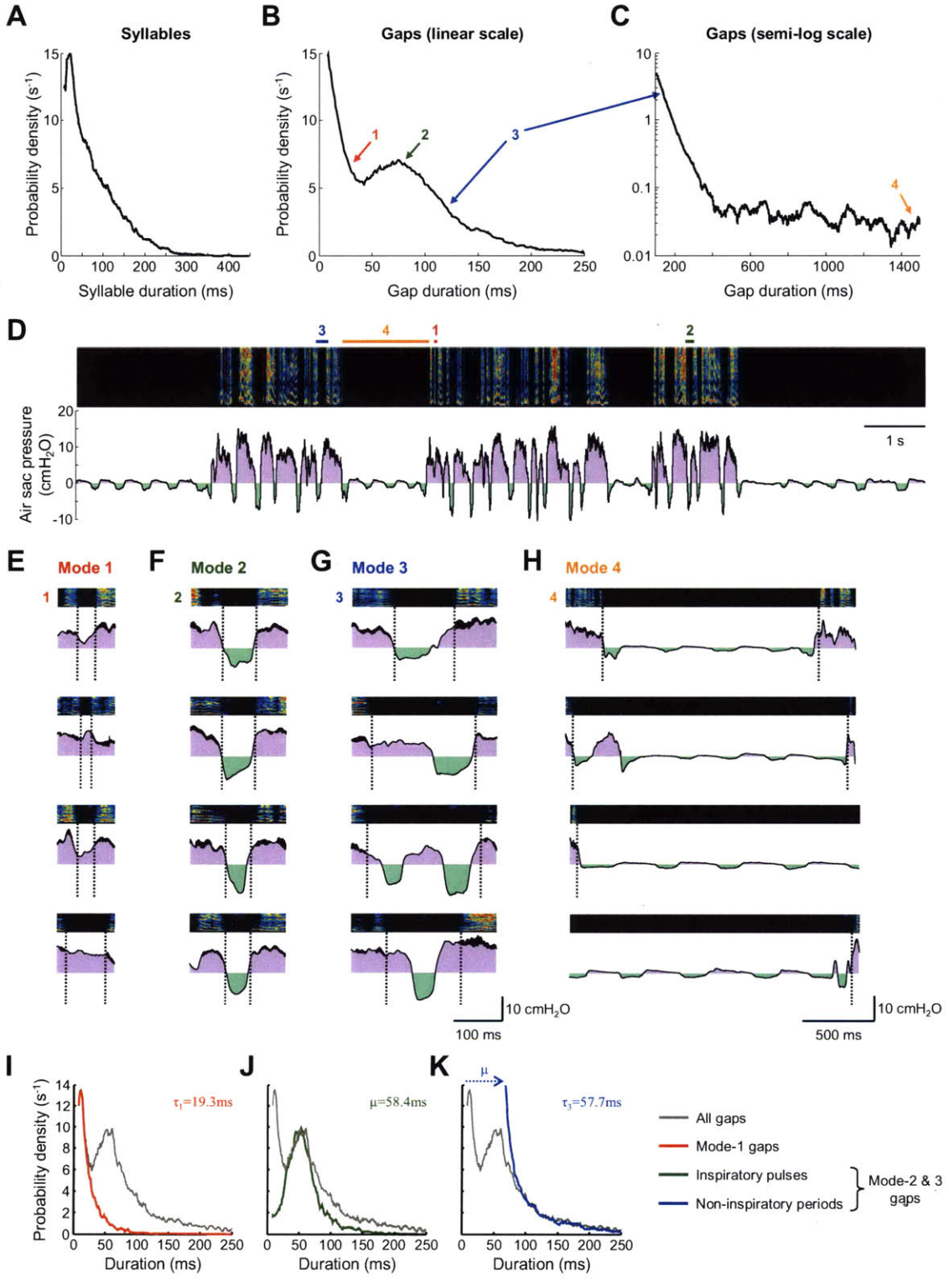
A
Syllables
Probability density (s-1)
Syllable duration (ms)
B
Gaps (linear scale)
Gap duration (ms)
C
Gaps (semi-log scale)
Gap duration (ms)
D
Air sac pressure (cmH2O)
1 s
E
Mode 1
F
Mode 2
G
Mode 3
H
Mode 4
10 cmH2O
100 ms
10 cmH2O
500 ms
I
J
K
τ1=19.3ms
μ=58.4ms
τ3=57.7ms
Duration (ms)
All gaps
Mode-1 gaps
Inspiratory pulses
Non-inspiratory periods
Mode-2 & 3 gaps

Figure 3. Early song development is characterized by temporal refinement. (a) Sonograms of typical songs produced by a single bird at three developmental stages. Red circles: syllables 140-240 ms long. Blue circles: gaps 30-90 ms long. (b) Syllable and gap duration distributions for the bird shown in (a) at various ages. Brackets indicate duration ranges marked in (a). Peak in gap durations ("proto-gaps") appears earlier than the one in syllable durations ("proto-syllables"). (c) Median heights of peaks in syllable and gap duration distributions across birds in different age groups. Calculation of the peak in syllable durations is shown in Fig. S1. The peak in gap durations is calculated as the magnitude of the component corresponding to mode-2 gaps (Fig. S2). Error bars: bootstrap standard errors of the median. (d) Distributions of proto-syllable and proto-gap durations across all birds. (e) Blue trace: gap duration distribution of an early plastic song-producing bird. Red trace: syllable duration distribution of the same bird. Color plot: duration probabilities of syllables that precede or follow gaps of a particular duration. Each row is individually normalized to a sum of 1. (f) Duration distributions of syllables that precede and follow gaps of various durations. Proto-gaps and proto-syllables tend to follow each other.

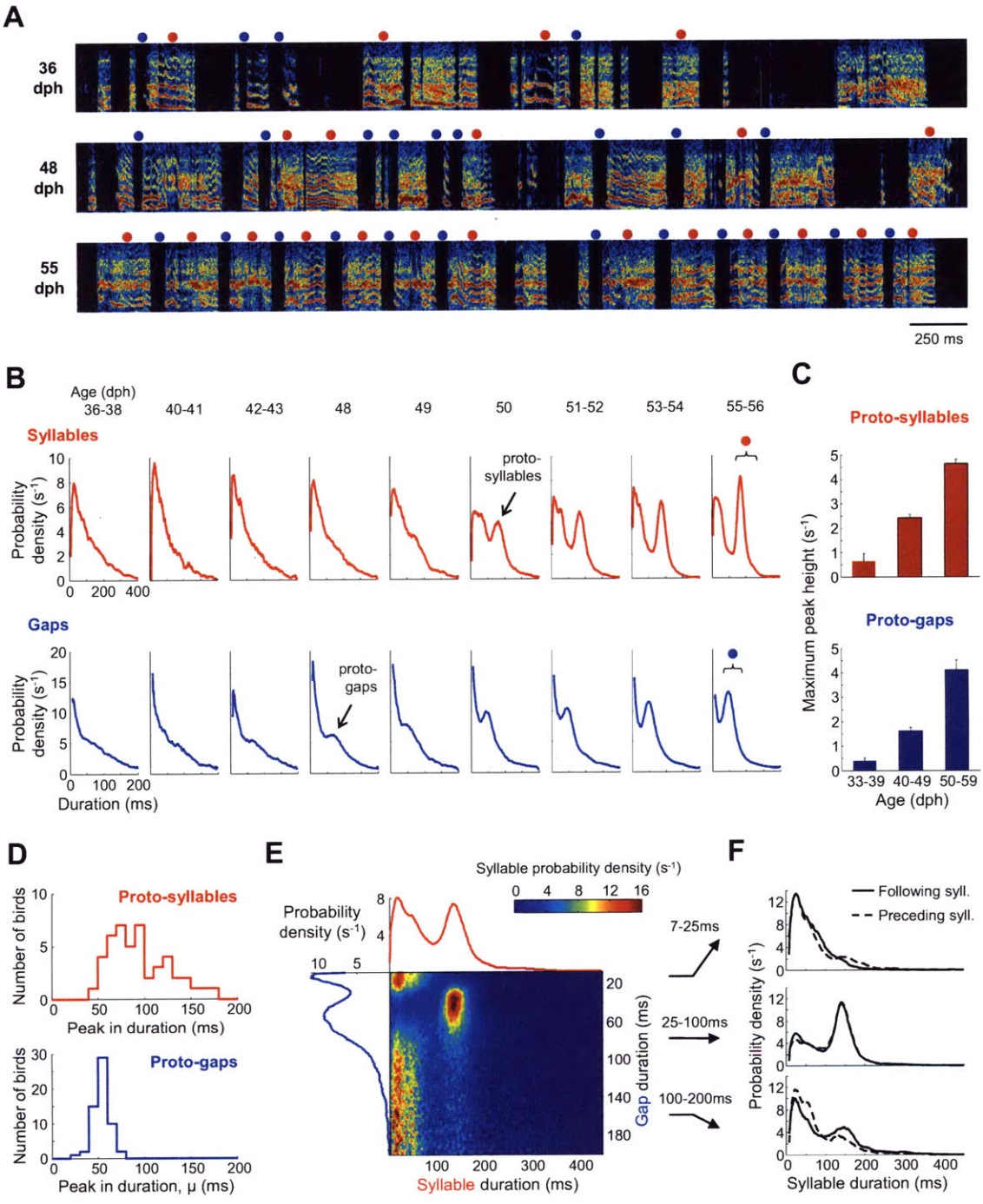
A
36 dph
48 dph
55 dph
250 ms
B
Age (dph)
36-38
40-41
42-43
48
49
50
51-52
53-54
55-56
Syllables
Probability density (s-1)
proto-syllables
Gaps
proto-gaps
Duration (ms)
C
Proto-syllables
Maximum peak height (s-1)
Proto-gaps
33-39
40-49
50-59
Age (dph)
D
Proto-syllables
Number of birds
Peak in duration (ms)
Proto-gaps
Peak in duration, μ (ms)
E
Syllable probability density (s-1)
Probability density (s-1)
7-25ms
25-100ms
100-200ms
Gap duration (ms)
Syllable duration (ms)
F
Following syll.
Preceding syll.
Probability density (s-1)
Syllable duration (ms)

Figure S1. Analysis of syllable durations in subsong and plastic song. (a) Grey trace: syllable duration distribution of a subsong-producing bird. Red trace: exponential fit to the distribution on the interval 25-400 ms. (b) Same plots as in (a), but shown on a semi-logarithmic plot. (c) Grey trace: residual following the subtraction of the exponential fit from the syllable duration distribution. Red trace: Gaussian fit to this residual. (d) Grey: trace: syllable duration distribution, replicated from (a). Red trace: sum of the exponential and Gaussian fits from panels (a) and (c). (e-h) Same plots as in (a-d) for a bird in the early plastic song stage, with the exception that the exponential function is fit only to the tail of the distribution (200-400 ms). The Gaussian accounts for a greater fraction of the overall distribution than it does for the subsong-producing bird.

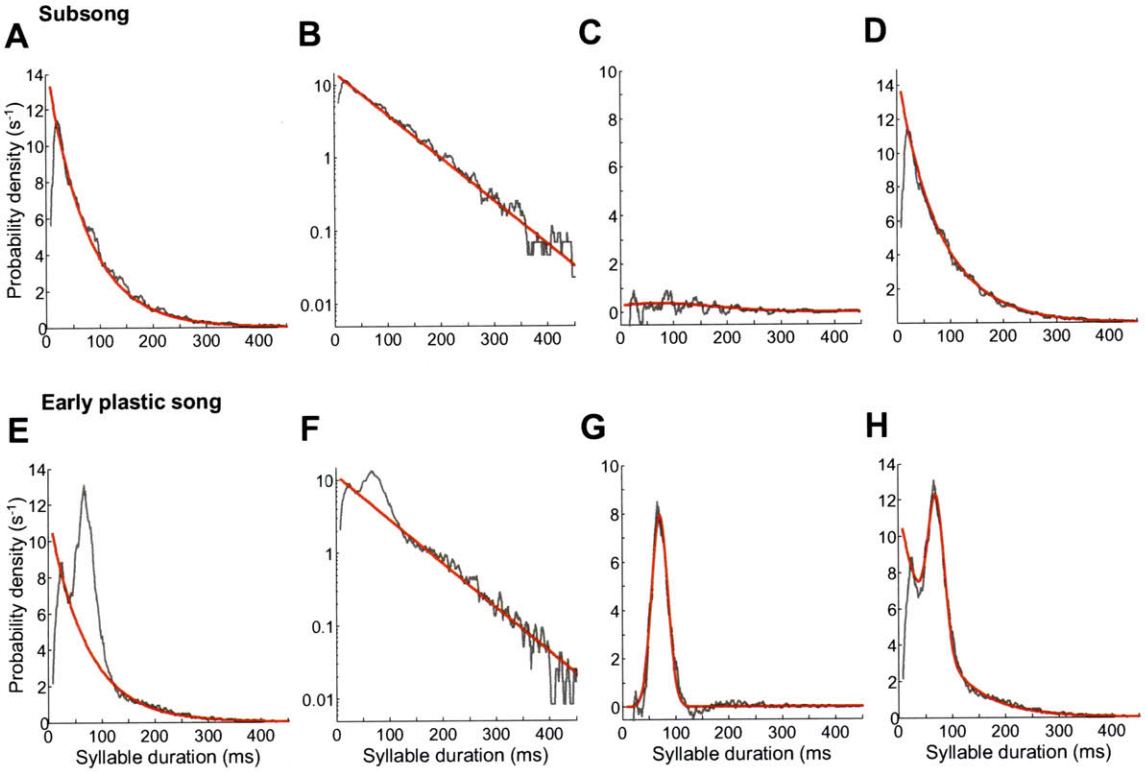
Subsong
A
B
C
D
Probability density (s-1)
Early plastic song
E
F
G
H
Syllable duration (ms)
Syllable duration (ms)
Syllable duration (ms
Syllable duration (ms)

Figure S2. Analysis of gap durations in subsong and plastic song. (a) Model of the respiratory dynamics that generate different modes of gap durations. Schematics illustrate all parameters of the gap duration distributions described in the text. (b) Grey trace: gap duration distribution of a subsong-producing bird. Red trace: exponential fit to brief gap durations (see text), estimating the parameters of mode-1 gaps. (c) Grey trace: residual following the subtraction of the exponential from the gap duration distribution. Blue trace: exponential fit to this residual at long durations (100-200 ms), estimating the exponential component of mode-3 gaps. (d) Fit of a weighted sum of an Gaussian and an ex-Gaussian distribution to the same residual, estimating the parameters of mode-2 and mode-3 gaps. (e) Grey-traces: residual shown in (d), following subtractions of each of the individual components of the fit (Gaussian and ex-Gaussian). Green and orange traces: Gaussian and ex-Gaussian components of the fit, respectively. (f) Grey trace: gap duration distribution, replicated from (a). Black trace: fit of the full model (weighted sum of an exponential, a Gaussian, and an ex-Gaussian) to the distribution. (g-k) Same plots as in (B-F), for a bird in the early plastic song stage. Amplitude of the Gaussian component (green trace), describing the contribution of mode-2 gaps, is substantially greater in the plastic song than in subsong.

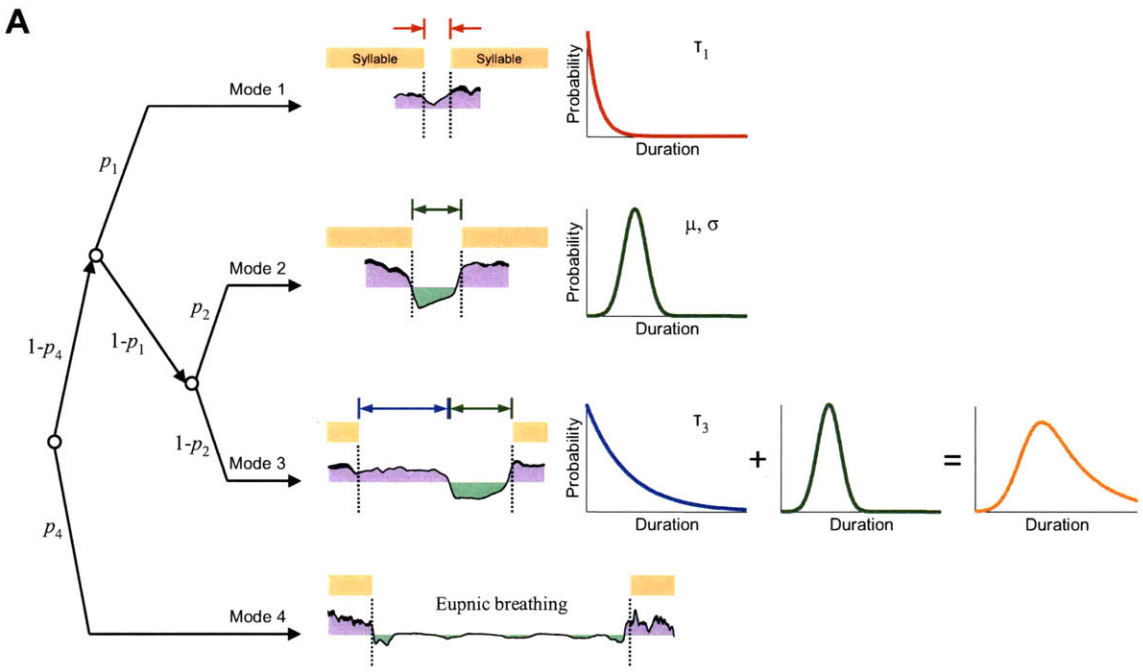
A
Syllable
Syllable
Mode 1
Mode 2
Mode 3
Mode 4
p_1
p_2
p_4
1-p_4
1-p_1
1-p_2
Probability
Duration
τ_1
μ, σ
τ_3
+
=
Eupnic breathing

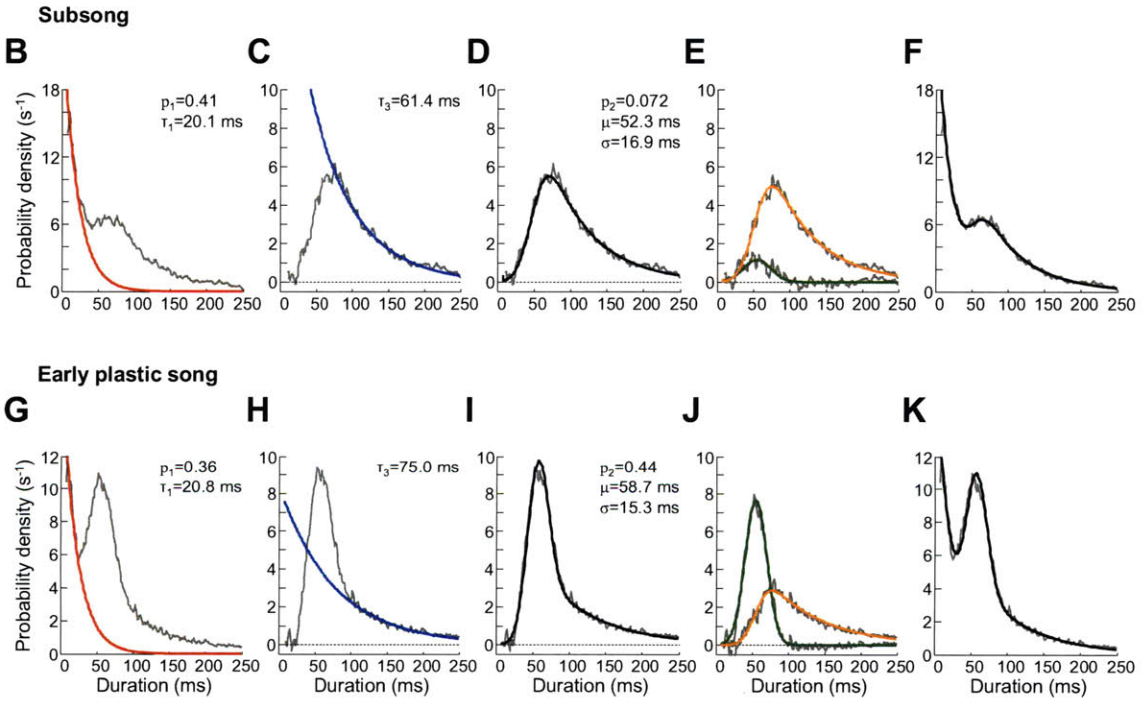
Subsong
B
C
D
E
F
p_1=0.41
τ_1=20.1 ms
τ_3=61.4 ms
p_2=0.072
μ=52.3 ms
σ=16.9 ms
Probability density (s^{-1})

Early plastic song
G
H
I
J
K
p_1=0.36
τ_1=20.8 ms
τ_3=75.0 ms
p_2=0.44
μ=58.7 ms
σ=15.3 ms
Probability density (s^{-1})
Duration (ms)

Figure S3. Gaps that contain eupnic breathing exhibit power-law distributions of duration. (a) Gap duration distribution of a young bird, combining subsong and early plastic song periods. (b) Grey trace: same distribution of a semi-logarithmic scale. Red line: exponential fit to the tail of the distribution between 100 and 200 ms. The distribution deviates from an exponential fit at ~300 ms. Almost all gaps longer than 300 ms contain eupnic breathing (mode-4 gaps; see text). (c) Grey trace: same distribution on a log-log plot. Red line: power-law fit to the distribution on a wide range of durations (300 ms – 30 s).

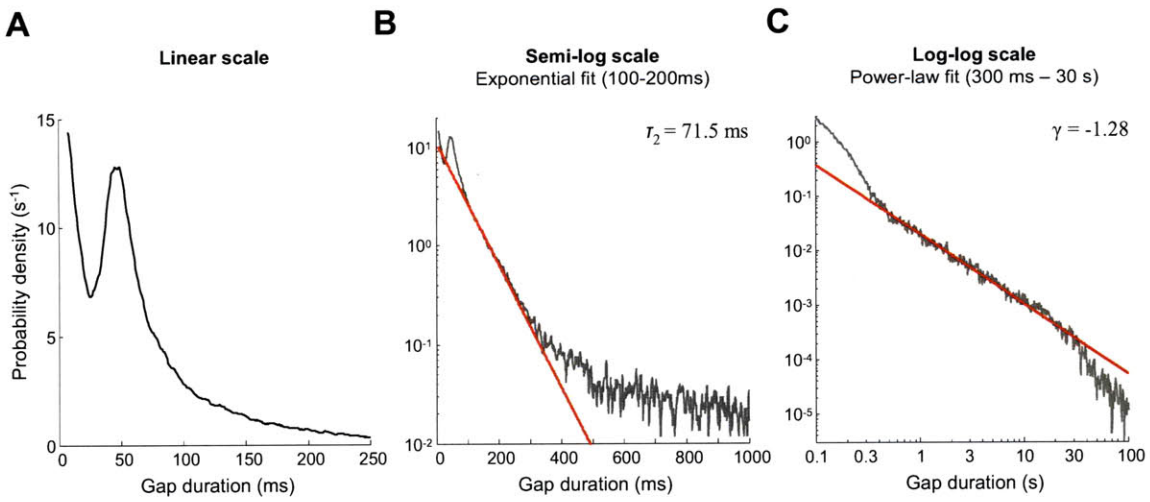
A
Linear scale
Probability density (s-1)
15
10
5
0
0
50
100
150
200
250
Gap duration (ms)
B
Semi-log scale
Exponential fit (100-200ms)
τ2 = 71.5 ms
10¹
10⁰
10-1
10-2
0
200
400
600
800
1000
Gap duration (ms)
C
Log-log scale
Power-law fit (300 ms – 30 s)
γ = -1.28
10⁰
10-1
10-2
10-3
10-4
10-5
0.1
0.3
1
3
10
30
100
Gap duration (s)

Chapter 4

Two distinct forms of circuit dynamics underlie early vocal behavior

Our results in Chapter 3 indicate that early singing is characterized by the presence of distinct, temporally alternating behavioral processes. These processes are shaped by different acoustic and respiratory patterns and follow consistent developmental changes across birds. Importantly, each process exhibits characteristic timescales, which form distinct "modes" in the distributions of gap and syllable durations. Decomposition of a song into these modes therefore allows one to quantify each underlying timescale, solely from the acoustic recording.

Where in the song system are the biophysical dynamics that produce these timescales? Chapter 2 makes the first step toward answering this question by identifying brain areas involved in the overall singing behavior. The goal of the present chapter is to separately localize circuit dynamics involved in the production of each underlying temporal process. The hope of this approach is to understand the roles of different song nuclei in sound production, coordination of singing with breathing, and developmental progression of song timing. On a more general level, component-by-component analysis can provide information about the types of biophysical circuit dynamics produced by each premotor brain area.

Involvement of HVC and LMAN in early song timing

Chapter 2 shows that subsong persists in the absence of HVC, and that subsong syllables are essentially unchanged by HVC elimination. In contrast, HVC is necessary for the production of consistently-timed "proto-syllables," which appear during the plastic song phase and form peaks in syllable duration distributions. Paradoxically, our data so far indicate that even during subsong, birds produce consistently-timed

inspiratory "proto-gaps", which become more common during development. These results suggest an intriguing possibility that HVC is also involved in the production of these gaps, implying that HVC controls inspiration-related timing early in development, possibly before it begins to controls syllable production.

To test this possibility, we analyzed gap distributions and air sac pressure patterns in young birds before and after bilateral elimination of HVC (Fig. 1, see Methods). As shown previously, HVC elimination did not change syllable duration distributions in subsong-producing birds (N=8 birds, Fig. 1a,b; also see Chapter 2 and (Aronov et al. 2008)), but abolished the peaks corresponding to proto-syllables in plastic song (N=11 birds, peak size 10.9±2.6 s^{-1} across birds, 1.3±0.2 s^{-1} in the same birds following HVC elimination, $p<0.001$; Figs. 1d,e, 2a). Following HVC elimination, birds continued producing deep inspirations during singing (Fig. S1). However, the peak in gap duration distributions was largely abolished in both subsong- and plastic song-producing birds (peak size 2.8±0.7 s^{-1} across birds, 0.35±0.05 s^{-1} in the same birds after HVC elimination, $p<0.01$; Figs. 1c,f, 2b). This result indicates that HVC is involved in the production of consistently-timed gaps that contain a single inspiration, and whose durations closely match the duration of that inspiration (mode-2 gaps, Fig. S2).

In contrast to mode-2 gaps, brief non-inspiratory (mode-1) gaps remained prominent and were largely unaffected by HVC elimination. The peak probability density for brief gaps was 13.6±1.0 s^{-1} across all birds (N=18) and 13.4±1.0 s^{-1} in the same birds following HVC elimination ($p=0.84$; Fig. 2c). This indicates that non-inspiratory gaps may be produced by an HVC-independent mechanism distinct from that which produces inspiratory gaps.

Because subsong production requires LMAN activity (Chapter 2, (Aronov et al. 2008)), we hypothesized that LMAN is involved in the generation of mode-1 gaps. To test this possibility, we inactivated LMAN in birds producing early plastic song (N=9, ages 45-56 dph, see Methods). As previously shown, plastic songs following LMAN inactivation were strikingly less variable that those prior to inactivation ((Ölveczky et al. 2005), Fig. 1g). LMAN-inactivated birds produced distinct syllable types, which formed peaks in the distributions of syllable durations (Fig. 1h). These peaks became the dominant feature of syllables following LMAN inactivation, increasing in size relative to the broad underlying distribution of syllable durations (peak size 8.8±2.2 s^{-1} across birds, 25.9±5.3 s^{-1} in the same birds following LMAN inactivation, $p<0.01$; Fig. 2d). A similar narrowing of the syllable duration distribution has been previously shown (Scharff & Nottebohm 1991).

The peak in gap duration distributions at also remained following LMAN inactivation and increased in size (peak size 9.3±3.2 s^{-1} across birds, 28.0±6.8 s^{-1} in the same birds following LMAN inactivation; Figs. 1i, 2e). However, mode-1 gaps were largely eliminated (peak probability density 15.0±2.6 s^{-1} across birds, 1.48±0.49 s^{-1} in the same birds following LMAN inactivation; Fig. 2f). This effect is, in a way, opposite of the effect of HVC elimination, which left mode-1 gaps intact but abolished the peaks in gap duration distributions. These results suggest that inspiratory and non-inspiratory gaps may be produced by distinct neural mechanisms, one of which is HVC-dependent, while the other is LMAN-dependent.

Role of HVC and LMAN dynamics in the control of song timing

The HVC and LMAN elimination experiments described above suggest that these brain areas are necessary for the production of distinct components of early singing. However, our results so far provide no information about a possible active role these nuclei might play in the timing of neural processes that produce these song components. For instance, an interesting possibility is that the biophysical dynamics within HVC control the durations of consistently-timed (~60 ms) proto-gaps. An alternative hypothesis is that the timing of these gaps is produced by a biophysical process elsewhere in the song system, but whose expression is HVC-dependent. To distinguish between these alternatives, we would like to leave HVC intact, but modify its intrinsic biophysical dynamics.

Because the speeds of most biophysical processes are temperature-dependent, mild cooling of HVC has been previously used as a way of modifying its intrinsic dynamics (Long & Fee 2008). Cooling HVC, but not its target area RA, produces uniform dilation of adult songs, suggesting that the dynamics of HVC circuitry are actively involved in mature song timing. We asked whether HVC dynamics play a similar role in the timing of gaps or syllables early in development. To use cooling for addressing this question, we developed a new lightweight Peltier device applicable for temperature manipulations in young juvenile birds (see Appendix A). We cooled HVC bilaterally by an average of ~7°C in 8 young birds and compared songs produced during cooling to those produced when HVC was maintained at normal body temperature. We isolated various components of gap and syllable duration distributions and quantified their fractional change ("stretch") normalized by the average amount of temperature change in

HVC (% $°C^{-1}$), similarly to (Long & Fee 2008). A negative amount of stretch indicates a slowing down of the dynamics as a result of cooling.

In 5 subsong-producing birds, HVC cooling had no effect on the durations of syllables (0.06±0.08% $°C^{-1}$, p=0.45; Fig. 3a). This is consistent with the finding that HVC is not necessary for the production of normal subsong syllables. There was also no effect on the long tails of syllable durations in 8 plastic song-producing birds (Fig. S3a). However, the peak in syllable duration distributions in these birds was shifted toward longer durations with HVC cooling (-1.36±0.16% $°C^{-1}$, p<0.001; Fig. 3b). Thus, HVC dynamics are involved in controlling the durations of proto-syllables in plastic song (which form peaks in the distributions), whereas they have no influence on the broadly distributed durations of syllables at any developmental stage.

Similarly to proto-syllables, proto-gaps became longer with HVC cooling (Fig. 3c). The peak in gap durations changed by -1.44±0.11% $°C^{-1}$ when HVC was cooled (N=8 birds, p<0.001). Thus, the dynamics within HVC are indeed involved in the consistent timing of inspiratory gaps early in development. Interestingly, the durations of mode-1 gaps did not change with HVC cooling (0.18±0.30% $°C^{-1}$, p=0.58). There was also no effect of HVC cooling on the time constant of long (100-200ms) gaps, which quantifies the non-inspiratory periods in mode-3 gaps (Fig. S3b). These data suggest that the role of HVC timing in young birds is specific to the inspiration-containing components of gaps.

Our results so far indicate that HVC dynamics are involved in the timing of both subsong and plastic song. However, unlike the role of HVC in adult singing, this involvement in younger birds is partial: HVC cooling affects the timing of consistently-

timed proto-syllables and consistently-timed inspiratory proto-gaps, but has no effect on the timing of subsong syllables and non-inspiratory gaps. Because LMAN is necessary for the production of these latter song components, we hypothesized that the biophysical dynamics within LMAN are actively involved in timing them. To test this possibility, we cooled LMAN bilaterally in subsong and plastic-song producing birds by ~6-8°C and analyzed the effects of cooling on gap and syllable durations (see Appendix A).

LMAN cooling indeed prolonged the durations of subsong syllables (Fig. 3d). Although distributions of syllable durations remained exponential, the time constant of this exponential became longer during LMAN cooling (-1.86±0.52% $°C^{-1}$, N=5 birds, $p<0.05$). This suggests that LMAN dynamics are actively involved in the timing of subsong syllables; i.e., determining when a syllable is terminated relative to its onset. In plastic song-producing birds, LMAN cooling had no effect on the timing of peaks in syllable duration distributions (-0.60±0.32% $°C^{-1}$, N=6 birds, $p=0.12$; Fig. 3e). However, the tails of these distributions became longer when LMAN was cooled (Fig. S3c). These results are again the opposite of that of HVC cooling, which changed the peaks in plastic-song syllable distributions, but did not affect the timescale of syllables in subsong.

The effects of LMAN cooling on gaps were similar: cooling did not change the durations of inspiratory proto-gaps (-0.005±0.178% $°C^{-1}$, N=6 birds, $p=0.98$; Fig. 3f). However, brief non-inspiratory (mode-1) gaps became longer with LMAN cooling (-4.13±0.60% $°C^{-1}$, $p<0.002$). Similarly, LMAN cooling stretched long (100-200 ms) gaps, indicating that LMAN is involved in timing non-inspiratory periods of mode-3 gaps as well (Fig. S3d).

In summary, the biophysical dynamics intrinsic to HVC and LMAN both play a role in the timing of subsong and early plastic song, but these roles are disjoint (Fig. 3g-j). LMAN dynamics are involved in controlling the durations of subsong syllables and non-inspiratory components of gaps. The timing of these events appears to be independent of HVC. On the other hand, HVC dynamics play a role in the timing of inspiratory gaps. In plastic song, they are additionally involved in the consistent timing of syllables. Durations of these HVC-controlled events appear to be independent of LMAN.

Supplementary material

Methods

Methods for sound recordings and analysis are provided in Chapter 3. Lesions and inactivations are discussed in Chapter 1. Construction of the devices for HVC and LMAN cooling are discussed in Appendix A. To cool these brain areas in awake, behaving birds, we attached the devices using light, flexible cables to custom-made mercury commutators following the post-surgery recovery period. Current was passed continuously through the devices during the day, flipping between 0.5 and -1.5 A every 100 s. For syllable and gap analysis, only data recorded during the last 80 s of each current pulse were used to ensure that the temperatures had reached values close to the steady state.

Effects of cooling on long tails of the distributions

As mentioned in the main text, HVC cooling in plastic song had an effect on the peaks in syllable duration distributions. However, it did not affect the long tails of these distributions (Fig. S3a). In 8 plastic song-producing birds, the time constant of the tail, measured between 200-400 ms did not change (stretch -0.14±0.39% $°C^{-1}$, p=0.84). HVC cooling also had no effect on the long tails of gap duration distributions (Fig. S3b), which are formed by the non-inspiratory components of mode-3 gaps (see Chapter 2). The time constant of this tail, measured between 100-200 ms was unaffected (stretch -0.05±0.49% $°C^{-1}$, p=0.90).

On the other hand, LMAN cooling affected the tails of both syllable and gap duration distributions, albeit more weakly than it affected other song features (see main text). Across 6 plastic song-producing birds, the time constant of the tail in syllable

duration distributions increased following LMAN cooling (-1.04±0.48% $°C^{-1}$, $p<0.05$; Fig. S3c). The time constant of the tails in gap duration distributions also increased (-0.60±0.22% $°C^{-1}$, $p<0.02$; Fig. S3d). These results indicate that LMAN activity may be involved in the timing of long tails in the distributions of acoustic components, whereas the peaks in the distributions of these components are HVC-dependent.

Histological analysis of LMAN cooling experiments

As shown in Appendix A, temperature in the brain in cooling experiments is strongly dependent on the distance from the cooling probe. Consequently, the positioning of probes in LMAN can have a substantial effect on the average amount of cooling achieved in this nucleus. To approximate the amount of cooling, we estimated the location of the cooling probes relative to LMAN boundaries in each bird by slicing the brain following each experiment (see Chapter 2) and noting the tract created by the probes. Fig. S4a shows probe locations in all birds discussed in the text. Probes were implanted nearest to the center of LMAN in the bird shown as the example in Fig. 3d.

To estimate the average amount of cooling in LMAN, we simulated the 3-dimensional spatial profile of temperature around the probes in each bird using the standard model of thermal diffusion in cylindrical coordinates (Appendix A). The parameters of this model were estimated from the spatial calibration experiments in Appendix A. A horizontal slice of one such solution is shown in Fig. S4b. For calculating the amount of temporal stretch due to cooling in % $°C^{-1}$ (see text), we obtained a single-value estimate of cooling by averaging the estimated amounts across the two hemispheres.

Figure 1. HVC and LMAN are necessary for different components of early singing. (a) Typical sonograms of a subsong bird before and after complete bilateral HVC lesions. Blue circles: gaps 30-90 ms long. (b) Syllable duration distributions for the bird shown in (a), before and after the lesions. (c) Gap duration distributions for the same bird. Bracket indicates the duration range marked in (a). (d-f) Early plastic song-producing bird before and after HVC lesion, plotted as in (a-c). Red circles: syllables 80-120 ms long. Blue circles: gaps 30-90 ms long. (g-i) Early plastic song-producing bird before and after bilateral LMAN inactivation, plotted as in (a-c). Red circles: syllables 60-110 ms long. Blue circles: gaps 30-60 ms long.

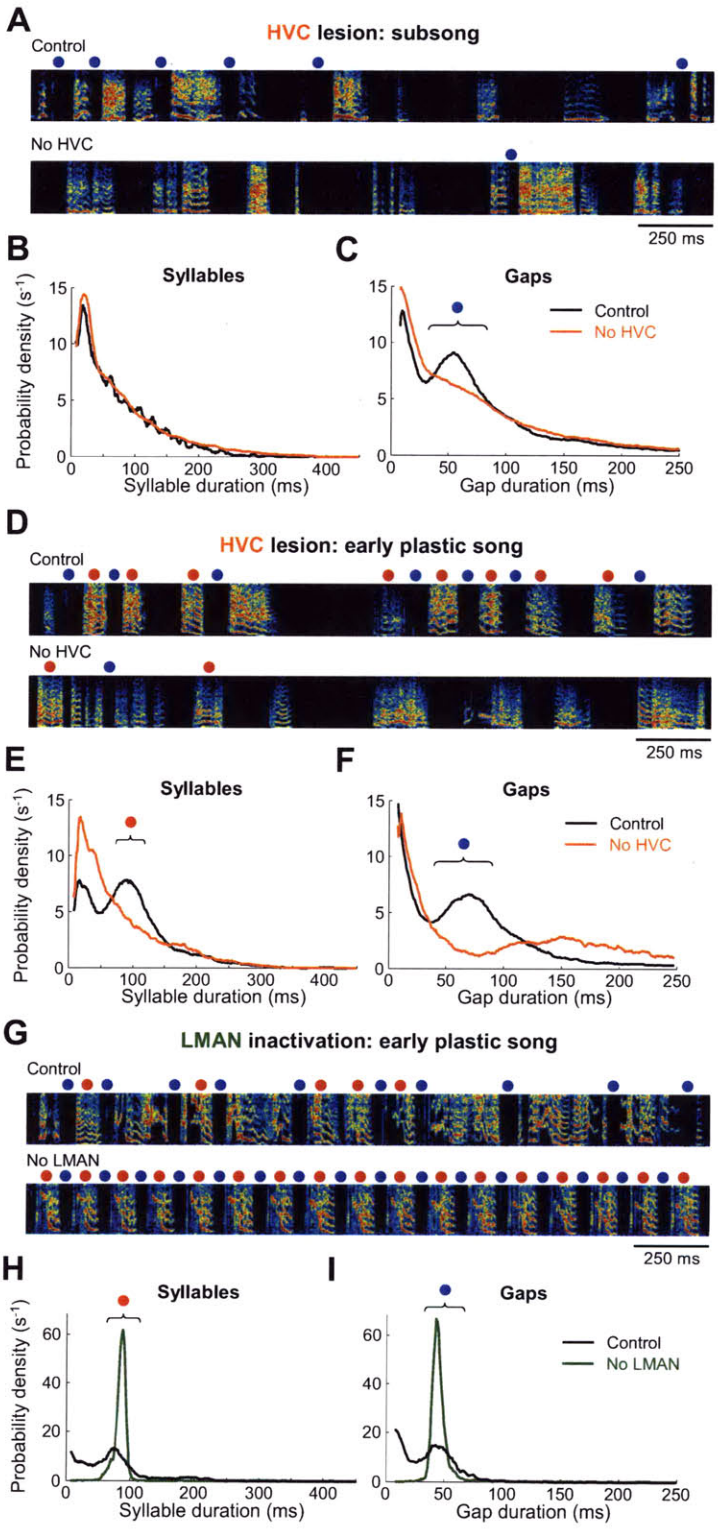
A
HVC lesion: subsong
Control
No HVC
250 ms
B
Syllables
Probability density (s-1)
Syllable duration (ms)
C
Gaps
Control
No HVC
Gap duration (ms)
D
HVC lesion: early plastic song
Control
No HVC
250 ms
E
Syllables
Probability density (s-1)
Syllable duration (ms)
F
Gaps
Control
No HVC
Gap duration (ms)
G
LMAN inactivation: early plastic song
Control
No LMAN
250 ms
H
Syllables
Probability density (s-1)
Syllable duration (ms)
I
Gaps
Control
No LMAN
Gap duration (ms)

Figure 2. Summary of bilateral HVC and LMAN elimination experiments across birds. Note that subsong-producing birds do not sing following LMAN inactivations (see Chapter 2, (Aronov et al. 2008)) and are thus only shown for HVC lesion experiments. (a) Effect of HVC elimination on the size of the peak in syllable durations ("proto-syllables"). (b) Effect of HVC elimination on the size of the peak in gap durations ("proto-gaps"), calculated as the magnitude of the components corresponding to mode-2 gaps (Fig. S1). (c) Effect of HVC elimination of the mode-1 (non-inspiratory) gaps. (d-f) Effects on LMAN elimination on the same parameters as shown in (a-c).

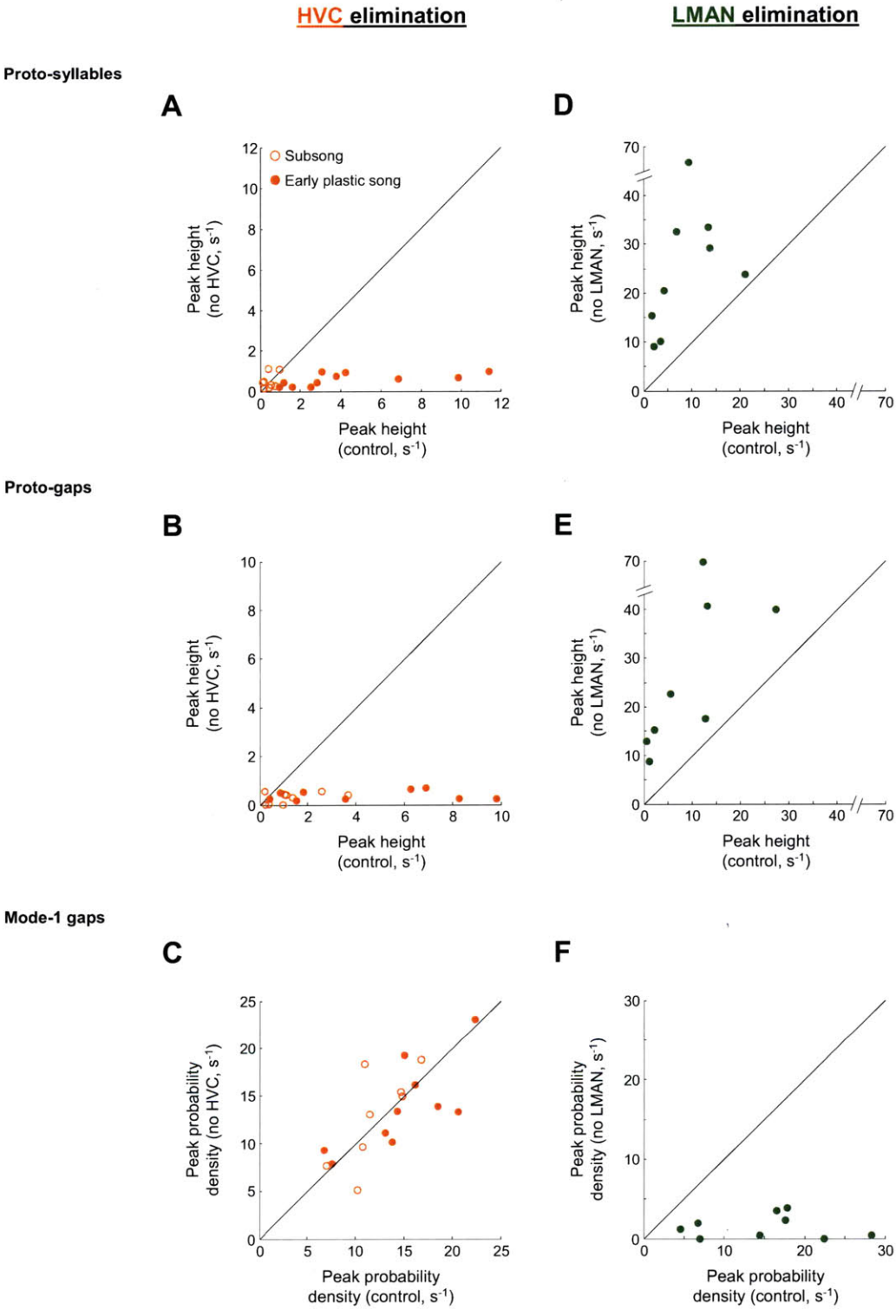
HVC elimination
LMAN elimination
Proto-syllables
A
D
Subsong
Early plastic song
Peak height (no HVC, s-1)
Peak height (control, s-1)
Peak height (no LMAN, s-1)
Peak height (control, s-1)
Proto-gaps
B
E
Peak height (no HVC, s-1)
Peak height (control, s-1)
Peak height (no LMAN, s-1)
Peak height (control, s-1)
Mode-1 gaps
C
F
Peak probability density (no HVC, s-1)
Peak probability density (control, s-1)
Peak probability density (no LMAN, s-1)
Peak probability density (control, s-1)

Figure 3. Biophysical dynamics intrinsic to HVC and LMAN are involved in timing different components of early singing. Top: Schematics of the devices for cooling HVC and LMAN. (a) Distributions of subsong syllable durations produced at normal body temperature and during HVC cooling, plotted on a semi-logarithmic scale. HVC cooling had no effect on subsong syllable durations. (b) HVC cooling prolonged proto-syllable duration in plastic song. (c) Effect of HVC cooling on gap duration distributions. (1) Detail of the gap duration distribution at brief durations, plotted on a semi-logarithmic scale. HVC cooling had no effect on mode-1 (non-inspiratory) gaps. (2) Detail of the gap duration distribution, showing the peak. HVC cooling prolonged proto-gaps. (d-f) Effects of LMAN cooling on syllable and gap durations, plotted as in (a-c). (d) LMAN cooling prolonged subsong syllables. (e) LMAN cooling had no effect on the durations of proto-syllables in plastic song. (f) (1) LMAN cooling prolonged mode-1 (non-inspiratory) gaps. (2) LMAN cooling had no effect on the durations of proto-gaps. (g) Population summary of the effect of HVC cooling (orange) and LMAN cooling (green) on subsong syllable durations. Each dot indicates the effect for an individual bird. Open dots indicate the examples shown in (a) and (d). Error bars: standard errors across all birds. (h) The effects of cooling on proto-syllable duration, plotted as in (g). (i) The effects of cooling on mode-1 (non-inspiratory) gaps, plotted as in (g). (j) The effects of cooling on proto-gap durations, plotted as in (g).

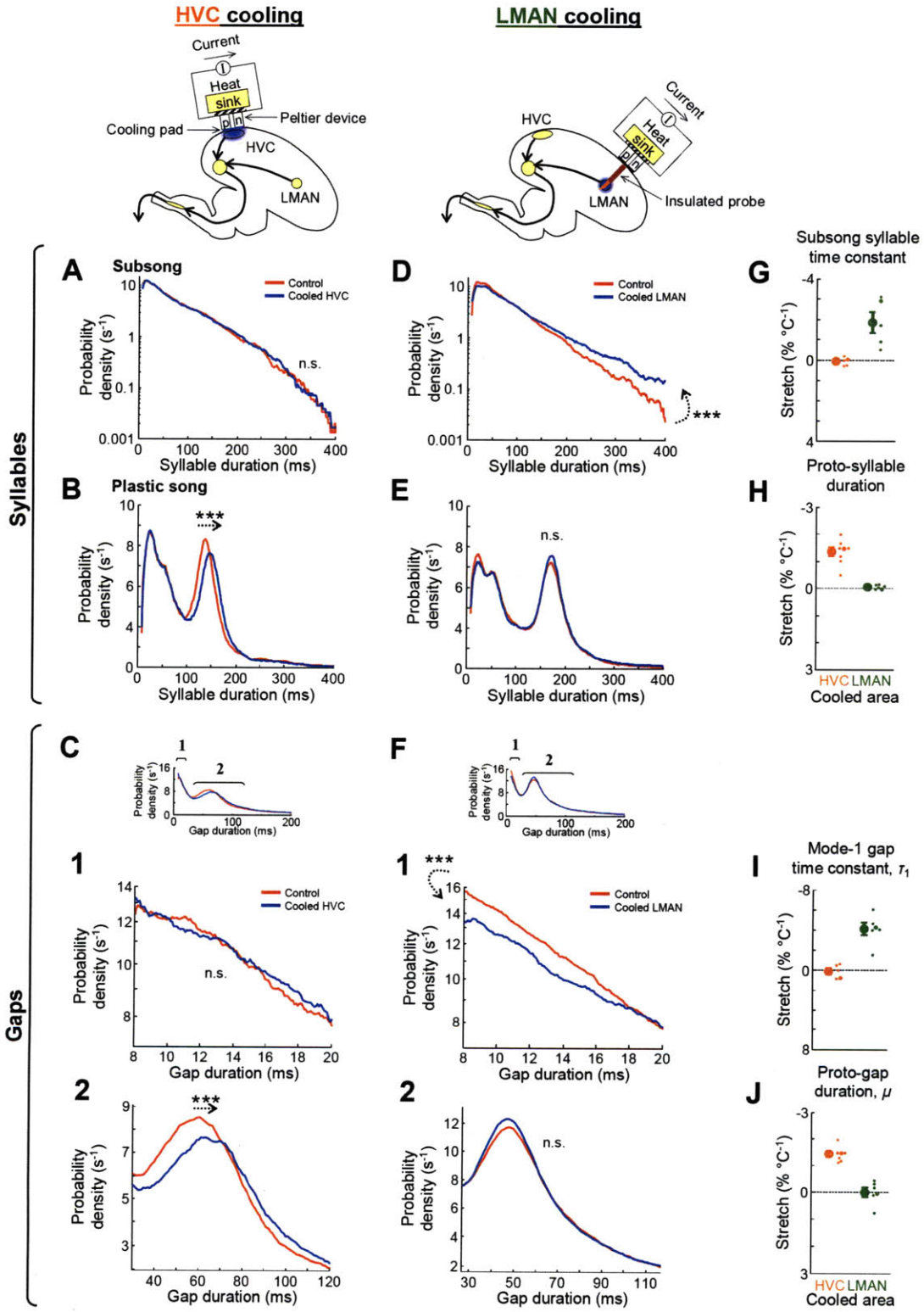
HVC cooling
LMAN cooling
Current
Heat sink
Peltier device
Cooling pad
HVC
LMAN
Insulated probe
Syllables
Gaps
A
Subsong
Control
Cooled HVC
n.s.
Probability density (s⁻¹)
Syllable duration (ms)
B
Plastic song
***
C
Gap duration (ms)
1
2
D
Cooled LMAN
E
F
G
Subsong syllable time constant
Stretch (% °C⁻¹)
H
Proto-syllable duration
HVC LMAN
Cooled area
I
Mode-1 gap time constant, τ_1
J
Proto-gap duration, μ

Figure S1. Respiratory measurements before and after bilateral HVC elimination. (a) Top: sonogram of a typical subsong bout. Bottom: simultaneous recording of air-sac pressure, indicating periods of expiration (positive pressure) and inspiration (negative pressure). (b) Recording from the same bird following bilateral lesions of HVC, plotted as in (a). Brief inspiratory pressure pulses remain following HVC elimination.

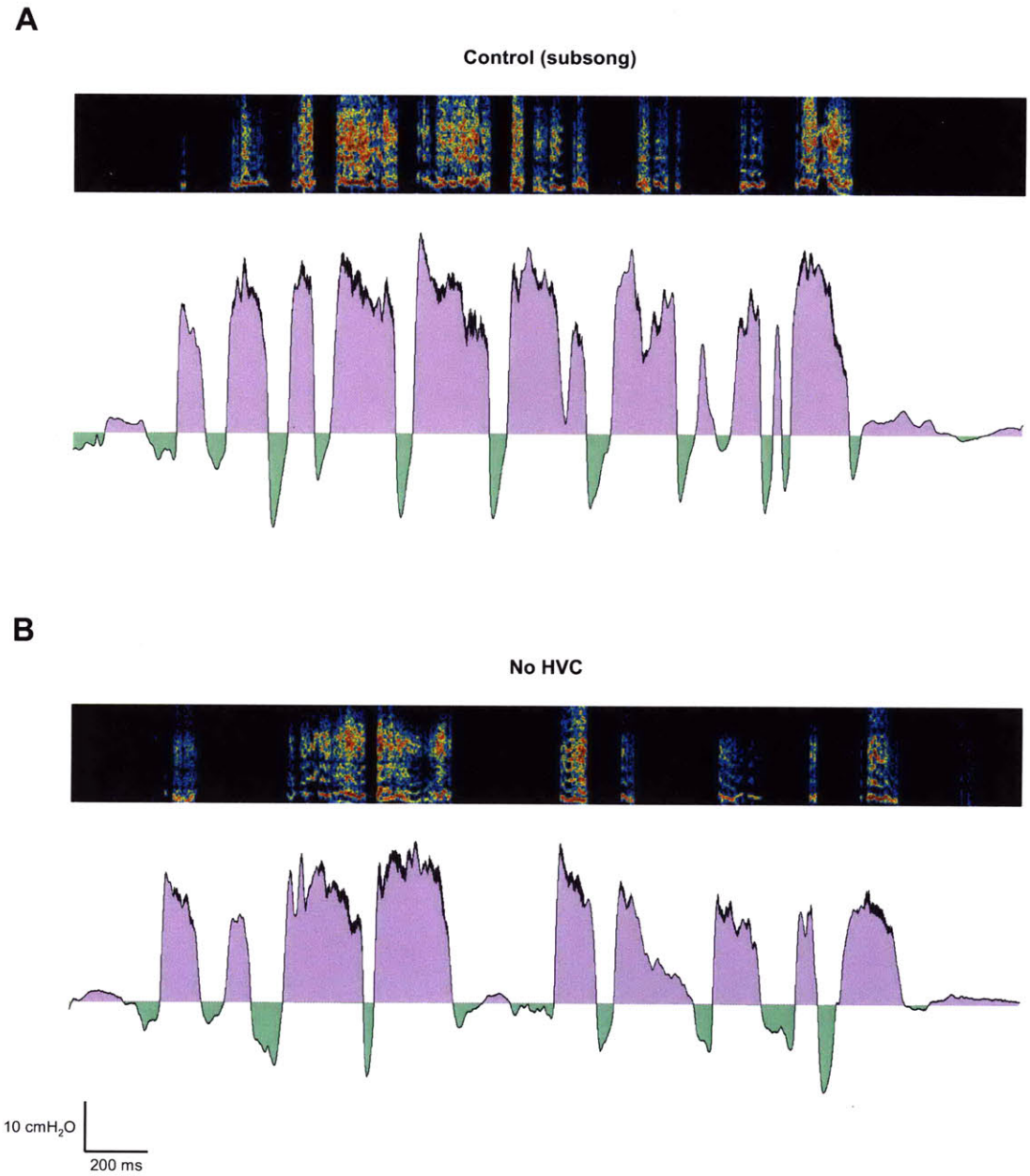
A
Control (subsong)
B
No HVC
10 cmH2O
200 ms

Figure S2. Effect of HVC elimination on the modes of gap durations in subsong. (a) Analysis of the temporal modes in normal subsong. Data is plotted the same way as in Fig. S2 of Chapter 3. (b) Analysis of gaps produced by the same bird after bilateral HVC lesions. Note that a major effect of the lesion was the elimination of mode-2 gaps (Gaussian fit, green trace).

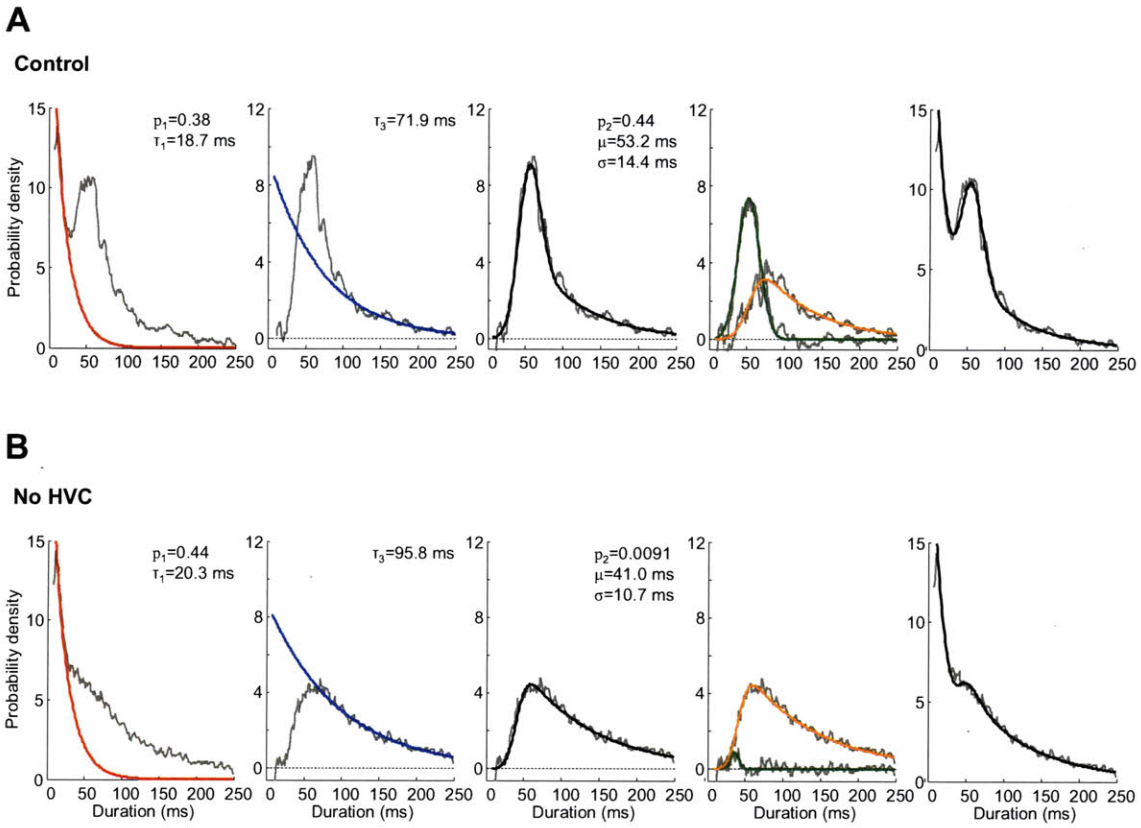
A
Control
p1=0.38
τ1=18.7 ms
τ3=71.9 ms
p2=0.44
μ=53.2 ms
σ=14.4 ms
Probability density
B
No HVC
p1=0.44
τ1=20.3 ms
τ3=95.8 ms
p2=0.0091
μ=41.0 ms
σ=10.7 ms
Probability density
Duration (ms)
Duration (ms)
Duration (ms)
Duration (ms)
Duration (ms)

Figure S3. Effects of HVC and LMAN cooling on the long tails of syllable and gap duration distributions. All distributions are plotted on a semi-logarithmic scale. (a) HVC cooling does not effect the timescale of long syllable durations. Note that the tail is slightly shifted due to the change in the peak of the distribution (Fig. 3c), but its slope is not effected. (b) LMAN cooling increases the timescale of long syllable durations. (c) HVC cooling does not affect the timescale of long gap durations (exponential component of mode-3 gaps, τ_3). (d) LMAN cooling increases the timescale of long gap durations.

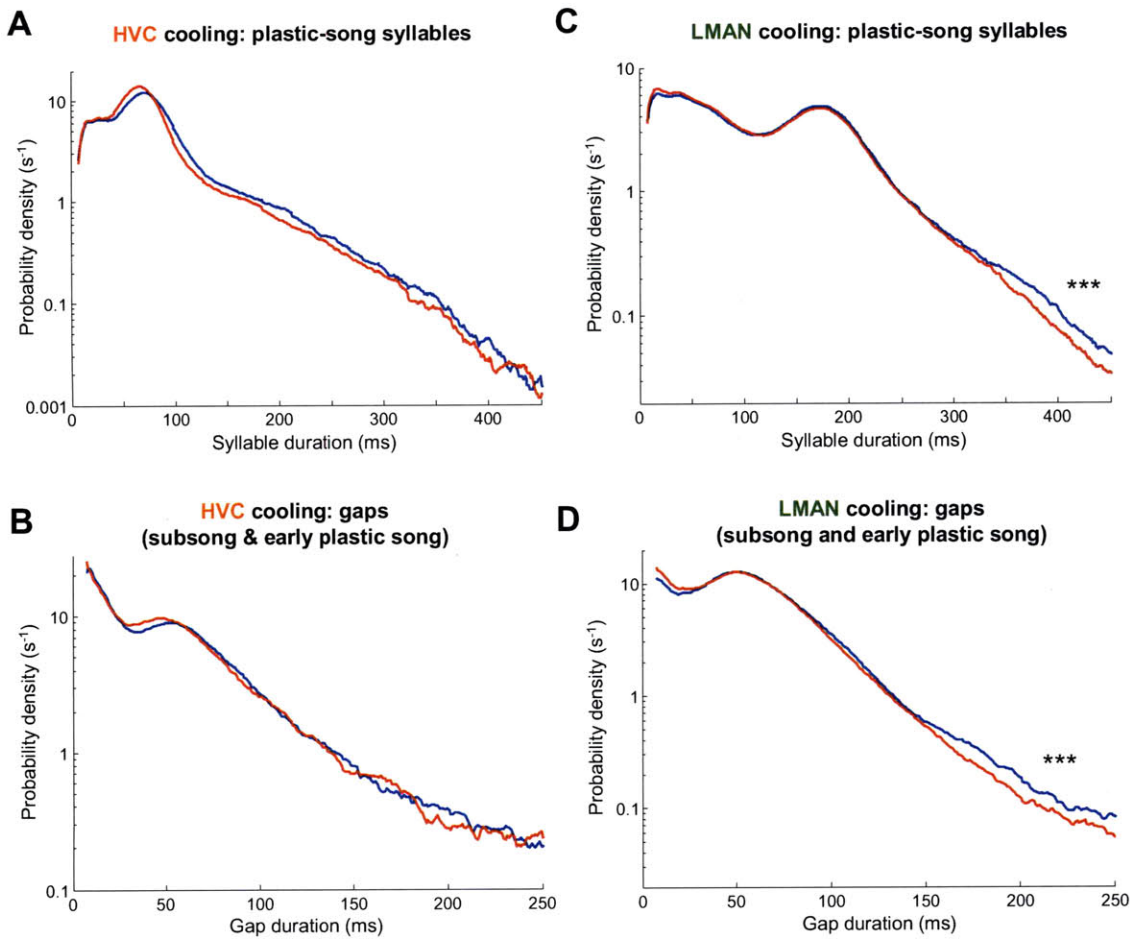
A
HVC cooling: plastic-song syllables
Probability density (s-1)
Syllable duration (ms)
C
LMAN cooling: plastic-song syllables
***
B
HVC cooling: gaps
(subsong & early plastic song)
Gap duration (ms)
D
LMAN cooling: gaps
(subsong and early plastic song)

Figure S4. Histological analysis of LMAN cooling experiments. (a) Approximate locations of cooling probes in LMAN. The probes in each bird are indicated by matching circles in the two hemispheres. Probes were implanted nearest to the center of LMAN in the bird shown in Fig. 3d. Note that probe diameter was 250 μm in some birds and 330 μm in others. A: anterior; L: lateral. (b) Simulated temperature around the probe in a horizontal section of LMAN.

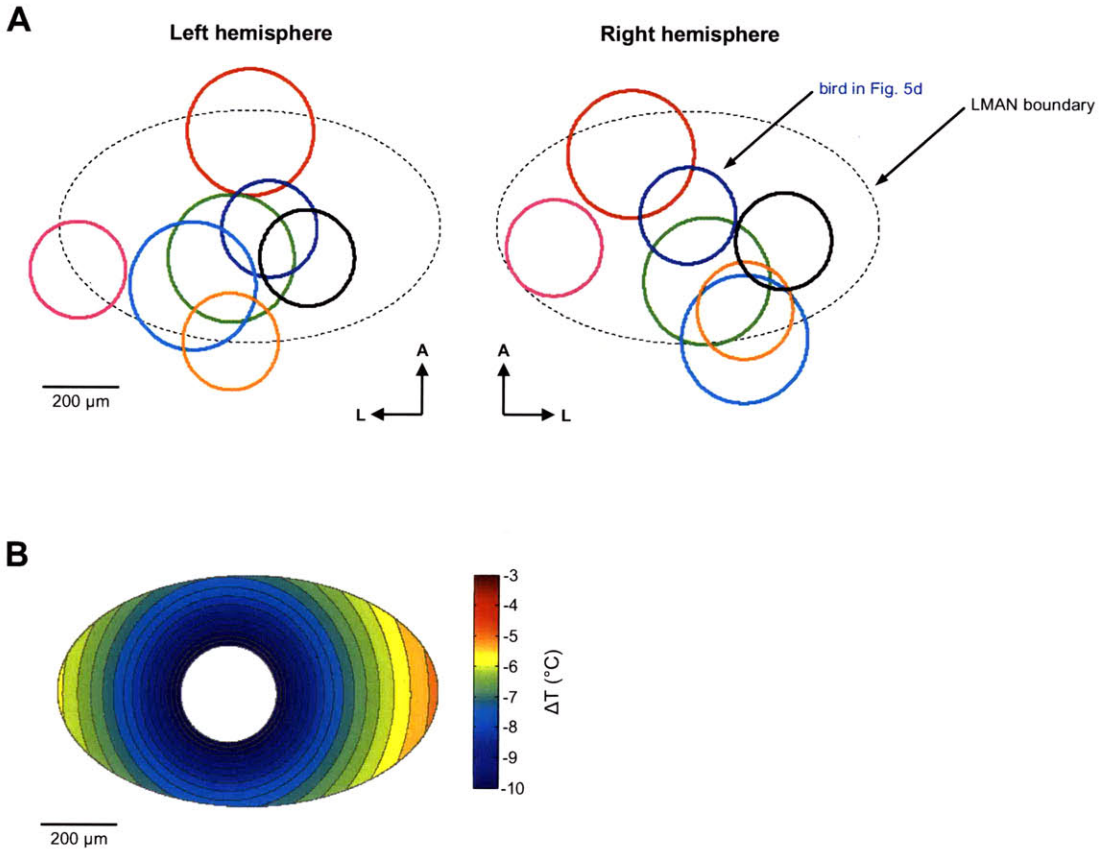
A
Left hemisphere
Right hemisphere
bird in Fig. 5d
LMAN boundary
200 µm
A
L
A
L
B
-3
-4
-5
-6
-7
-8
-9
-10
ΔT (°C)
200 µm

Chapter 5

Discussion

Previous chapters provide a detailed account of our results concerning early song production in zebra finches. A number of methods, including lesions and inactivations, recordings, quantitative behavioral analysis, and mild cooling have been used to understand various aspects of this behavior. In this chapter, I attempt to combine these results into a coherent model that explains, to a large extent, the neural mechanisms of early singing. I discuss the implications of this model for understanding how the brain generates behaviorally-relevant dynamics. Finally, I return to the questions asked in the introductory chapter of this thesis and discuss our results in the general context of exploratory activity in the brain.

Dynamical model of early song production

Previous chapters show that both HVC and LMAN generate activity patterns that contribute to the timing of early singing. We first consider activity intrinsic to LMAN and illustrate its involvement in singing in the absence of HVC. This is a model of the song system at the earliest stages of development, when contributions from HVC are weak or nonexistent; it also applies to the more mature system following HVC elimination. We then introduce the role of HVC dynamics in driving song production and discuss possible forms of interaction between HVC- and LMAN-driven motor control.

The term "dynamics" is often used in neuroscience to describe a wide range of time-dependent processes. Throughout this chapter, however, we use this term in a strictly physics-defined sense.[4] When describing neural circuits, "dynamics" refer to the

[4] Classical mechanics, for instance, distinguish between *dynamics* – a study of the processes that generate movement, and *kinematics* – a study of movement without consideration of its causes. For instance, tension forces in a spring create oscillatory dynamics. As a result, a ball attached to this spring exhibits oscillatory kinematics (movement).

actual biophysical processes that generate timescales in neural activity (Wilson 1999; Vogels et al. 2005). Although these timescales are also present in downstream activity and eventual movements, these latter processes do not exhibit the dynamics.

This concept is clearly illustrated by simple oscillator circuits, such as the circuit for swimming in the leech (Stent et al. 1978). In this example, oscillatory *dynamics* are generated by inhibitory interactions within a small group of neurons. Perturbing these neurons affects timing of the oscillation throughout the neuromuscular system. Rhythmic *activity*, on the other hand, is present in several downstream parts of the system, including other central neurons, motor neurons, and even the muscles themselves that produce swimming movements. Perturbing these components of the system can disrupt local activity or the behavioral output, but it does not affect the ongoing global oscillation.

LMAN is involved in generating subsong components

We find that early subsong, as well as singing in the absence of HVC, is characterized by several types of distinct transitions in the behavioral output. In the respiratory domain, subsong consists of relatively long expiratory pressure pulses (EPs) that alternate with brief inspiratory pressure pulses (IPs). In the acoustic domain, subsong consists of syllables that alternate with silent gaps. We find that syllables occur almost exclusively during EPs, but that a single EP can contain several syllables separated by non-inspiratory (mode-1) gaps. Thus, early subsong consists of syllables, mode-1 gaps, and gaps that contain IPs, which can also include silent, non-inspiratory periods (mode-2 and 3 gaps).

What generates these behavioral transitions in subsong, and where are the neural dynamics that determine the durations between these transitions? Using inactivation experiments, we find that activity in LMAN is necessary for subsong production. Furthermore, cooling LMAN prolongs subsong syllables, mode-1 gaps, and non-inspiratory periods in mode-3 gaps. These results suggest that LMAN is actively involved in generating dynamics that influence the timing of acoustic elements in subsong.[5]

How might LMAN-dependent dynamics generate acoustic transitions in subsong? One possibility is that LMAN (possibly in conjunction with other brain areas) exhibits two types of population activity states – some that generate sounds and others that generate silences. By continuously evolving in time, population activity in this case "wanders" between the vocal and the silent regions of a state space, producing the observed transitions between syllables and gaps. One way such behavioral bimodality could be implemented is via a downstream – perhaps even peripheral – mechanism that applies a nonlinear threshold to a continuous LMAN output (Fee et al. 1998). By slowing down the biophysical processes in LMAN, cooling would reduce the frequency of the transitions, prolonging both syllables and gaps.

Another possibility, which is not mutually exclusive with the above model, is that LMAN actively generates transitions from syllables to gaps and vice versa. Specifically, a distinct subset of neurons in LMAN could trigger a switch in downstream brain areas (or in other LMAN neurons) from a vocalized state to a silent state, whereas other LMAN neurons could trigger the reverse switch. In fact, our neuronal recordings during subsong

[5] Note that the stretching of both syllables and gaps is crucial to make this argument; if only one component had stretched, our result could be explained by a mechanism unrelated to LMAN dynamics. For instance, weakening of the output drive from LMAN due to cooling might lengthen gaps by reducing the fraction of activity states that pass some downstream threshold for vocalization. Such process, however, would shorten – not lengthen – the syllables.

and following HVC lesions are suggestive of this possibility. We find that some RA-projecting neurons in LMAN exhibit bursts of activity related to acoustic transitions, preceding either syllable onsets or syllable offsets by durations consistent with premotor latencies.

What is the involvement of LMAN dynamics in respiratory transitions during subsong? One possibility is that LMAN plays no role in these transitions. Specifically, the alternation of EPs and IPs may be generated by activity elsewhere in the brain – perhaps by the brainstem respiratory system. In this scenario, LMAN generates fluctuations that produce in syllables and gaps during EPs, but has no influence on the underlying respiratory pattern. Another possibility is that LMAN activity is involved in some respiratory events, either by triggering them in downstream brain areas or by actively driving them and determining their durations. Our experiments only characterize the role of LMAN in sound production; replicating electrophysiological and cooling experiments with simultaneous air sac pressure measurements is critical for addressing its role in respiration.

HVC is involved in generating consistently-timed gaps

Our results indicate that subsong is also characterized by the appearance of gaps whose durations are consistently ~60 ms (mode-2 gaps), likely before the developmental onset of consistent timing in syllable durations. These gaps are almost entirely filled by a single IP. We find that mode-2 gaps become more frequent during development, and that HVC lesions abolish their production. Furthermore, we find that HVC cooling, but not LMAN cooling, prolongs these gaps. This result suggests that HVC is not only necessary

for the production of mode-2 gaps, but that the biophysical dynamics intrinsic to HVC may be involved in their timing.

What is the mechanism by which HVC influences the timing of inspiratory gaps in early singing? One possibility is that HVC activity triggers the production of some IPs that interrupt ongoing song production. If the frequency of generating such IPs increases developmentally, this process can account for the increase in the incidence of mode-2 gaps. It is also possible that HVC not only triggers IPs, but actively drives their production, generating a sequence of activity states that produce an inspiratory motor pattern.

However, it is important to distinguish between the gap and the IP contained in it. The former is an acoustic motor feature – namely, the absence of vocal output for some period of time; the latter is a respiratory motor gesture. Although these two events are coincident during mode-2 gaps, they may not be driven by the same forebrain circuits. Our experiments characterize acoustic features and thus only address the production of gaps. Therefore, a possible alternative explanation of our results is that HVC is not involved in respiratory control, but is activated simultaneously (or at a fixed time relative to) the initiation of an IP. It could then controls gap duration by initiating the following syllable ~60 ms after the onset of the IP. HVC recordings and cooling with simultaneous respiratory measurements are necessary to characterize the nature of the relationship between HVC activity and IP production.

HVC is involved in generating consistently-timed syllables

We find that early song development is also characterized by the appearance of syllables that exhibit relatively consistent durations ("proto-syllables"), although these syllables remain variable in acoustic structure. Proto-syllable production is abolished following bilateral elimination of HVC, implying that, similarly to the production of consistently-timed mode-2 gaps, this developmental process requires HVC activity. Furthermore, we find that HVC cooling prolongs proto-syllables, suggesting that the biophysical dynamics intrinsic to HVC are actively involved in their timing. Previous studies have shown that early syllables transform into mature adult syllables via a continuous developmental trajectory, which involves refinement of their acoustic structure and differentiation into distinct syllable types (Tchernichovski et al. 2004). Neural dynamics within HVC are also involved in the timing of adult syllables (Long & Fee 2008). In conjunction with these studies, our results are suggestive of the possibility that similar biophysical processes in HVC are involved in generating early proto-syllables and mature syllables later in development.

Our analysis of early plastic songs indicates that HVC-dependent proto-syllables and consistently-timed "proto-gaps" not only appear during this stage, but tend to precede and follow each other, forming long, rhythmic sequences. These sequences remain and become more prominent following LMAN elimination. These results suggest that HVC activity is not only involved in the timing of proto-syllables and proto-gaps, but may play a role in the initiation of a gap following the completion of a syllable and vice versa. Consistently-timed syllable/gap sequences transform into adult motifs during development, suggesting that the role of HVC in timing these sequences may be similar to its role in the timing of adult singing (Long & Fee 2008).

Interestingly, early onset of relatively precise syllable timing we observe is a feature of human babbling as well. Infants in the pre-lingual stage vocalize by producing rhythmic mandibular movements ("frames"), even before the appearance of identifiable acoustic content in these vocalizations (Davis & MacNeilage 1995). Rhythmicity is also an early feature of "hand babbling" in sign language (Petitto & Marentette 1991). Similarly to plastic song in zebra finches, later babbling stages are characterized by the refinement of motor control and the introduction of linguistic content to the rhythmic frames.

Possible interaction between HVC and LMAN

Subsong and early plastic song are interesting developmental stages because they involve contributions of two distinct pathways to the production of timing. For example, mode-2 gaps, whose timing is HVC-dependent, are intermingled during subsong with syllables, whose timing is LMAN-dependent. What interaction, if any, exists between the two pathways? It is possible that the production of HVC- and LMAN-dependent song components is completely uncoordinated. In this scenario LMAN produces continuous premotor activity fluctuations that generate syllables and gap. At certain times, HVC generates activity that "inserts" an inspiratory period into the song, independently of LMAN activity during this time. Following the completion of this period, ongoing LMAN activity continues resulting in acoustic output.

Alternatively HVC- and LMAN-dependent processes in early singing are coordinated in time. For instance, a process in HVC involved in terminating mode-2 gaps may provide feedback input to LMAN that initiates syllables. Similarly, the completion

of an LMAN-generated syllable may initiate a gap-related process in HVC. Anatomically, multiple feedback pathways to HVC and to LMAN have been described (Nottebohm et al. 1982; Bottjer et al. 1989; Vates et al. 1997; Coleman & Vu 2005; Ashmore et al. 2008). Elimination of these pathways is young birds, as well as recordings from them are necessary to characterize their involvement in early song production, as well as their possible role in the coordination of HVC- and LMAN-dependent activity.

Specialized premotor circuits for producing distinct types of dynamics

In addition to identifying brain areas actively involved in early song timing, our results attribute distinct types of circuit dynamics to these areas. Two approaches – an ethological one and a neurobiological one – have been instrumental to such a level of circuit function analysis. We outline the novelty of these two approaches and discuss possible biophysical mechanisms underlying the production of the dynamics we identified.

Ethological approach: analysis of timing in behavior

Movements that comprise complex behaviors, like speech or locomotion, are temporally organized into coordinated sequences. Relative timing of these movements is therefore a basic aspect of behavior, and localizing the neural processes that generate timing is critical for understanding how behaviors are produced. Such localization has been achieved for simple rhythmic behaviors, which are essentially characterized by a single timescale (Stent et al. 1978), but is more difficult for behaviors that contain multiple timescales, which are often hierarchically organized. One issue is that all

processes that contribute to a complex behavior are not always directly observable. We find that birdsong, which consists of respiratory and acoustic fluctuations is an excellent example of this problem. Although respiration influences the timing of sounds in early singing, only the sound is often directly observable by an experimenter (and presumably by other birds during vocal communication).

Our approach toward this problem has been to attempt to decompose the observable behavior into multiple underlying processes. By analyzing the durations of syllables and gaps in early singing, we identified what appear to be distinct temporal "modes" characterized by different timescales. Using this decomposition, we then set out to determine if the biophysical dynamics generating each timescale can be localized to a particular region of the neural circuit. We suggest that similar decomposition of other complex behaviors into distinct modes (Drai et al. 2000) may be critical for understanding the underlying neural mechanisms.

Neurobiological approach: localized temperature modulation

Traditional methods for localizing motor function in the brain include lesions and inactivations, stimulation, and neural recordings. These techniques are useful for demonstrating the involvement of neural circuits in behavior, but they are inadequate for understanding the role of these circuits in producing behaviorally-relevant dynamics. Small localized temperature changes, on the other hand, are a powerful method for specifically targeting circuit dynamics (Long & Fee 2008). Our results distinguishing HVC- and LMAN-dependent dynamics strongly emphasize these points.

Temperature modulation is particularly effective in a typical feedforward motor system, where an oscillator circuit projects onto a premotor area, which then converts the oscillatory signal into a sequence of motor commands (Stent et al. 1978). In this case, traditional methods often fail at recognizing that the former, but not the latter, circuit is the one generating behaviorally-relevant dynamics. For instance, because both brain areas are necessary for the production of movements, lesioning or inactivating either one can be equally disruptive to the behavior. Similarly, global stimulation of either brain area can disrupt the behavior, particularly if feedback connections are present between them (Ashmore et al. 2005). Finally, recording in either set of neurons can reveal premotor activity time-locked to the rhythmic behavioral output (Stent et al. 1978; Chi & Margoliash 2001; Hahnloser et al. 2002). Cooling, on the other hand, clearly distinguishes between these areas. Cooling the oscillator circuit slows down its biophysical dynamics, resulting in an equivalent slowing of the behavior itself (Bauer & von Helversen 1987; Pires & Hoy 1992). On the other hand, cooling of the premotor area downstream of the oscillator may be somewhat disruptive to the behavior, but cannot change its speed. Such localization of the timing circuit is particularly elegant in the complex song system, where cooling HVC, but not its effect nucleus RA, affects song timing (Long & Fee 2008).

A caveat of this technique is that alternative anatomical arrangements of premotor areas can make the results of cooling experiments more ambiguous. One case is that of a brain area that provides excitatory input unrelated to timing to an oscillator circuit. Cooling this area may weaken its excitatory output and slow down the downstream oscillator circuit by prolonging response latencies of individual neurons in it (e.g., due to

hyperpolarization of the oscillator neurons). Another hypothetical example is that of two or more brain areas interconnected in a loop. In this case, behavioral dynamics could be generated by activity that rapidly cycles through the loop. Cooling any area in the loop could slow down the behavior by introducing a delay to each cycle (Volgushev et al. 2000b). This issue is particularly relevant in complex motor systems like the zebra finch song system, where multiple feedback loops exist (Ashmore et al. 2005; Vates et al. 1997; Perkel et al. 2002).

Distinct types of circuit dynamics in the song system

We find that HVC-dependent components of early singing – proto-syllables and mode-2 gaps – exhibit Gaussian-like distributions of durations. This is apparent in the songs produced following LMAN inactivation, as well as in the analyses that isolate HVC-dependent modes from the overall distributions of syllable and gap durations. The center of a Gaussian is a single timescale characterizing these song components, and our results show that the generation of this timescale may involve HVC activity. This is consistent with earlier work that demonstrated uniform stretching of adult songs following HVC cooling (Long & Fee 2008), suggesting that HVC at all developmental stages is specialized in generating dynamics that produce motor sequences of consistent durations. In other words, following the initiation of a motor program, circuitry within HVC may step through a stereotyped sequence of activity states, each state triggering a downstream pattern of muscle activations at the corresponding point in time.

How might HVC generate sequential dynamics? Theoretical studies have suggested "synfire chain" organization in neural circuits – a pattern in which each neuron

belongs to a node, and neurons within a given node exhibit strong excitatory connections to neurons in the next node (Abeles 1991; Vogels et al. 2005; Jin et al. 2007; Fee et al. 2004). When triggered, activity in such a network reliably propagates through successive nodes, generating a stereotyped output sequence. Recordings in HVC are suggestive of this model: during an adult song, RA-projecting neurons generate a single brief burst of spikes, whose timing is highly consistent across motif renditions, but different across neurons (Hahnloser et al. 2002). Our results indicate that HVC may be specialized for producing sequential dynamics even at the earliest stages of development. Recent theoretical work suggests that synfire-chain organization can, in fact, arise early in development from simple spike timing-based synaptic learning rules, even before the onset of sensorimotor learning (Jun & Jin 2007; Fiete et al. 2010).

We find that, unlike the stereotyped sequential elements of adult songs, LMAN-dependent components in early singing are characterized by temporal randomness. In fact, these components (subsong syllables, as well as mode-1 gaps and non-inspiratory portions of mode-3 gaps) exhibit exponential duration distributions. In a loose sense, exponential distributions indicate an extreme level of randomness; a sequence of activity underlying these behavioral components proceeds with no memory, terminating the motor gesture at a time fully independent of the start time. A different sequence is generated each time, allowing the underlying circuit timescale to be analyzed only from a distribution of many motor renditions.

What kind of network architecture might generate such random activity patterns in LMAN, and possibly other brain areas? Theoretical studies suggest that stochastic activity in neural circuits can be produced by chaotic dynamics (van Vreeswijk &

Sompolinsky 1998; Vogels et al. 2005; Wilson 1999). Such dynamics may be generated by recurrent networks with sparse, random connectivity, or even by biophysical processes in single neurons. Although chaotic dynamics are fully deterministic, they are extremely sensitive to initial conditions. On behaviorally-relevant timescales, a chaotic network would thus produce a unique output sequence following each activation, even if the input signal triggering network activity is identical each time.

Whether chaotic dynamics are responsible for randomness in neural networks is an open question. Similarly, connectivity patterns and synaptic learning rules that result in such dynamics are currently only in the realm of theoretical studies. Although chaos in neural systems has been studied for a long time, chaotic processes have been mainly used to model spontaneous background activity in sensory cortical regions (Vogels et al. 2005). Dynamics in motor areas, however, are more amenable to study because they produce easily measurable and quantifiable outputs. Our results suggest that LMAN may therefore be a superior model for studying stochastic aspects of cortical function.

Our results demonstrate that HVC and LMAN are involved in generating behaviorally-relevant dynamics, but they do not prove an exclusive role of these circuits. Because these areas are components of several feedback loops, they could, in principle, be driven by activity that rapidly cycles through these loops during singing. The speeds of neural processes in loops would be affected by temperature modulation of a single brain area, since cooling may introduce a delay to each cycle. Such dynamics were shown to be unlikely in adult birds by cooling RA – the brain area downstream of HVC in a loop – and finding that this manipulation has no effect on song timing (Long & Fee 2008). This experiment, however, must be repeated in young juvenile birds to determine whether

RA activity plays a role in subsong timing. In addition to RA, area X and/or DLM must be cooled in juvenile birds to test their involvement in early singing, since LMAN forms two feedback pathways with these areas.

Finally, one aspect of early song timing has not been addressed by our experiments – the timescale of mode-4 silent gaps. We find that these long gaps, which contain eupnic breathing, exhibit power-law distributions on a very wide range of durations, from 300 ms to 30 s. These distributions consistently deviate from a power law at durations greater than 30 s, suggesting that gaps shorter than ~30 s may represent a distinct mode of song production, rather than transitions to a purely non-singing state during which the animal is engaged in other behaviors.

On a physical level, power-law dynamics can arise from a number of different mechanisms and represent an intermediate regime between fully predictable and completely random dynamics (Drew & Abbott 2006). Because mode-4 gaps are essentially intervals between successive bouts of singing, these dynamics imply some presence of memory in the song initiation behavior. Specifically, the timing of each song partially depends on when the previous one occurred, and consecutive singing bouts tend to occur in clusters. Biologically, a memory trace underlying such organization may represent a slowly-varying "motivation" signal that, when strong, stimulates the song system to produce bouts in close succession. The location of such a process is clearly unknown and may even be outside of the song system, perhaps in neuromodulatory centers. The localization of these slow dynamics is therefore an open question, which aims at the heart of understanding how behaviors are initiated in the brain.

Our analysis of HVC- and LMAN-dependent dynamics is suggestive of an interesting organizational scheme in the song system. Traditionally, cortical circuits are characterized by the types of receptive fields exhibited by their neurons. In primary motor systems, this concept is manifested in myotopy – a pattern of anatomical organization in which groups of neurons are specialized for activating individual muscles or sets of muscles. Neurons can also be organized according to specific action patterns or targets they encode (Graziano 2006). Our results suggest another type of cortical organization, in which neuronal populations are organized not only by the type of actions they perform, but also by the kinds of circuit dynamics they produce. Of course, in the mammalian brain such specialization may not necessarily involve anatomically distinct regions, but could occur in subregions (such as cortical layers) or even specific classes of neurons (Cardin et al. 2009; Bonifazi et al. 2009).

Summary: specialized circuits for exploratory behavior

Models of developmental learning often presume that juvenile behaviors are immature versions of their adult counterparts, produced by the same neural circuits in an initial, undeveloped state. In such models, experience-dependent plasticity operates on the motor programs in these circuits to select only those that produce desired actions, and to eliminate those that do not (Forssberg 1999; Edelman 1987; Sporns & Edelman 1993; Marler 1997; Hadders-Algra 2000). Building on a body of recent work, we propose a different model, in which neural pathways distinct from those that drive motor control in adults are specialized for producing exploratory juvenile behaviors. We find that, beyond simply modulating or injecting variable fluctuations into motor sequences, such a

pathway in the songbird actively drives behavior, generating random dynamics that dominate motor control early in development.

Exploration analogous to subsong is ubiquitous in developing motor systems, manifested in behaviors that range from simple muscle twitches to highly complex play (Forssberg 1999; Fagen 1981). Homology across motor systems is also present on the neural level: the pathway we describe is a component of the basal ganglia-related forebrain circuitry – a set of evolutionarily conserved structures present in many vertebrate species (Smeets et al. 2000; Farries & Perkel 2002). In mammals, as in birds, these structures are implicated in motor learning, as well as in a wide array of motor and cognitive disorders (Graybiel 2008). One is left to wonder how far the homology among vertebrates extends, and whether similar basal ganglia-forebrain circuits are specialized for the production of exploratory behaviors in mammals, including humans.

Broadly speaking, what are the implications of specialized exploratory circuits in the brain? Beyond trial-and-error learning, even mature animals produce purposefully randomized or erratic behaviors that facilitate fast exploration and adjustment to their surroundings (Humphries & Driver 1970; Fonio et al. 2009). In the cognitive domain, exploratory thought generation may allow an individual to sample from a range of possible decisions and, in social settings, to introduce advantageous unpredictability into one's behavior (Miller 1997). Such processes have been used to explain the roots of creative thinking and – on a philosophic level – even the concept of free will (Wilson 1999). Specialized neural circuitry for exploration would represent a remarkable evolutionary adaptation of animal brains to the uncertainties in the world around them.

Appendix A

Analyzing the dynamics of brain circuits with temperature:
design and implementation of a miniature thermoelectric device

Where is the "engine" that drives brain dynamics? Complex behaviors, like speech and locomotion, are temporally coordinated on a wide range of timescales, and many brain areas are typically implicated in the production of any one of these behaviors. Is there a specialized circuit that generates the dynamics underlying a behavioral sequence, or do these dynamics arise from network interactions across different brain areas? Do different brain regions control different timescales of a behavior? Similar questions can be asked about the origin of internal dynamics of the brain, such as oscillations (Buzsáki 2006) or neuronal sequences (Abeles 1991; Hahnloser et al. 2002; Pastalkova et al. 2008).

Questions about brain dynamics are difficult to address using standard techniques of electrophysiological recording and inactivation. These methods tell us whether a brain region is involved in the expression of a particular behavior (or brain oscillation), but they do not reveal whether the biophysical dynamics within that region are actively involved in timing the behavior. The most direct way to localize the dynamics is to manipulate the biophysics in different regions and observe the resulting effect on behavior. This has been done by transiently disrupting neuronal activity (Stent et al. 1978; Bonifazi et al. 2009) or with temperature changes (Arbas & Calabrese 1984; Bauer & von Helversen 1987; Pires & Hoy 1992; Katz et al. 2004; Yamaguchi et al. 2008; Long & Fee 2008). Temperature affects the speed of all cellular processes, including synaptic transmission, action potential generation, and axonal conduction (Thompson et al. 1985; Volgushev et al. 2000a; Volgushev et al. 2000b). This approach is therefore broadly applicable, allowing one to slow down or speed up the dynamics of individual brain regions.

Temperature modulation is, in fact, effective at changing the speeds of simple, rhythmic behaviors that are driven by central pattern generators (CPGs), such as the heart-beat in leech (Arbas & Calabrese 1984), wing-beat in locusts (Foster & Robertson 1992), locomotion in the *Tritonia* mollusk (Katz et al. 2004), as well as communication signals in fish (Feng 1976), insects (Bauer & von Helversen 1987; Pires & Hoy 1992), and frogs (Gerhardt 1978; Yamaguchi et al. 2008). Furthermore, experimentally focusing temperature changes to specific regions of the nervous system is effective at localizing the biophysical processes that produce these motor rhythms (Bauer & von Helversen 1987; Pires & Hoy 1992). Recent work indicates that this technique can be extended to the study of more complex behaviors in the vertebrate brain. In zebra finches, cooling the high vocal center (HVC) changes song speed uniformly across all timescales, whereas temperature changes in its efferent nucleus RA have no effect on song timing (Long & Fee 2008). These findings suggest that the dynamics intrinsic to HVC are actively involved in the control of song timing.

Cooling of brain structures in small, behaving, warm-blooded animals poses several technological challenges. For instance, probes that use liquid or gas flow for cooling are generally not lightweight or flexible enough for this application (Zhang et al. 1986; Lomber et al. 1999). Alternatively, commercially-available Peltier thermoelectric devices have been used to cool parts of the brain, but these also require water flow to remove excess Ohmic heat generated by electric currents (Ferster et al. 1996; Chafee & Goldman-Rakic 2000; Imoto et al. 2006). Recently, a Peltier device that uses water cooling has been miniaturized to be carried by a small songbird (Long & Fee 2008). For wide applicability, however, it is desirable to eliminate the water cooling system, which

partially restrains the animal with attached tubing. Another challenge is that cooling deep brain structures requires efficient heat transfer across long distances in the brain – a process opposed by the animal's homeostatic temperature maintenance.

Here, we discuss the design, optimization, and implementation of a device that is light (<1 g), does not require water cooling, and is useful for changing temperature in both superficial and deep brain structures. For structures in the forebrain song system of the zebra finch, this device is capable of generating up to ~7°C of cooling – an amount sufficient for manipulating biophysical dynamics (Long & Fee 2008). The principles of this method are generally applicable for constructing devices that use temperature to probe circuit dynamics in behaving animals.

Design of a miniature thermoelectric device for brain cooling

1. Basics of thermoelectric devices

When different conducting materials are brought into contact, a voltage difference is generated that is proportional to the temperature difference between the conductors. This phenomenon – known as the *Peltier effect* – is the basis of thermoelectric devices (Rowe 1995). The voltage difference can be quite large when materials like semiconductors commonly used in these devices are placed in contact with a metal. The converse effect also occurs: when electric current is passed across the junction between these materials, it causes heat to be pumped across the junction. If the semiconductor is doped with positively charged ions (p-type), then the flow of electrons from the semiconductor to the metal causes heat to be pumped from the semiconductor to the metal as well. On the contrary, if the semiconductor is doped with negatively charged

ions (n-type), then heat is pumped in the opposite direction. P- and n-type semiconductors can be cleverly alternated between two plates (Fig. 1a), so that heat is pumped from one plate (the cold plate) and into another (the hot plate) as current flows back and forth through the device. At each junction, the amount of heat pumped is given by $\dot{Q} = \alpha TI$, where T is the absolute temperature of the junction, I is the amount of current, and α is a property of the semiconductor material known as the Seebeck coefficient. (In this formula, α is the average of the coefficients for the n- and p-type elements, which can be different.)

Unfortunately, two additional phenomena limit the efficiency of this arrangement. First, semiconductors are, by definition, not perfect electrical conductors, and the flow of current through them causes a dissipation of heat. It can be shown that half of this Ohmic heat flows into the hot plate and the other half into the cold plate. Combined with the Peltier effect, the net amount of heat pumped into the cold plate is therefore

$$\dot{Q}_C = 2N(aT_C I + \frac{1}{2}RI^2) \tag{1-1}$$

where $2N$ is the number of semiconductor elements (forming N junctions), T_C is the absolute temperature of the cold plate, and R is the electrical resistance of each semiconductor element. Note that the sign of the first term in Eqn. 1-1 is chosen such that, by convention, negative current causes cooling at the cold plate. Similarly, the net amount of heat pumped into the hot plate is

$$\dot{Q}_H = 2N(-aT_H I + \frac{1}{2}RI^2) \tag{1-2}$$

where T_H is the absolute temperature of the hot plate. For mild cooling applications, the first term in Eqn. 1-2 is close in magnitude to the first term in Eqn. 1-1 (since absolute

temperatures T_C and T_H, in Kelvin, are numerically close).[6] Thus, we can roughly think of the first term in these expressions as representing the pumping of heat out of the cold plate and into the hot plate. The second term represents Ohmic heat that flows into both plates. For negative values of *I*, the two effects produce heat flow in opposite directions at the cold plate; thus, Ohmic heating reduces the effectiveness of cooling.

A second problem is that the semiconductor elements between hot and cold plates can have substantial thermal conductivity, allowing heat to flow back from the hot plate to the cold plate, also reducing the effectiveness of cooling. The amount of heat that flows back is given by the thermal conductance *K* of each semiconductor element and the temperature difference $\Delta T = T_H - T_C$ between the two plates:

$$\dot{Q}_S = 2NK\Delta T \tag{1-3}$$

By analogy with electrical circuits, we can represent semiconductors as a thermal resistance (inverse of thermal conductance) connecting the two plates (Fig. 1b). In this circuit, temperature is treated analogously to voltage in an electrical circuit and heat transfer is treated analogously to current. The relationships between these thermal quantities are identical to those present between their analogs in electrical circuits.

The hot plate is usually connected to the external world through a thermal conductor called the *heat sink*. In the simplest, ideal scenario the heat sink is perfect – i.e., by analogy with electrical circuits, the hot plate is "grounded" (Fig. 1b). In this case, the hot-plate temperature remains at a constant value, whereas the cold-plate temperature

[6] We limit analytical treatment of the device to small temperature changes (~10K from a baseline of ~314K) because these are sufficient for mild brain cooling applications, but also because semiconductor properties are temperature-dependent and cannot be treated as constants in the general case. For applications that require stronger cooling, dynamical simulation of the device using empirical measurements of semiconductor properties is required for accurate analysis (Kondratiev & Yershova 2001).

is changed by an amount $-\Delta T$ relative to this value. In the following sections, we investigate the dependence of ΔT on the amount of electrical current I in this ideal case; subsequently we analyze the effects of imperfect heat sinking on device performance.

2. Properties of semiconductors

Three properties of the semiconductor elements are present in Eqns. 1-1 through 1-3 and therefore affect heat transfer in the Peltier device. These are the Seebeck coefficient α, the electrical resistance R, and the thermal conductance K. The latter two quantities depend on the shape of a semiconductor element in addition to its material properties. For a semiconductor block of height h and cross-sectional area A, we can define the *geometric constant* $G = A/h$. Electrical resistance of this block is then given by $R = \rho/G$ and thermal conductance by $K = \kappa G$, where ρ is the electrical resistivity of the material and κ is the thermal conductivity. These equations suggest that changing G can have opposing effects on the efficiency of the device: whereas increasing G reduces Ohmic heating due to the effect on R, it also reduces thermal isolation between the hot and the cold plate due to the effect on K. The principles behind choosing an optimal value of G will be discussed later.

3. Behavior of the isolated device

In steady state and in the absence of thermal conductances linking the device to the external world, heat transfers given by Eqns. 1-1 and 1-3 must add to zero at the cold plate. That is, heat transfer away from the cold plate due to the Peltier effect must be equal to the heat transfer into the plate due to Ohmic heating and thermal diffusion:

$$2N\alpha T_C I + \frac{N\rho}{G} I^2 + 2N\kappa G\Delta T = 0 \tag{3-1}$$

Although T_C is not independent of ΔT, for mild brain cooling experiments these values are very different numerically ($\Delta T << T_C$). When solving for the steady-state value of ΔT, we can therefore assume that T_C is a constant value T (e.g. the brain temperature of a zebra finch; (Bech & Midtgård 1981)). Given this assumption, the solution to Eqn. 3-1 is

$$\Delta T = -\frac{\alpha T}{\kappa G} I - \frac{\rho}{2\kappa G^2} I^2 \tag{3-2}$$

This concave-down quadratic form implies the existence of a maximum temperature difference between the two plates at some "optimal" amount of current (Fig. 1c). Beyond this amount of current, marginal increases in Ohmic heating are greater than the marginal increases in Peltier cooling (since the former is quadratic in current, whereas the latter is only linear). Optimizing Eqn. 3-2 to find the minimum achievable steady-state ΔT, we find the optimum current I_{opt}:

$$I_{\text{opt}} = \frac{\alpha G T}{\rho} \tag{3-3}$$

The temperature difference ΔT_{opt} at this current is

$$\Delta T_{\text{opt}} = \frac{\alpha^2 T^2}{2\kappa\rho} = Z\frac{T^2}{2} \tag{3-4}$$

where the quantity $Z = \alpha^2/\kappa\rho$ is a figure of merit for the semiconductor material.

4. Behavior of the device attached to a load

In practice, the purpose of a thermoelectric device is to pump heat from a thermal *load* (in our case, the brain). By analogy to electrical circuits, the load in steady-state can be represented by a thermal conductance K_L connecting the cold plate to "ground." The ground in a thermal circuit is a fixed temperature, relative to which cooling is measured; in the case of brain cooling, it is the normal temperature of the brain (314K in zebra finches; (Bech & Midtgård 1981)).

Introducing the load as a conductor to the thermal circuit (Fig. 1d), we can solve for the steady-state temperature as a function of current:

$$\Delta T = -\frac{\alpha T}{\kappa G + K_L} I - \frac{\rho}{2\kappa G^2 \left(1 + K_L / 2N\kappa G\right)} I^2 \tag{4-1}$$

In the case of $K_L = 0$, this equation simplifies to Eqn. 3-2, derived above. Again, the relationship of temperature on current is quadratic, exhibiting an optimum. The main effect of the load is the reduction in the optimal cooling achieved at the cold plate (Fig. 1c). The optimum current is

$$I_{\text{opt}} = \frac{\alpha G T \left(\kappa G + K_L / 2N\right)}{\rho\left(\kappa G + K_L\right)} \tag{4-2}$$

which simplifies to Eqn. 3-3 in the absence of a load, and the temperature difference at this current is

$$\Delta T_{\text{opt}} = \frac{\alpha^2 T^2 G\left(\kappa G + K_L / 2N\right)}{2\rho\left(\kappa G + K_L\right)^2} \tag{4-3}$$

which simplifies to Eqn. 3-4. Note that the amount of heat pumped from the load at the optimal current is $\Delta T_{\text{opt}} K_L$.

5. Behavior of the device with imperfect heat sinking

In reality, miniature heat sinks applicable for use in small behaving animals are likely to be highly limited. We thus need to expand the above model to include imperfect heat sinks attached to the hot plate of the thermoelectric device. In the simplest case, the device is cooled convectively by a fluid (e.g. water or air). Such a heat sink can be represented by a single thermal conductance K_C linking the hot plate to the temperature of the fluid relative to the body, ΔT_F. This temperature is analogous to a voltage source in electrical circuits (Fig. 1e).

It is also possible to place a heat sink in direct contact with the animal's body ("body-coupled heat sink"). Because we define the body temperature as the "ground" in our the thermal circuits, this configuration can be represented by a single conductance K_B connecting the hot plate to ground. If both convective and body-coupled heat sinks are present, the total heat sink conductance is $K_C + K_B$, and the temperature differential of the fluid can be represented by constant "bias" heat transfer $K_C \Delta T_F$ to the hot plate. The advantages of introducing a body-coupled heat sink to the device will be discussed later.

Treating Fig. 1e as a circuit analogous to electrical circuits, we can solve for the steady-state temperature of the cold plate relative to the brain, ΔT_C:

$$\Delta T_C = \frac{2N\kappa G\left(2N\alpha TI - N\rho I^2/G - K_C\Delta T_F\right) - \left(2N\alpha I + 2N\kappa G + K_B + K_C\right)\left(2N\alpha TI + N\rho I^2/G\right)}{\left(2N\alpha I - 2N\kappa G - K_L\right)\left(2N\alpha I + 2N\kappa G + K_B + K_C\right) + \left(2N\kappa G\right)^2} \tag{5-4}$$

Since Eqn. 5-4 is not only demonstrative, but expresses the full model we use to characterize the device, it no longer assumes that the hot and cold plates are at a constant temperature when calculating the magnitude of the Peltier effect (see Section 3). Again,

the value of this analytic solution at any amount of current can be used to determine the amount of heat pumped from the brain: $\Delta T_C K_L$.

Thermal propagation in the brain

Equations so far have represented the thermal load on the device by a single conductance K_L. In the case of brain cooling, this conductance depends on the biophysical properties of the brain tissue, as well as on the spatial properties of the contact between the device and the brain. In this section, we consider the effects of these parameters on heat propagation. The first goal of this analysis is to determine K_L, a quantity necessary in the above equations to quantify heat transfer from the brain. The second goal is to characterize the spatial properties of thermal propagation in the brain itself, which is necessary to understand how temperature changes as a function of distance from the device.

In some cases, the region of interest is located near the brain surface (e.g., area HVC in songbirds or superficial cortical layers in mammals), permitting temperature to be modulated by directly placing the cold plate of the device on the surface of the brain (Long & Fee 2008). We refer to this arrangement as the *planar geometry*. In other cases, the region of interest is located deep in the brain, requiring that a thermally conductive probe be attached to the cold plate and placed within the brain. We call this *cylindrical geometry*. Our next goal is to characterize temperature changes in the brain in each of these two geometries.

6. Planar geometry

Temperature changes are the easiest to analyze in planar geometry, in which a cooling surface is placed directly in contact with the brain. In this arrangement, temperature as a function of time t and distance x from the surface is described by the standard one-dimensional model of thermal diffusion in solids, which includes an additional term to describe the loss of heat due to the perfusion of the brain with blood (Kastella & Fox 1971; Jafari & Higgins 1989):

$$\kappa_B \frac{\partial^2 \Delta T}{\partial x^2} - wc\Delta T - \rho_B c_B \frac{\partial \Delta T}{\partial t} = 0 \tag{6-1}$$

Here, κ_B is the thermal conductivity of the brain, w is the blood supply per units of volume and time, c is the specific heat of the blood, ρ_B is the density of the brain, and c_B is the specific heat of the brain. Note that temperature ΔT is measured relative to the normal brain temperature (i.e., temperature of the blood). In steady state, Eq. 5-1 has an exponential solution $\Delta T(x) = \Delta T_C e^{-x/\lambda}$, where T_C is the steady-state temperature of the cooling surface and $\lambda \equiv (\kappa_B / wc)^{1/2}$. The length constant λ is a critical property of the brain, roughly indicating the spatial extent of temperature changes produced by the device. This solution ignores the edges of the cooling surface and is therefore only accurate at small distances ($x < \lambda$).

Heat flux from the brain into the cold plate is proportional to the slope of the temperature profile at the cold plate ($\kappa_B \partial \Delta T / \partial x$ at $x = 0$). Evaluating this quantity for the exponential solution given above, dividing by ΔT_C, and multiplying by the surface area of the cold plate, A_C, yields the thermal conductance of the load:

$$K_L = \frac{A_C \kappa_B}{\lambda} \tag{6-2}$$

In reality, the cold plate is linked to body temperature not only via a direct contact with the brain, but also by contacting the nearby cranium through some insulation material. Because some regions of the cranium are unavoidably very close to the cold plate, and any insulation material that may be used is imperfect, this contact must be represented by a conductance K_I (Fig. 1f). The total load on the cold plate is therefore $K_L + K_I$, and the size of K_I determines what fraction of the heat is pumped into the cold plate from the brain, rather than via the insulation.

7. Cylindrical geometry

When the region of interest is located deep in the brain, a thermally conductive probe must be attached to the cold plate and inserted into the brain to facilitate heat transfer. We first consider how temperature in the brain changes as a function of distance from the surface of a cylindrical probe. We assume that temperature changes along the length of the probe are very gradual in comparison with radial changes in the brain. This assumption is accurate for probes made of highly conductive materials, such as silver, which is almost four orders of magnitude more conductive than the brain (see Methods). In cylindrical coordinates, the model of thermal diffusion in perfused tissues yields the following equation for temperature (Jafari & Higgins 1989):

$$\frac{1}{r}\frac{d}{dr}\left(r\frac{d\Delta T}{dr}\right) - \lambda^2 \Delta T = 0 \qquad (7\text{-}2)$$

where λ is the same length constant of the brain as discussed above, and r is the radial distance from the center of the probe. The solution to this equation is

$$\Delta T(r) = \Delta T_P \frac{K_0(r/\lambda)}{K_0(r_P/\lambda)} \qquad (7\text{-}3)$$

where ΔT_P is the steady-state temperature of the probe surface, r_P is the radius of the probe, and $K_0(r)$ is the zero-order modified Bessel function of the second kind (Bowman 1958). (Here, we used $\Delta T(r_P) = \Delta T_P$ and $\Delta T(\infty) = 0$ as the boundary conditions). $K_0(r)$ has a steeper decrease than an exponential function at small radii; at large distances, it decreases approximately exponentially. By fitting Eqn. 7-3 to the data obtained in (Long & Fee 2008), we obtain an approximation of the length constant for the zebra finch forebrain, $\lambda = 1.59\,\text{mm}$.

In addition to characterizing the spatial profile of temperature in the brain, Eqn. 7-3 can be used to calculate the surface thermal conductivity of the probe-brain interface (this is conceptually the same as the electrical membrane resistivity of neuronal axons in the traditional Cable Theory, (Rall 1962; Dayan & Abbott 2001)). Heat transfer from the brain into the probe is proportional to the spatial derivative of $\Delta T(r)$ at the surface of the probe. Accounting for the thermal conductivity of the brain and the geometry of the probe, this leads to an expression for the surface conductivity of an un-insulated probe, κ_S, expressed per unit length of the probe

$$\kappa_S = \frac{2\pi r_P \kappa_B K_1(r_P/\lambda)}{\lambda K_0(r_P/\lambda)} \tag{7-4}$$

where K_1 is the first-order modified Bessel function of the second kind (the derivative of K_0).

In the most general case, some portion of the probe can be surrounded by several concentric layers of insulation. The conductivity of each insulation is derived via integration in cylindrical coordinates, which yields a logarithmic solution. Conductances of insulation layers act in series with the probe-brain interface conductance (Fig. 1g) and

can therefore be represented by a single surface conductivity of the probe per unit length of the probe, κ'_S (to distinguish from κ_S in the un-insulated case)

$$\kappa'_S = \left[\sum_{i=1}^{N} \frac{\ln(r_i / r_{i-1})}{2\pi\kappa_i} + \frac{\lambda K_0(r_N/\lambda)}{2\pi r_N \kappa_B K_1(r_N/\lambda)} \right]^{-1} \tag{7-5}$$

Here $r_1,\ldots,r_N$ are the outer radii of the N insulation layers, $\kappa_1,\ldots,\kappa_N$ are the material conductances of these layers, and $r_0 \equiv r_P$. Note that the expression for the conductivity of the insulation-brain interface, the inverse of which is the second term of this equation, has been changed from Eqn. 7-4 to account for the increased radius of the interface. The ratio of κ'_S to this interface conductivity represents the efficiency of the insulation, expressing temperature at the surface of the insulation as a fraction of the probe temperature ΔT_P underneath the insulation. This fractional reduction in temperature is equivalent to the effect of a voltage divider in electrical circuits.

8. Conduction along the probe

In a typical cooling application, the probe in the brain would consist of two sections: an insulated segment of length l_1, and an un-insulated segment of length l_2 located deeper in the brain within the targeted area (a third section, located above the brain, will be considered later). We would like to determine how the probe temperature ΔT_P changes as a function of depth. Following the conventions of Cable Theory (Rall 1962; Dayan & Abbott 2001), we characterize the two segments of the probe by their length constants, λ_1 and λ_2, which represent how gradually temperature falls off along the length of the probe. Taking into account the geometry of the probe, we obtain

$$\lambda_1 = \sqrt{\frac{\pi r_P{}^2 \kappa_P}{\kappa_S}} \tag{8-1}$$

where κ_P is the thermal conductivity of the probe material and κ_S is the surface conductivity given by Eqn. 7-5. The length constant of the second segment, λ_2 is calculated using the same equation, but with the value of κ_S' given by Eqn. 7-4 instead of κ_S. Because the first segment has a lower surface conductivity due to insulation, it has a higher length constant than the second segment.

From Cable Theory, the general expression for temperature along the first segment, as a function of depth x is

$$\Delta T_P(X) = a_1 \cosh(L_1 - X) + b_1 \sinh(L_1 - X) \tag{8-2}$$

where $L_1 \equiv l_1/\lambda_1$, $X \equiv x/\lambda_1$, and a_1 and b_1 given by boundary conditions. Similarly, temperature along the second segment is

$$\Delta T_P(X) = a_2 \cosh(L_2 - X) + b_2 \sinh(L_2 - X) \tag{8-3}$$

where $L_2 \equiv l_2/\lambda_2$, $X \equiv x/\lambda_2$ (here, x is measured from the upper end of the second segment rather than from the brain surface), and a_1 and b_1 are given by boundary conditions. Boundary conditions require that both temperature and its derivative are continuous at the contact between the two segments. Further, we assume that no heat flows through the tip of the probe, implying that the derivative of temperature is 0 at the tip. (This is a reasonable boundary condition because the cross-sectional area of the tip is small relative to the overall exposed surface area). Using these considerations, we derive

$$a_1 = \Delta T_S \left[\cosh L_1 + (\lambda_1/\lambda_2)\sinh L_1 \tanh L_2\right]^{-1} \tag{8-4}$$

$$b_1 = \Delta T_S \left[\sinh L_1 + (\lambda_2/\lambda_1)\cosh L_1 \coth L_2\right]^{-1} \tag{8-5}$$

$$a_2 = \Delta T_S \left[\cosh L_1 \cosh L_2 + (\lambda_1/\lambda_2)\sinh L_1 \sinh L_2\right]^{-1} \tag{8-6}$$

$$b_2 = 0 \tag{8-7}$$

where ΔT_S is the temperature of the probe at the surface of the brain (the fourth boundary condition).

By taking the derivative at zero of the expression in Eqn. 8-2 and accounting for the probe conductivity, we can determine the input thermal conductance K_P of the entire probe, measured at the surface of the brain:

$$K_P = \frac{\pi {r_P}^2 \kappa_P}{\lambda_1}\left(\frac{1}{\coth L_1 + (\lambda_1/\lambda_2)\tanh L_2} + \frac{1}{\tanh L_1 + (\lambda_2/\lambda_1)\coth L_2}\right) \tag{8-8}$$

As mentioned above, another segment of the probe, of length l_0, is located between the cold plate of the device and the brain surface. The thermal conductance of this segment acts in series with K_P (Fig. 1f), allowing us to calculate the overall thermal load on the cold plate:

$$K_L = K_I + N_P\left(\frac{l_0}{\pi {r_P}^2 \kappa_P} + \frac{1}{K_P}\right)^{-1} \tag{8-9}$$

where K_I is the conductance of the cold-plate insulation discussed in Section 6 and N_P is the number of probes attached to the cold plate (e.g., 2 for bilateral cooling experiments).

Optimization of the thermoelectric device

Previous sections have derived equations that provide a detailed description of heat transfer and temperature changes in the thermoelectric device for brain cooling. Some aspects of this device are strongly constrained by an experiment (e.g., the necessary

length of the probe in the brain). Other aspects, such as the shape of the semiconductor blocks or the probe diameter, can be chosen from a range of alternatives. In the following sections, we use the derived equations to characterize the dependence of device performance on various parameters of its construction. The goal is to learn how to optimize these parameters, as well as to gain a better understanding of experimental constraints on the device.

To discuss each parameter independently, we show the effect of changing it on the performance of a "core" device, which contains two probes for bilateral cooling of a structure 2 mm deep in the brain. Various aspects of this core device are measured or approximated in Table 1. The construction of this device, as well as the measurements of the parameters in Table 1 are discussed in the Methods section.

9. Semiconductor geometry

As mentioned earlier, a semiconductor block can be characterized by the geometric constant G, the ratio of its cross-sectional area to its height. Large values of G are advantageous because they reduce Ohmic heating in the device. Small values of G, on the other hand, improve thermal isolation between the hot and cold plates of the device. Given these opposing influences, one would expect an optimal value of G to exist for a given device.

Fig. 2a shows steady-state temperatures at the cold plate as a function of current for three devices with different values of G. As expected from the above derivations, temperature exhibits a minimum at an optimal value of the current for each configuration. The temperature at this minimum is the lowest for values of G near 1.7 mm. Changing

the shape of the semiconductors in either direction from this minimum worsens the performance of the device. Fig. 2b quantifies the minimum achievable temperature at the cold plate for a range of geometric constants, showing that the optimal value of G is indeed near 1.7 mm.

The optimal value of G depends on other device parameters, such as the load on the cold plate and the efficiency of the heat sink. Fig. 2c shows minimum achievable temperatures for different loads in a reasonable range. Smaller loads allow lower temperatures to be achieved at the cold plate, and the optimal value of G is somewhat lower for smaller loads. Efficiency of the heat sink also has a dramatic effect on the lowest achievable temperatures, as illustrated by increasing the thermal conductance of the convective heat sink, K_C (Fig. 2d). Higher values of G are optimal in the presence of an efficient heat sink, although the temperature minimum is fairly broad across values of G in this case.

Clearly, minima of these relationships are only relevant for device construction if the lowest possible temperature is desired. If that is not the goal, it is reasonable to choose the smallest value of G that achieves the desired temperature, because smaller values of G require smaller currents. For instance, to achieve a temperature differential of $\Delta T_C = -10°\text{C}$ relative to body temperature, the device with G=0.5 mm requires about half as much current as the device with G=5 mm (Fig. 2a).

10. Number of semiconductor junctions

The device considered so far contains two semiconductor blocks, forming a single junction (N=1). What is the effect of changing the number of junctions? For simplicity,

consider increasing N by a factor of 2 and simultaneously decreasing G by the same factor. With this modification, the overall surface area of the semiconductor blocks does not change, leaving all thermal conductances in the device the same. For a given amount of current, heat production produced by the Peltier effect doubles due to increased number of junctions. Ohmic heat production, however, increases by a factor of 4 due to the combined effect of increasing the length of the current's path and decreasing the cross-sectional area of this path. Because the Peltier effect in linear and Ohmic heating is quadratic in current, these changes imply that equivalent temperature is achieved by the device at half the original amount of current. Fig. 2e confirms this reasoning: increasing N and decreasing G shifts the minimum of the temperature-current relationship to lower values of current, but leaves temperature at this minimum the same.

Thus, increasing N and leaving the product NG at its optimal value does not improve or worsen device performance. However, it allows smaller currents to be used – a property advantageous for behavioral experiments on small animals, in which thin cables and small electrical commutator contacts must be used (Fee & Leonardo 2001). The need to connect a large number of small semiconductor blocks can, in principle, make device construction difficult. However, some commercially-available thermoelectric modules have sizes and values of G suitable for brain cooling in small animals (see Methods).

11. Heat sinking

The device we are considering contains a convective heat sink attached to the hot plate (see Section 5). This heat sink is constructed by attaching conductive "fins" to the

hot plate, which are exposed to the air surrounding the animal (see Methods). In addition, the device includes a "body-couple heat sink," constructed by attaching a conducting material to the hot plate, and establishing thermal contact between that material and the surface of the animal's cranium. The convective and body-coupled heat sinks have thermal conductances K_C and K_B, respectively.

Fig. 3a shows the maximum amount of cooling achievable by the device as a function of K_C and K_B. Unsurprisingly, our model suggests that increasing the conductivity of either heat sink generally improves device performance. An exception to this rule is that the body-coupled heat sink slightly worsens performance when the convective heat sink is exceptionally efficient (K_C>~20 mW/K). This occurs because such strong convection actually maintains the hot plate below body temperature, causing the body-coupled heat sink to pump heat into the plate, rather than away from it. Highly efficient convection can be achieved using active water cooling of the hot plate (Long & Fee 2008). However, because we specifically set out to design a device without water cooling, out heat sinks are constrained to relatively small conductance values ($K_B \approx 7$ mW/K and $K_C \approx 5$ mW/K; see Methods). What are the effects of having either one of these heat sinks, and is including both of them in the device necessary?

Fig. 3b illustrates the effects of including or omitting each of the two heat sinks. Without either heat sink, the device does not generate cooling in steady-state at any amount of current (note that this device still produces a temperature differential between the hot and cold plates, but Ohmic heating keeps both plates above brain temperature). If either of the two heat sinks is included, the device is capable of generating some amount

of cooling. The convective heat sink is more effective than the body-coupled one because it is linked to room temperature, which is about 18°C below body temperature.

The maximal cooling achieved by a device with both heat sinks is only marginally stronger than the maximal cooling achieved by the convective heat sink alone. However, these two devices are very different at zero current. Due to the exposure to room temperature, convective heat sinking alone cools the cold plate by almost 8°C when no current is being passed. This is a fairly large amount for brain cooling experiments (e.g., it is near the maximal cooling used in (Long & Fee 2008)). Generally, cooling at zero current is not problematic, because an offset positive current can be passed through the device to maintain the cold plate at body temperature. However, this is not an option at some times, such as during a post-surgery recovery period, when an animal cannot be tethered. Including the body-coupled heat sink roughly halves the amount of cooling at zero current, reducing possible problems associated with chronic cooling of brain structures.

12. Probe dimensions

So far, we have analyzed the effects of various device parameters on the temperature of the cold plate. If a probe is attached to the cold plate, however, the temperature at the tip of this probe in the brain is only a fraction of the cold plate temperature, for two reasons. One reason is that the probe itself has limited axial conductance that acts in series with the conductance of the brain, similarly to a voltage divider in electrical circuits. The second reason is that some amount of heat is transferred through the imperfect insulation along the length of the probe, reducing the efficiency of

the device at changing the temperature deep in the brain. These phenomena are dependent on the dimensions of the probe and the insulation, which we now consider.

Clearly, a weakly-conducting material must be selected for insulating the probes. Because air has very low thermal conductivity, we chose to insulate probes with polyimide tubes that were wide enough to leave some air between the probe surface and the polyimide wall (see Methods). Fig. 4a shows the simulated effect of such insulation on temperature in the brain near the probe. Unsurprisingly, increasing the inner diameter of the polyimide tube improves insulation, as indicated by a greater fractional drop in temperature across the insulation. However, this improvement is small beyond a certain range of diameters (e.g. when increasing the inner diameter from 160 to 200 μm; Fig. 4a) and is made at the expense of increasing the outer diameter as well. Damage to brain tissue is a concern with large probes and should be taken in account when selecting insulation thickness, especially if increasing this thickness only marginally improves device performance.

If the inner and outer diameters of the polyimide tube are held fixed, what is the effect of changing the diameter of the probe itself? On the one hand, increasing the diameter reduces the thickness of the air insulation. On the other hand, such manipulation increases the cross-sectional area of the probe, which improves its axial conduction. Increasing the diameter also causes temperature fall-off to be less steep at small distances from the probe surface in the targeted brain area (Section 7). These opposing effects suggest a possible existence of an optimal probe diameter. Fig. 4b,c confirms that this is indeed the case. For inner polyimide tube diameters in the range of several hundred microns, optimal cooling (2 mm deep in the brain, 200 μm away from the surface) is

achieved by probes that fill approximately 2/3 of the tube's interior. Both thicker and thinner probes produce suboptimal cooling. Of course, it may sometimes be beneficial to choose a diameter smaller than the optimum, in order to reduce the amount of tissue damage in the targeted brain region.

Finally, probe length is a parameter that cannot be optimized, since probes must be long enough to reach the region of interest. However, using a highly conductive material like silver and covering it with efficient insulation ensures that the length constant of the probe is long compared to the targeted depth. For the probes of our "core" device (see Methods), the length constant according to Eqn. 8-1 is $\lambda_1 = 72\,\text{mm}$ for the insulated section and $\lambda_2 = 41\,\text{mm}$ for the un-insulated section. Fig. 4d shows the amount of cooling achieved at the tip of the probe for various probe lengths. For experiments that deep target structures (e.g. 8 mm), the amount of cooling may be insufficient. In such case, it may be necessary to increase the diameter of the probe and its insulation.

Performance of the implemented devices

We constructed two types of miniature devices for brain cooling in the zebra finch (Fig. 5) – one for targeting a superficial nucleus HVC using the planar geometry (Section 6) and another for targeting nucleus LMAN 2 mm deep in the brain using cylindrical geometry (Section 7). In the following sections, we characterize temperature changes produced by these devices in awake juvenile birds using small thermocouples implanted in the brain (see Methods) or attached to the devices themselves.

13. Device for HVC cooling

Our device achieves HVC cooling via metal plates pressed against the surface of the brain (see Methods). To characterize the performance of this device, we measured temperatures of these cooling plates at various amounts of electric current in 3 birds. In 2 of these birds, we also measured temperature near the center of HVC, about 500 μm below the cooling plates in the brain. Fig. 6a shows temperature measurements at these two locations. For each amount of current, we estimated the steady-state temperature by fitting an exponential to measurements in the last 70 s of the corresponding current pulse (Fig. 6b).

Following a change in current, temperature typically achieved values close to the steady-state within 10-20 s. At currents of -1.5 A and above, temperature following these initial changes was relatively stable, typically drifting by less than 1°C during a 100-s current pulse. As expected, convective heat loss from the device produced slight cooling even at zero current. At about 0.5 A, however, heating maintained the cooling plates and HVC close to normal body temperature. Optimal cooling by roughly 10°C at the cooling plate was achieved at about -1.5 A. At the center of HVC, temperature changes were roughly 3/4 of those at the cooling plate. Given a distance of 500 μm, this fraction is accurately predicted by an exponential fall-off with a space constant of $\lambda = 1.59\,\text{mm}$ (Section 6).

In order to maximize the range of achieved temperatures for our behavioral measurements (see Chapter 4), we flipped current between 0.5 and -1.5 A every 100 s. Fig. 6c shows temperature changes produced by this protocol. The total range of temperatures was about 10°C at the cooling plate and about 7°C in the center of HVC. To

ensure that temperature has reached values close to the steady state, we only used data recorded during the last 80 s of each current pulse.

14. Device for LMAN cooling

In 4 additional birds, we measured temperature changes produced by the device for LMAN cooling. LMAN is located ~2 mm deep in the brain and is therefore cooled by implanting thermally conductive probes into the brain (see Methods). Figs. 6d,e show temperature measurements at the cold plate of the device, at the tip of the probe, and at about 500 μm from the surface of the probe in the brain. Timecourses of temperature changes were similar to those produced by the HVC cooling device described above. At the cold plate, optimal cooling by roughly 15°C was achieved at currents near -1.5 A. As expected, temperature changes at the tip of the probe were smaller, resulting in roughly 11°C of cooling. These values are remarkably similar (within 1°C) to those predicted by the thermal model of the "core" device described in the previous section. Also according to expectations, temperature fall-off in cylindrical coordinates was substantially greater than in the planar coordinates – only about 4°C of cooling were achieved at 500 μm from the surface of the probe in the brain.

Because temperature changes greatly with distance from a cooling probe, average amount of cooling achieved in LMAN depends on the exact positioning of the probes within the nucleus (see Chapter 4 for details). Therefore, it is important to precisely characterize this spatial relationship. We measured temperature at various distances of up to 1 mm from the probes. Fig. 6f shows temperature measurement at three of the locations, during the current protocol described above (flipping between 0.5 and -1.5 A

every 100 s). About 10°C of cooling were achieved near the probe, but temperature fell off steeply with increasing distances – to about half this amount at 300 μm from the probe. The fall-off became more gradual beyond this range; about 3°C of cooling were achieved at 1 mm from the probe. These values close to those predicted by the thermal diffusion model in cylindrical coordinates described above (Section 7).

Methods

We constructed two small Peltier thermoelectric devices for bilaterally cooling brain areas in juvenile zebra finches. One device was used for cooling HVC, which is located near the surface of the brain. The other device was used for cooling LMAN, which is located ~2 mm deep in the brain.

Device construction

We constructed a small Peltier thermoelectric device (Fig. 5a,b) using commercially-available bismuth-telluride (Bi_2Te_3) semiconductor elements (Custom Thermoelectric). These elements were trimmed using a razor blade to a 1.5x1.5 mm cross-sectional area, 1.35 mm height, achieving an approximate value of G=1.7 mm. A single p-type and a single n-type element (N=1 junction) were soldered to metalized pads on a thermally-conductive ceramic "hot plate" (8x8 mm) using bismuth-tin solder (Custom Thermoelectric). The distance between the two elements was ~1 mm. Note that complete miniature thermoelectric modules with larger values of N and similar values of the product NG are also commercially available and can be used instead of this process. This allows the use of smaller currents to achieve optimal cooling (see Section 10).

To deliver current to the device, we soldered a miniature connector (Omnetics) to the hot plate, making electrical contacts with the two semiconductor elements. For HVC cooling (Fig. 5a), a thin annealed silver sheet (1x10 mm, 5 mil thick) was soldered to the bottom of the semiconductor blocks. The sheet was gold-plated (cyanide-free gold-plating solution; Neuralynx) to prevent silver toxicity and bent to form two cooling pads (1x2 mm) with 3 mm spacing between the inner edges.

For LMAN cooling (Fig. 5b), a small stainless-steel "cold plate" instead of the silver sheet was soldered to the bottom of the semiconductor blocks. Two sharpened gold-plated annealed silver wires (250 μm diameter, 3.5 mm long) were soldered to the cold plate. These wires were thermally insulated with polyimide tubing (1 mil-thick walls), with an inner diameter of 320 μm, leaving 35 μm of air between the wire and the inner surface of the polyimide tube. The last 1 mm of each wire was left un-insulated, and the bottom tip of each polyimide tube was sealed with a drop of a silicone elastomer (KwikCast, WPI). The un-insulated segments of the wires were inserted bilaterally into LMAN. For both HVC and LMAN cooling devices, the semiconductor blocks and the cold plate were insulated with a 1 mm-thick layer of Styrofoam, which was further coated with a thin layer of KwikCast for moisture sealing.

A convective heat sink was constructed by soldering a copper wire mesh (2 mil wires, 200 threads per inch; from TWP) around the perimeter of the hot plate, extending 8 mm above the device. Thin silver strips were soldered to the edges of the mesh (above the corners of the hot plate) for structural support, as well as to improve thermal conduction away from the hot plate. At two locations, the top of the mesh was also glued to the connector to improve structural stability.

A body-coupled heat sink was constructed from a 5-mil annealed silver sheet, which soldered to the hot plate on one end. At the other end, the sheet was cut longitudally into 1 mm-thin strips. These strips were bent to follow the curvature of the skull, forming contact with a total surface area of ~6x8 mm. The space between the silver and the skull surface (~200 μm) was filled with light-cured dental acrylic (Pentron Clinical) to facilitate heat transfer. Note that acrylics that use methyl methacrylate are not

compatible with this device because methyl methacrylate fumes dissolve Styrofoam insulation.

Surgery

Subjects were juvenile zebra finches (male or female, 35-50 days-post-hatch). Birds were obtained from the Massachusetts Institute of Technology breeding facility. Animal care and experiments were carried out in accordance with the National Institute of Health guidelines and approved by the local Institutional Animal Care and Use Committee.

Birds were anesthetized and placed in a stereotaxic apparatus. Craniotomies were made bilaterally, and HVC or LMAN were targeted using stereotaxic coordinates. For HVC cooling, 1x2 mm windows of the skull over HVC were thinned using a dental drill, and the cooling pads of the device were placed in contact with these windows. For LMAN cooling, small (~400x400 μm) craniotomies were made above LMAN and probes were slowly inserted into the brain, advancing by 100-200 μm per minute. Probe tips were implanted 2.5 mm deep, such that the un-insulated segments of the probes spanned the dorso-ventral extent of LMAN (1.5 - 2.5 mm deep).

Calibration of temperature in the brain

For temperature calibrations, measurements were made with thin (40-gauge) thermocouples (Omega) implanted in the brain. Following surgery, birds were placed into a foam restraint and allowed to recover from anesthesia for 10 min. Various amounts of stable DC current (see text) were passed through the device using a current source

(Lambda). Temperature measurements were acquired at 100 samples/s and recorded with custom-written software in Matlab. Following temperature calibration, birds were sacrificed and the distance between the device and the thermocouple was verified by taking x-ray images of the bird.

Measurement of semiconductor properties

To estimate properties of semiconductor elements we constructed a device without cooling pads or probes, but with Styrofoam insulation covering the cold plate (Fig. S1a). We placed the hot plate in contact with the surface of a large water bath to maintain it at near-constant temperature and used two thermocouples to simultaneously monitor the temperatures of the hot and cold plates. We varied the current I flown through the device from -10 to 5A in steps of 0.1A and measured the difference ΔT between the hot- and cold-plate temperatures. We also used an instrumentation amplifier to measure the voltage drop across the two elements. Each current was passed for 90 s; steady-state voltage and temperatures were calculated by taking the average in the last 60 s of each current pulse.

At currents near zero, voltage across the device changed linearly with current (Fig. S1b). We estimated the slope of this relationship in the temperature range relevant for our experiments (25-42°C of the average temperature between the hot and cold plates). Using this slope, we estimated the electrical resistivity ρ in this temperature range to be about 1740 μΩ cm. According to Eqn. 3-2, we fit a quadratic function to the relationship between ΔT and I (Fig. S1c). Using the coefficients of this fit, we estimated the Seebeck coefficient of the semiconductor material to be 148 μV/K and the thermal

conductivity to be 1.38 W m^{-1} K^{-1}. The estimated value of the Seebeck coefficient is somewhat lower (by ~25%) that the values typically reported in the literature (Rowe 1995; Kondratiev & Yershova 2001); the estimated value of the electrical resistivity is about 50% higher. These differences could be due to the influences of some aspects of our device construction (such as the solder joints) on performance.

Measurement of heat sink conductances

We sought to roughly estimate the thermal conductances K_B of the body-coupled heat sink and K_C of the convective heat sink in our device (Fig. 1d). For this, we constructed devices identical to our normal devices, but with no probes or cooling pads attached, and with surface-mount resistors (total resistance R=10 Ω) soldered to the hot plate instead of the similarly-sized semiconductor elements. For any given current I passed through the device, this allowed us to estimate the total power ($P = I^2R$) dissipated by the device. Resistors were insulated with a 1-mm thick layer of Styrofoam. Devices were attached to the cranium in 3 birds and a thermocouple (see above) was used to monitor the temperature of the hot plate. Brain and air temperatures were simultaneously monitored with two additional thermocouples. These latter two temperatures remained roughly constant throughout the experiment (~41°C for the brain, ~23°C for air).

We measured the temperature drop ΔT_1 from the hot plate to the air and the drop ΔT_2 from the hot plate to the brain. For a given amount of power P generated by current flow through the device, the equivalent thermal circuit (Fig. 1d) implies the relationship $P = \Delta T_1 K_C + \Delta T_2 K_B$. We took two measurements – one at zero current (generating P=0

mW) and one at a current generating P=200-250 mW of power – and used this relationship to solve for K_B and K_C. In the 3 birds, values of K_B were 9.2, 6.9, and 7.4 mW/K, and values of K_C were 6.2, 4.8, and 5.1 mW/K. For the simulation of our "core" device, we used approximate median values $K_B = 7\,\text{mW/K}$ and $K_C = 5\,\text{mW/K}$.

Parameter	Description	Value	Comment
Semiconductor properties			
α	Seebeck coefficient	148 μV K^{-1}	Measured (see Methods)
ρ	electrical resistivity	1740 μΩ cm	Measured (see Methods)
κ	thermal conductivity	1.38 W m^{-1} K^{-1}	Measured (see Methods)
G	geometric constant	1.7 mm	Dimensions (l×w×h): 1.5×1.5×1.35 mm
N	number of junctions	1	Two blocks (one each of n- and p-type)
Heat sink properties			
K_B	thermal conductance (body-coupled heat sink)	7 mW K^{-1}	Measured (see Methods)
K_C	thermal conductance (convective heat sink)	5 mW K^{-1}	Measured (see Methods)
ΔT_F	temperature of convective fluid relative to body	-18 °C	Air at room temperature (23°C)
Probe properties			
r_P	radius	125 μm	
l_0	length of segment above the brain	1.0 mm	
l_1	length of insulated segment	1.5 mm	
l_2	length of un-insulated segment	1.0 mm	Center of segment is 2.0 mm deep
κ_P	thermal conductivity of material (silver)	429 W m^{-1} K^{-1}	
N_P	number of probes	2	For bilateral cooling
Insulation properties			
K_I	thermal conductance of cold-plate insulation	0.17 mW K^{-1}	For Styrofoam sheet: 5mm^2 area, 1mm thick
r_1	outer radius of 1st insulation layer (air)	160 μm	
κ_1	thermal conductivity of air	0.025 W m^{-1} K^{-1}	
r_2	outer radius of 2nd insulation layer (polyimide)	185 μm	
κ_2	thermal conductance of polyimide	0.12 W m^{-1} K^{-1}	
Brain properties			
λ	length constant	1.59 mm	From data in (Long & Fee 2008)
κ_B	thermal conductivity	0.54 W m^{-1} K^{-1}	(Duck 1990)
T	baseline temperature	314 K	(Bech & Midtgård 1981)

Figure 1. Analysis of the thermoelectric device using equivalent thermal circuits. (a) Schematic of a device. Electric current flows back-and-forth between the hot and the cold plates along semiconductor elements. Peltier effect cools the cold plate and heats up the hot plate. One semiconductor pair (N=1) is shown. The device is attached to a perfect heat sink, represented by "grounding" the hot plate. (b) Equivalent thermal circuit for the device shown in (a). Semiconductor elements are represented by a thermal conductance. Heat is pumped from the cold plate due to the Peltier effect ($\dot{Q}_{\text{Peltier}}$). Equal amounts of Ohmic heat ($\dot{Q}_{\text{Ohmic}}$) are transferred to each of the plates. (c) Schematic of the steady-state temperature achieved at the cold plate for an isolated device and for the same device attached to a thermal load. Optimal cooling is achieved at current I_{opt}. (d) Equivalent circuit for a device attached to a load, represented by a conductance K_L. (e) Equivalent circuit of a device with non-ideal heat sinks represented by conductances: K_B is a body-coupled heat sink; K_C is a convective heat sink, cooled by a fluid of temperature ΔT_F below the body temperature. (f) Equivalent circuit of the load on the cold plate in the planar geometry. Insulation is represented by a thermal conductance K_I in parallel with the brain. (g) Equivalent circuit of the load on the cold plate in cylindrical geometry. Only one probe is shown. The probe has axial thermal conductivity (vertical resistors) that depends on its radius r_P and material conductivity κ_P. Segments within the brain also have substantial surface conductivity (κ_S for the un-insulated segment and κ'_S for the insulated one), expressed per unit length of the probe. From the surface of an insulated probe, conductances of insulation layers act in series with the brain conductance.

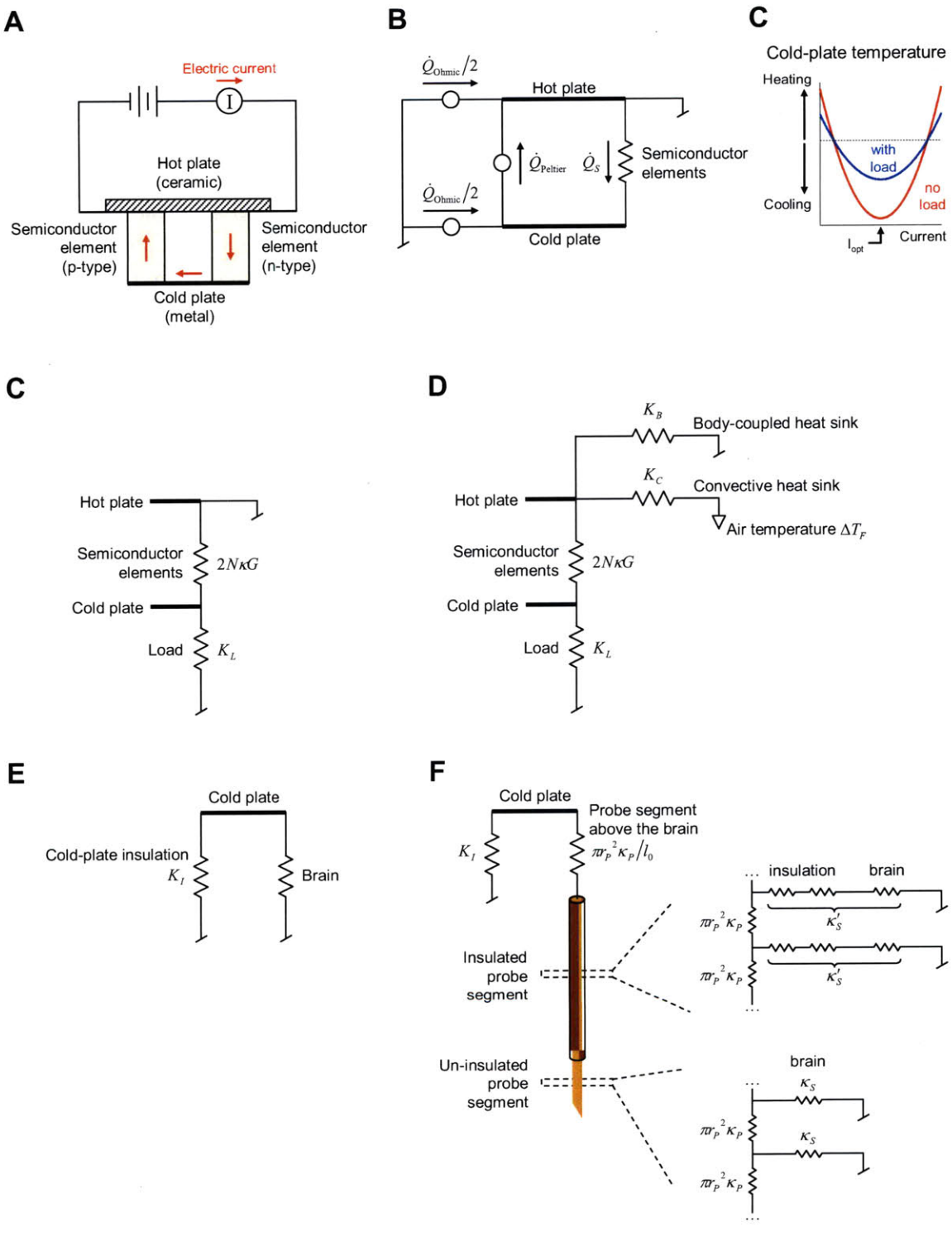
A
Electric current
I
Hot plate
(ceramic)
Semiconductor
element
(p-type)
Semiconductor
element
(n-type)
Cold plate
(metal)
B
$\dot{Q}_{\text{Ohmic}}/2$
Hot plate
$\dot{Q}_{\text{Peltier}}$
$\dot{Q}_S$
Semiconductor
elements
$\dot{Q}_{\text{Ohmic}}/2$
Cold plate
C
Cold-plate temperature
Heating
Cooling
with
load
no
load
I_{opt}
Current
C
Hot plate
Semiconductor
elements
$2N\kappa G$
Cold plate
Load
K_L
D
K_B
Body-coupled heat sink
K_C
Convective heat sink
Hot plate
Air temperature ΔT_F
Semiconductor
elements
$2N\kappa G$
Cold plate
Load
K_L
E
Cold plate
Cold-plate insulation
K_I
Brain
F
Cold plate
Probe segment
above the brain
K_I
$\pi r_P^2 \kappa_P / l_0$
insulation
brain
Insulated
probe
segment
$\pi r_P^2 \kappa_P$
κ'_S
$\pi r_P^2 \kappa_P$
κ'_S
Un-insulated
probe
segment
brain
κ_S
$\pi r_P^2 \kappa_P$
κ_S
$\pi r_P^2 \kappa_P$

Figure 2. Influence of semiconductor geometry on device performance. (a) Steady-state temperature of the cold plate ΔT_C as a function of current flow through the device, for three values of the geometric constant *G*. Geometric constant of the semiconductor elements effect the minimum-achievable temperature. (b) Minimum achievable ΔT_C as a function of *G*. The lowest temperature is achieved for $G \approx 1.7\,\text{mm}$. (c) Relationship between the minimum achievable ΔT_C and *G* for different conductances of the load K_L on the cold plate. Lower values of *G* are optimal for smaller loads. (d) Relationship between the minimum achievable ΔT_C and *G* for different conductances of the convective heat sink K_C. Larger values of *G* are optimal for more efficient heat sinks. (e) Relationship between ΔT_C and current for three devices with different numbers of semiconductor junctions (*N*). For each device, the value of *G* is scaled by *N* such that the overall surface area of the semiconductors remains the same. Devices achieve identical temperatures at the cold plate, but less current is required to achieve the minimum temperature for devices with more semiconductor junctions.

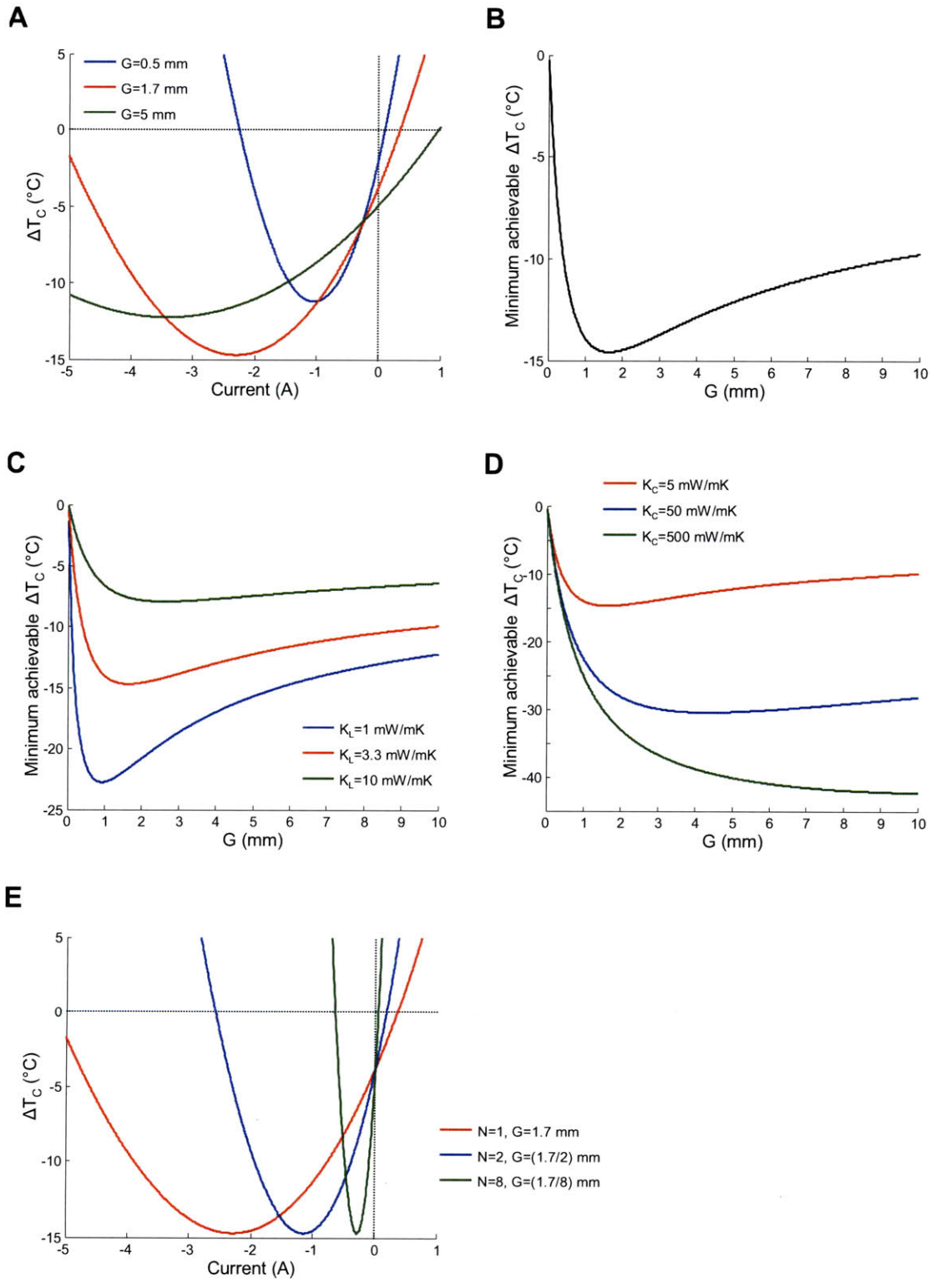
A
G=0.5 mm
G=1.7 mm
G=5 mm
ΔT_C (°C)
Current (A)
B
Minimum achievable ΔT_C (°C)
G (mm)
C
Minimum achievable ΔT_C (°C)
K_L=1 mW/mK
K_L=3.3 mW/mK
K_L=10 mW/mK
G (mm)
D
K_C=5 mW/mK
K_C=50 mW/mK
K_C=500 mW/mK
Minimum achievable ΔT_C (°C)
G (mm)
E
ΔT_C (°C)
Current (A)
N=1, G=1.7 mm
N=2, G=(1.7/2) mm
N=8, G=(1.7/8) mm

Figure 3. Influence of heat sinks on device performance. (a) Minimum steady-state temperature achievable at the cold plate, ΔT_C as a function of two heat sink conductances: conductance of the body-coupled heat sink K_B and conductance of the convective heat sink K_C. At small conductance values, improving either heat sink lowers the minimum achievable temperature at the cold plate. However, when the convective heat sink is efficient (>~20 mW/K), attaching a body-coupled heat sink does not improve performance. Contours are spaced at intervals of 2°C. (b) Effects of including or omitting small body-coupled (7 mW/K) and convective (5 mW/K) heat sinks. For each combination of heat sinks, the steady-state temperature at the cold plate is shown as a function of current flown through the device. The lowest temperature is achievable when both heat sinks are included (red trace). The optimal performance of such device is only marginally better than that of the device with the convective heat sink alone (green trace); however, including both heat sinks substantially reduces the amount of cooling at zero current.

A

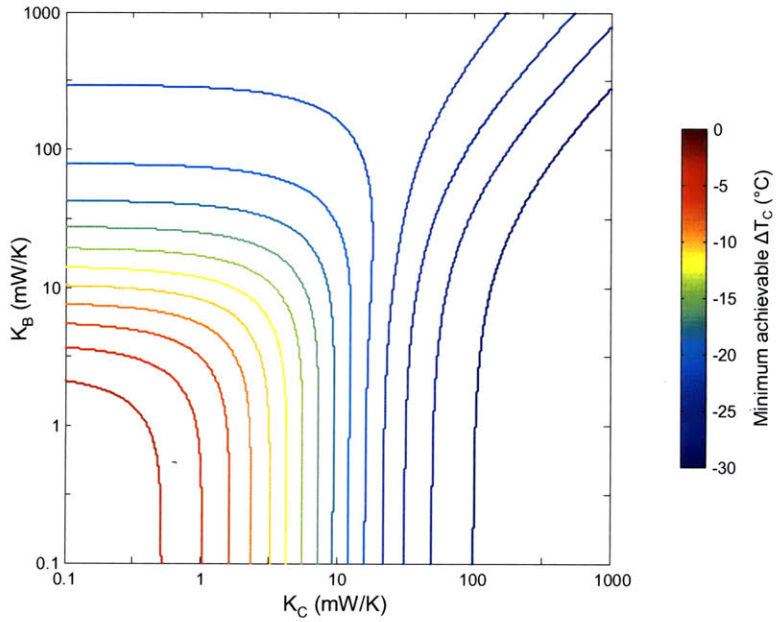

B

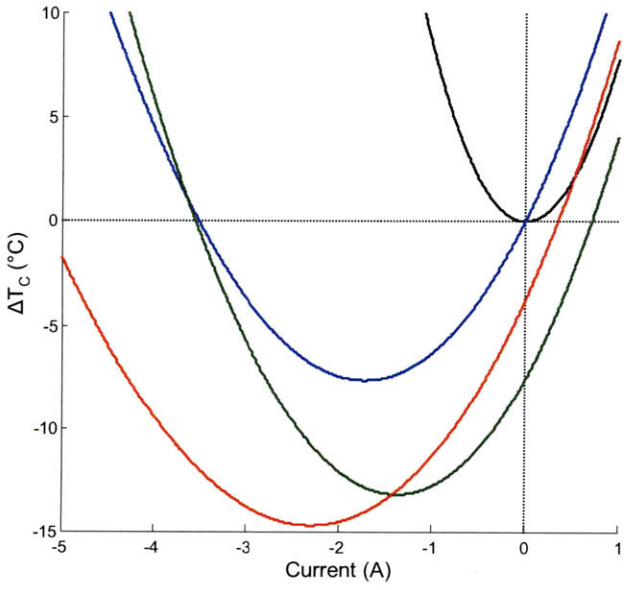

Heat sinks	K_B (mW/K)	K_C (mW/K)
none	0	0
body-coupled	7	0
convective	0	5
both	7	5

Figure 4. Influence of probe properties on device performance in cooling deep brain structures. (a) Effectiveness of various probe insulations in the brain. Leftmost plot shows the spatial profile of the steady-state temperature in the brain near an un-insulated probe. The three rightmost plots shown this profile for probes insulated with a polyimide tube (25 μm-thick wall), with different amounts of air insulation (0, 35, and 75 μm) between the probe and the polyimide tube. (b) Minimum temperature achievable in the brain (2 mm deep, 200 μm from the central axis of the probe), for different dimensions of the probe and the insulation. For each configuration, the polyimide wall is 25 μm thick and the space between the probe surface and the inner polyimide wall is filled with air. Contours are spaced at intervals of 0.5°C. (c) Effects of varying probe diameter while holding the polyimide tube diameter fixed, for different polyimide tubes. An optimum probe diameter exists for each polyimide tube. (d) Temperature profile along the length of the probe, for various probe lengths. For each probe, the initial 1-mm segment is above the brain and the final 1-mm segment is un-insulated, such that the targeted depth is at the center of the un-insulated segment. The rest of the probe is insulated.

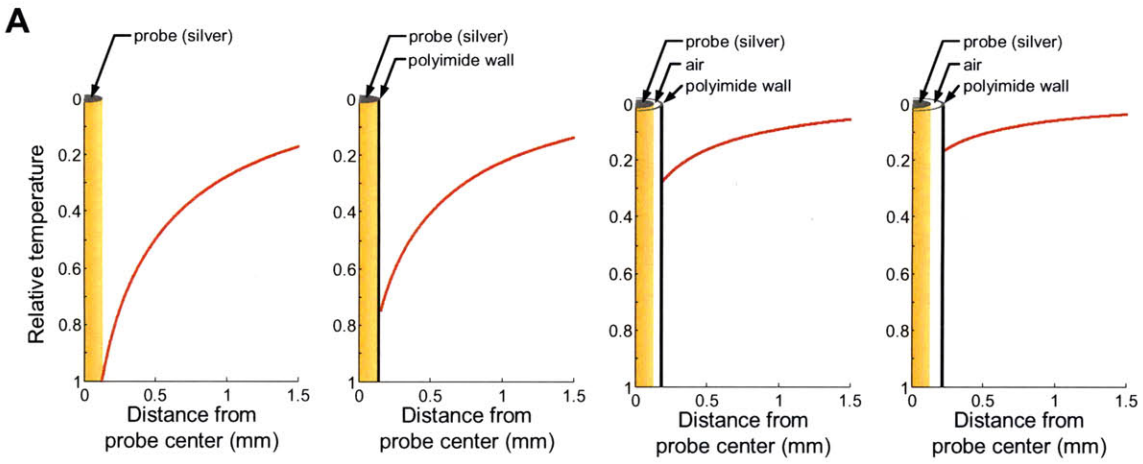
A
probe (silver)
polyimide wall
air
Relative temperature
Distance from probe center (mm)

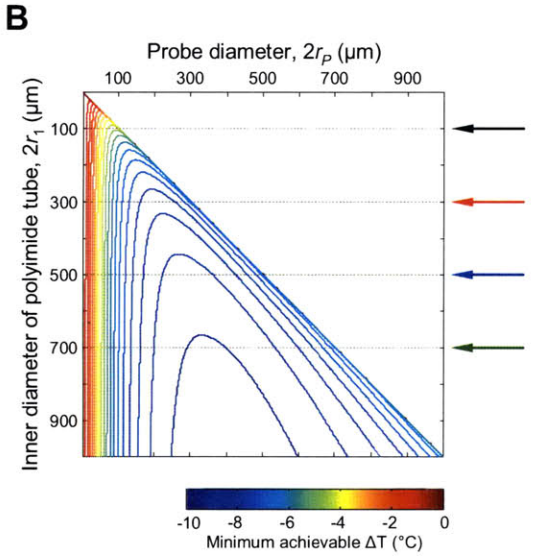
B
Probe diameter, $2r_P$ (μm)
Inner diameter of polyimide tube, $2r_1$ (μm)
Minimum achievable ΔT (°C)

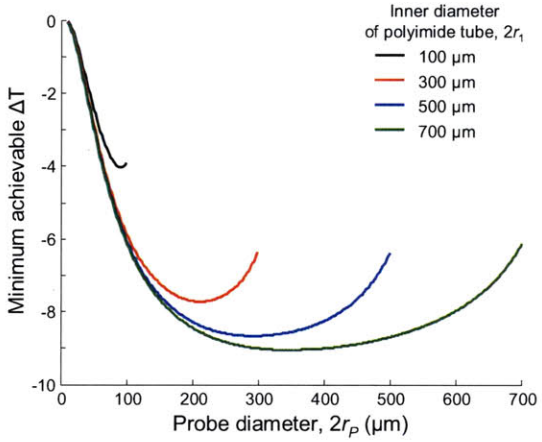
C
Inner diameter of polyimide tube, $2r_1$
100 μm
300 μm
500 μm
700 μm
Minimum achievable ΔT
Probe diameter, $2r_P$ (μm)

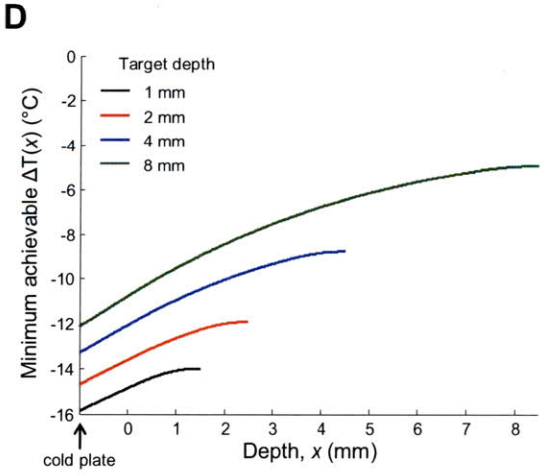
D
Target depth
1 mm
2 mm
4 mm
8 mm
Minimum achievable ΔT(x) (°C)
cold plate
Depth, x (mm)

Figure 5. Implementation of the Peltier thermoelectric devices. (a) Schematic of the device for cooling a structure located close to the surface of the brain (HVC) using cooling pads placed against thinned areas of the cranium. (b) Schematic of the device for cooling a structure deep in the brain (LMAN) using thermally conductive probes.

A

Peltier device for HVC cooling

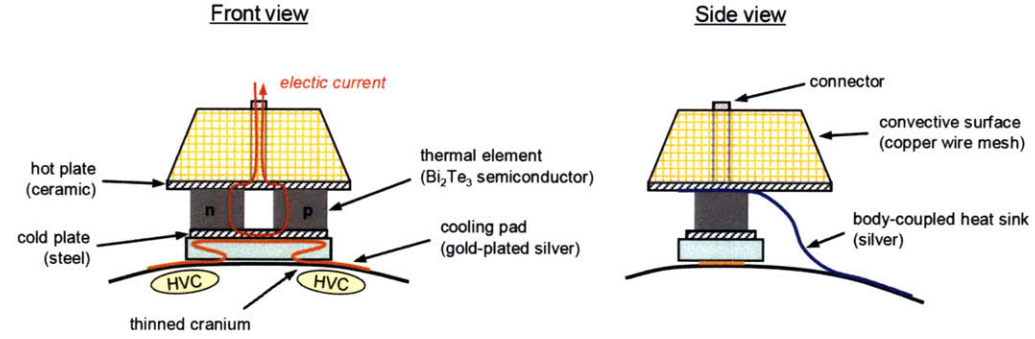

B

Peltier device for LMAN cooling

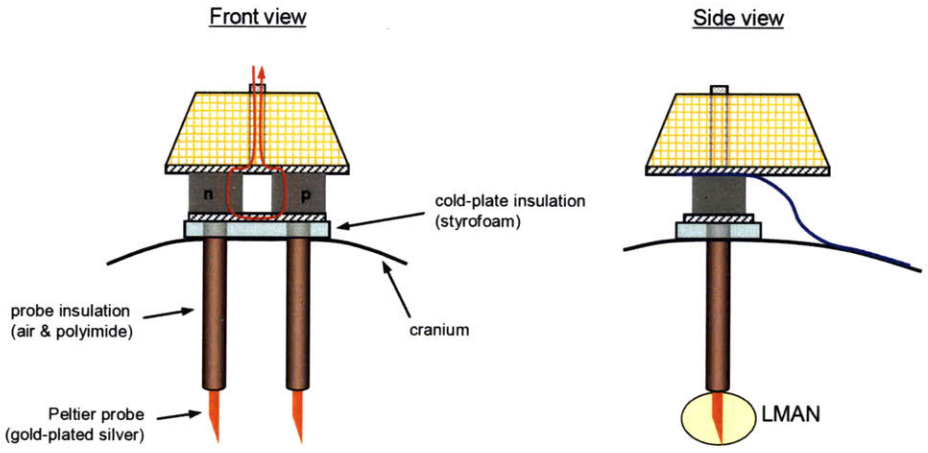

Figure 6. Measurements of temperature produced by thermoelectric devices. (a) Temperature at the cooling plate and in HVC at various amounts of current flown through the HVC cooling device. The amount of current is changed every 100 s, decreasing from 1 to -2.5 A in steps on 0.5 A. (b) Steady-state temperature as a function of current at the two locations. Steady-state is estimated by fitting an exponential curve to the last 70 s of each current pulse in (a). (c) Temperature at the same two locations during an experiment in which current is flipped between 0.5 and -1.5 A every 100 s. (c-d) Temperatures at the cold plate of the LMAN cooling device, at the probe tip, and at 500 μm away from the surface of the probe. Data are estimated and plotted as in (a-b). (e) Temperature at three distances from the probe surface of the LMAN cooling device, for the same experiment as in (c).

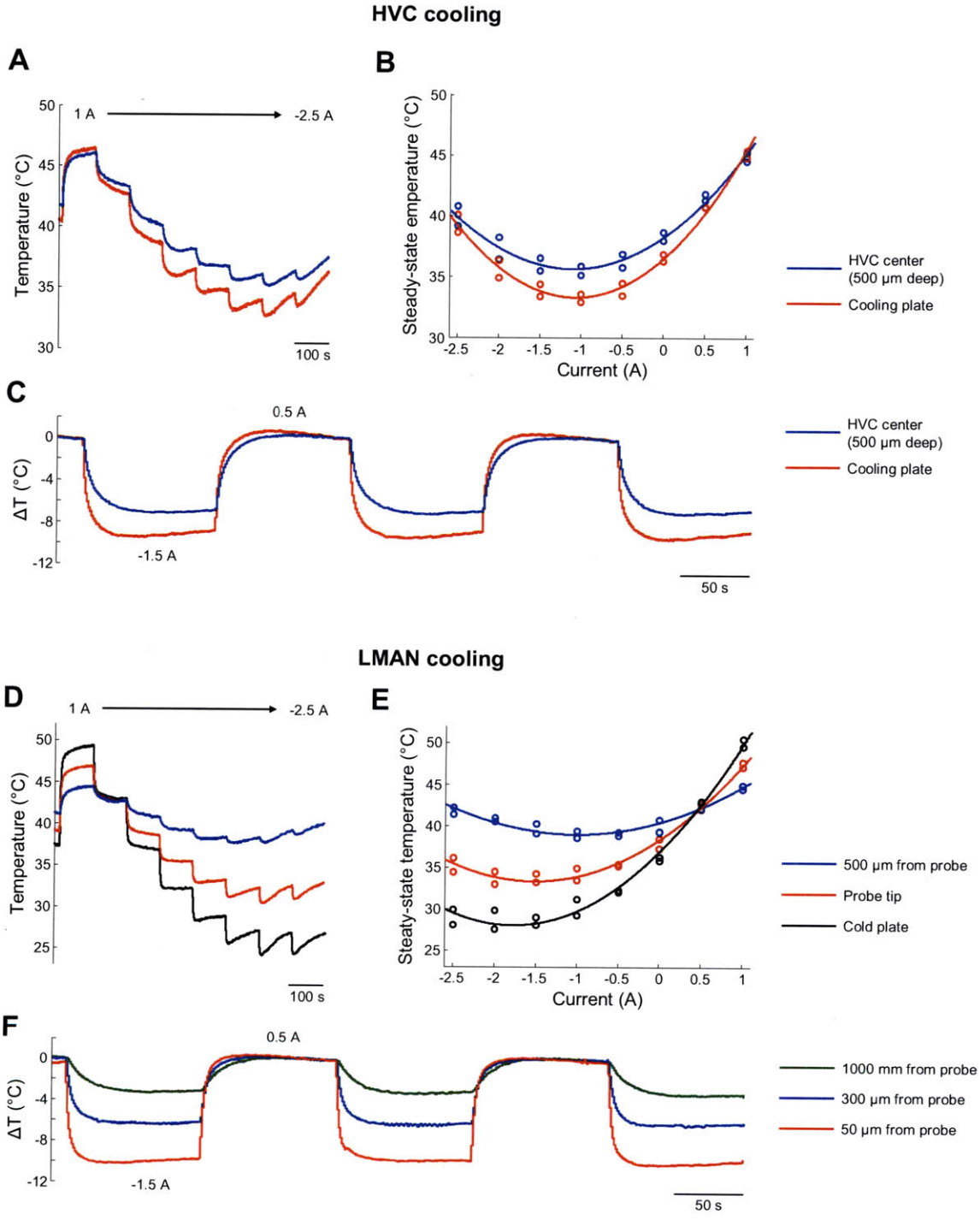
HVC cooling
A
1 A
-2.5 A
Temperature (°C)
100 s
B
Steady-state emperature (°C)
Current (A)
HVC center
(500 µm deep)
Cooling plate
C
0.5 A
ΔT (°C)
-1.5 A
50 s
HVC center
(500 µm deep)
Cooling plate
LMAN cooling
D
1 A
-2.5 A
Temperature (°C)
100 s
E
Steaty-state temperature (°C)
Current (A)
500 µm from probe
Probe tip
Cold plate
F
0.5 A
ΔT (°C)
-1.5 A
50 s
1000 mm from probe
300 µm from probe
50 µm from probe

Figure S1. Estimation of semiconductor properties. (a) Schematic of the setup. Electric current is flown through a small Peltier device that contains a single pair of p- and n-doped semiconductor elements. The hot plate of the device is maintained at a near-constant temperature using a large water bath; the cold-plate is insulated with Styrofoam. Temperatures of both the hot and cold plates are monitored with small thermocouples to estimate the temperature difference ΔT between them. An instrumentation amplifier is also used to record the voltage drop across the device. (b) Steady-state voltage across the device at different values of current. Blue symbols: average steady-state values. Red line: linear fit to the data in the relevant range (see text). Note that the data deviate from the linear fit, likely due to the temperature sensitivity of the semiconductor material. (c) Steady-state temperature difference between the hot and the cold plates at different amounts of current. Blue symbols: average steady-state values. Red curve: quadratic fit to the data (see text).

A

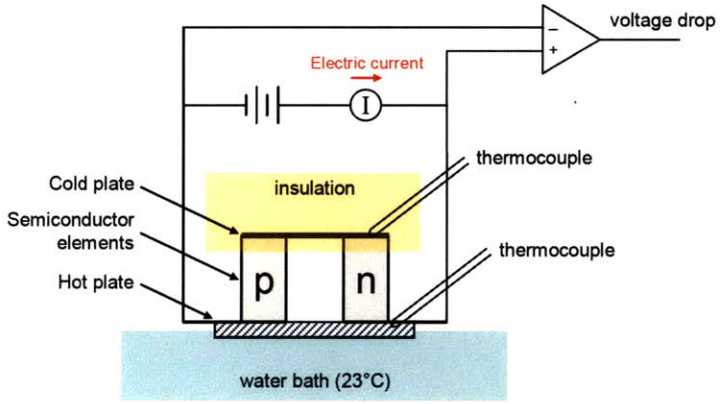
voltage drop
Electric current
I
thermocouple
Cold plate
insulation
Semiconductor elements
thermocouple
Hot plate
p
n
water bath (23°C)

B

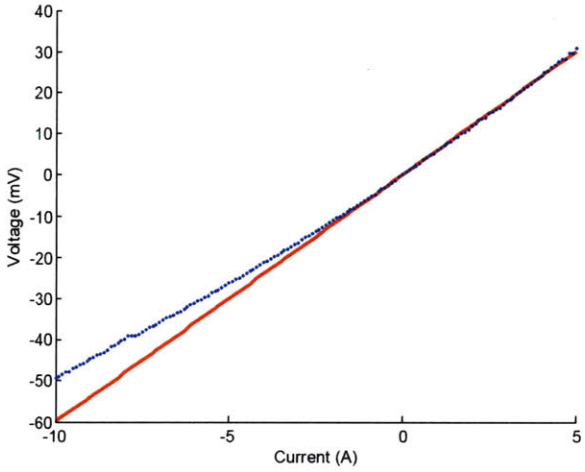
Voltage (mV)
Current (A)

C

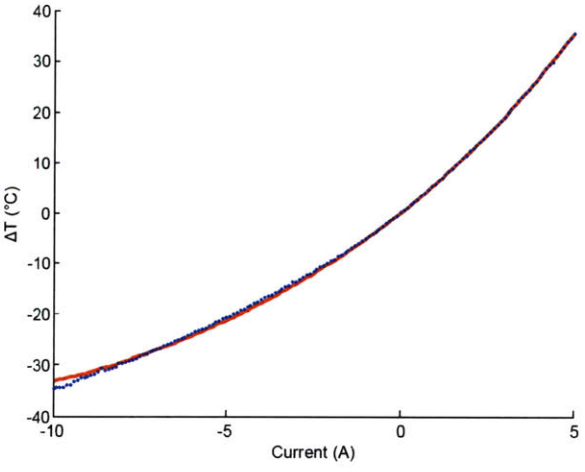
ΔT (°C)
Current (A)

Bibliography

Abeles, M., 1991. *Corticonics*, Cambridge University Press.

Akutagawa, E. & Konishi, M., 1994. Two separate areas of the brain differentially guide the development of a song control nucleus in the zebra finch. *Proc Natl Acad Sci*, 91(26), 12413-12417.

Alvarez-Buylla, A., Ling, C.Y. & Nottebohm, F., 1992. High vocal center growth and its relation to neurogenesis, neuronal replacement and song acquisition in juvenile canaries. *J Neurobiol*, 23(4), 396-406.

Andalman, A.S. & Fee, M.S., 2009. A basal ganglia-forebrain circuit in the songbird biases motor output to avoid vocal errors. *Proc Natl Acad Sci*, 106(30), 12518-12523.

Arbas, E.A. & Calabrese, R.L., 1984. Rate modification in the heartbeat central pattern generator of the medicinal leech. *J Comp Physiol A*, 155(6), 783-794.

Aronov, D., Andalman, A.S. & Fee, M.S., 2008. A specialized forebrain circuit for vocal babbling in the juvenile songbird. *Science*, 320(5876), 630-634.

Ashmore, R.C., Renk, J.A. & Schmidt, M.F., 2008. Bottom-up activation of the vocal motor forebrain by the respiratory brainstem. *J Neurosci*, 28(10), 2613-2623.

Ashmore, R.C., Wild, J.M. & Schmidt, M.F., 2005. Brainstem and forebrain contributions to the generation of learned motor behaviors for song. *J Neurosci*, 25(37), 8543-8554.

Bauer, M. & von Helversen, O., 1987. Separate localization of sound recognizing and sound producing neural mechanisms in a grasshopper. *J Comp Physiol A*, 161(1), 95-101.

Bech, C. & Midtgård, U., 1981. Brain temperature and therete mirabile ophthalmicum in the Zebra finch (Poephila guttata). *J Comp Physiol B*, 145(1), 89-93.

Bekoff, M. & Byers, J.A., 1998. *Animal play*, Cambridge University Press.

Bonifazi, P. et al., 2009. GABAergic hub neurons orchestrate synchrony in developing hippocampal networks. *Science*, 326(5958), 1419-1424.

Bottjer, S.W. et al., 1989. Axonal connections of a forebrain nucleus involved with vocal learning in zebra finches. *J Comp Neurol*, 279(2), 312-326.

Bottjer, S.W., Miesner, E.A. & Arnold, A.P., 1984. Forebrain lesions disrupt development but not maintenance of song in passerine birds. *Science*, 224(4651), 901-903.

Bowman, F., 1958. *Introduction to Bessel functions*, Courier Dover Publications.

Buzsáki, G., 2006. *Rhythms of the brain*, Oxford University Press US.

Cardin, J.A. et al., 2009. Driving fast-spiking cells induces gamma rhythm and controls sensory responses. *Nature*, 459(7247), 663-667.

Chafee, M.V. & Goldman-Rakic, P.S., 2000. Inactivation of Parietal and Prefrontal Cortex Reveals Interdependence of Neural Activity During Memory-Guided Saccades. *J Neurophysiol*, 83(3), 1550-1566.

Chi, Z. & Margoliash, D., 2001. Temporal precision and temporal drift in brain and behavior of zebra finch song. *Neuron*, 32(5), 899-910.

Coleman, M.J. & Vu, E.T., 2005. Recovery of impaired songs following unilateral but not bilateral lesions of nucleus uvaeformis of adult zebra finches. *J Neurobiol*, 63(1), 70-89.

Crépel, V. et al., 2007. A parturition-associated nonsynaptic coherent activity pattern in the developing hippocampus. *Neuron*, 54(1), 105-120.

Davis, B.L. & MacNeilage, P.F., 1995. The Articulatory Basis of Babbling. *J Speech Hear Res*, 38(6), 1199-1211.

Dayan, P. & Abbott, L.F., 2001. *Theoretical Neuroscience*, MIT Press.

Derégnaucourt, S. et al., 2005. How sleep affects the developmental learning of bird song. *Nature*, 433(7027), 710-716.

Doupe, A.J. & Kuhl, P.K., 1999. Birdsong and human speech: common themes and mechanisms. *Annu Rev Neurosci*, 22, 567-631.

Doya, K. & Sejnowski, T., 1995. A novel reinforcement model of birdsong vocalization learning. In G. Tesauro, D. S. Tourezky, & T. K. Leen, eds. *Advances in Neural Information Processing Systems*. Cambridge, MA: MIT Press, pp. 101-108.

Drai, D., Benjamini, Y. & Golani, I., 2000. Statistical discrimination of natural modes of motion in rat exploratory behavior. *J Neurosci Methods*, 96(2), 119-131.

Drew, P.J. & Abbott, L.F., 2006. Models and properties of power-law adaptation in neural systems. *J Neurophysiol*, 96(2), 826-833.

Duck, F.A., 1990. *Physical properties of tissue*, Academic Press.

Edelman, G., 1987. *Neural Darwinism: The Theory Of Neuronal Group Selection* First Edition., Basic Books.

Elowson, M.A., Snowdon, C.T. & Lazaro-Perea, C., 1998. `Babbling' and social context in infant monkeys: parallels to human infants. *Trends Cogn Sci*, 2(1), 31-37.

Eyre, J.A. et al., 2000. Functional corticospinal projections are established prenatally in the human foetus permitting involvement in the development of spinal motor centres. *Brain*, 123 (Pt 1), 51-64.

Fagen, R., 1981. *Animal Play Behavior*, Oxford University Press, USA.

Farries, M.A., Ding, L. & Perkel, D.J., 2005. Evidence for "direct" and "indirect" pathways through the song system basal ganglia. *J Comp Neurol*, 484(1), 93-104.

Farries, M.A. & Perkel, D.J., 2002. A telencephalic nucleus essential for song learning contains neurons with physiological characteristics of both striatum and globus pallidus. *J Neurosci*, 22(9), 3776-3787.

Fee, M.S. & Leonardo, A., 2001. Miniature motorized microdrive and commutator system for chronic neural recording in small animals. *J Neurosci Methods*, 112(2), 83-94.

Fee, M.S. et al., 1998. The role of nonlinear dynamics of the syrinx in the vocalizations of a songbird. *Nature*, 395(6697), 67-71.

Fee, M.S., Kozhevnikov, A.A. & Hahnloser, R.H.R., 2004. Neural mechanisms of vocal sequence generation in the songbird. *Ann N Y Acad Sci*, 1016, 153-170.

Feenders, G. et al., 2008. Molecular mapping of movement-associated areas in the avian brain: a motor theory for vocal learning origin. *PloS One*, 3(3), e1768.

Feng, A.S., 1976. The effect of temperature on a social behavior of weakly electric fish Eigenmannia virescens. *Comp Biochem Physiol A: Comp Physiol*, 55(2), 99-102.

Ferster, D., Chung, S. & Wheat, H., 1996. Orientation selectivity of thalamic input to simple cells of cat visual cortex. *Nature*, 380(6571), 249-252.

Fiete, I.R. et al., 2010. Spike-time-dependent plasticity and heterosynaptic competition organize networks to produce long scale-free sequences of neural activity. *Neuron*, 65(4), 563-576.

Fiete, I.R., Fee, M.S. & Seung, H.S., 2007. Model of Birdsong Learning Based on Gradient Estimation by Dynamic Perturbation of Neural Conductances. *J Neurophysiol*, 98(4), 2038-2057.

Fonio, E., Benjamini, Y. & Golani, I., 2009. Freedom of movement and the stability of its unfolding in free exploration of mice. *Proc Natl Acad Sci*, 106(50), 21335-21340.

Forssberg, H., 1999. Neural control of human motor development. *Curr Opin Neurobiol*, 9(6), 676-682.

Foster, J.A. & Robertson, R.M., 1992. Temperature Dependency of Wing-Beat Frequency in Intact and Deafferented Locusts. *J Exp Biol*, 162(1), 295-312.

Franz, M. & Goller, F., 2002. Respiratory units of motor production and song imitation in the zebra finch. *J Neurobiol*, 51(2), 129-141.

Fujii, N. & Graybiel, A.M., 2003. Representation of action sequence boundaries by macaque prefrontal cortical neurons. *Science*, 301(5637), 1246-1249.

Gerhardt, H.C., 1978. Temperature Coupling in the Vocal Communication System of the Gray Tree Frog, Hyla versicolor. *Science*, 199(4332), 992-994.

Glaze, C.M. & Troyer, T.W., 2006. Temporal structure in zebra finch song: implications for motor coding. *J Neurosci*, 26(3), 991-1005.

Goldberg, J.H. et al., 2010. Singing-related neural activity distinguishes two putative pallidal cell types in the songbird basal ganglia: comparison to the primate internal and external pallidal segments. *J Neurosci*, 30(20), 7088-7098.

Goldberg, J.H. & Fee, M.S., 2010. Singing-related neural activity distinguishes four classes of putative striatal neurons in the songbird basal ganglia. *J Neurophysiol*. Available at: http://www.ncbi.nlm.nih.gov/pubmed/20107125 [Accessed May 12, 2010].

Goldman-Rakic, P.S., 1995. Cellular basis of working memory. *Neuron*, 14(3), 477-485.

Goller, F. & Cooper, B.G., 2004. Peripheral motor dynamics of song production in the zebra finch. *Ann N Y Acad Sci*, 1016, 130-152.

Graybiel, A.M., 2008. Habits, Rituals, and the Evaluative Brain. *Annu Rev Neurosci*, 31(1), 359-387.

Graziano, M., 2006. The organization of behavioral repertoire in motor cortex. *Annu Rev Neurosci*, 29, 105-134.

Hadders-Algra, M., 2000. The neuronal group selection theory: promising principles for understanding and treating developmental motor disorders. *Dev Med Child Neurol*, 42(10), 707-715.

Hadders-Algra, M., Brogren, E. & Forssberg, H., 1996. Ontogeny of postural adjustments during sitting in infancy: variation, selection and modulation. *J Physiol*, 493 (Pt 1), 273-288.

Hadders-Algra, M., 2008. Reduced variability in motor behaviour: an indicator of impaired cerebral connectivity? *Early Hum Dev*, 84(12), 787-789.

Hahnloser, R.H.R., Kozhevnikov, A.A. & Fee, M.S., 2002. An ultra-sparse code underlies the generation of neural sequences in a songbird. *Nature*, 419(6902), 65-70.

Herrmann, K. & Arnold, A.P., 1991. The development of afferent projections to the robust archistriatal nucleus in male zebra finches: a quantitative electron microscopic study. *J Neurosci*, 11(7), 2063-2074.

Hohle, R.H., 1965. Inferred components of reaction times as functions of foreperiod duration. *Journal of Experimental Psychology*, 69, 382-386.

Humphries, D.A. & Driver, P.M., 1970. Protean defence by prey animals. *Oecologia*, 5(4), 285-302.

Imada, T. et al., 2006. Infant speech perception activates Broca's area: a developmental magnetoencephalography study. *Neuroreport*, 17(10), 957-962.

Immelmann, K., 1969. Song development in the zebra finch and other estrildid finches. In R. A. Hinde, ed. *Bird vocalizations*. Cambridge University Press, pp. 61-74.

Imoto, H. et al., 2006. Use of a Peltier chip with a newly devised local brain-cooling system for neocortical seizures in the rat. Technical note. *J Neurosurg*, 104(1), 150-156.

Jafari, F. & Higgins, P.D., 1989. Thermal modeling in cylindrical coordinates using effective conductivity. *IEEE Transactions on Ultrasonics, Ferroelectrics, and Frequency Control*, 36(2), 191-196.

Jarvis, E.D., 2004. Learned birdsong and the neurobiology of human language. *Ann N Y Acad Sci*, 1016, 749-777.

Jin, D.Z., Ramazanoğlu, F.M. & Seung, H.S., 2007. Intrinsic bursting enhances the robustness of a neural network model of sequence generation by avian brain area HVC. *J Comput Neurosci*, 23(3), 283-299.

Jun, J.K. & Jin, D.Z., 2007. Development of neural circuitry for precise temporal sequences through spontaneous activity, axon remodeling, and synaptic plasticity. *PloS One*, 2(1), e723.

Kao, M.H. & Brainard, M.S., 2006. Lesions of an avian basal ganglia circuit prevent context-dependent changes to song variability. *J Neurophysiol*, 96(3), 1441-1455.

Kao, M.H., Doupe, A.J. & Brainard, M.S., 2005. Contributions of an avian basal ganglia-forebrain circuit to real-time modulation of song. *Nature*, 433(7026), 638-643.

Kastella, K.G. & Fox, J.R., 1971. The Dynamic Response of Brain Temperature to Localized Heating. *Biophys J*, 11(6), 521-539.

Katz, P.S. et al., 2004. Cycle Period of a Network Oscillator Is Independent of Membrane Potential and Spiking Activity in Individual Central Pattern Generator Neurons. *J Neurophysiol*, 92(3), 1904-1917.

Kenet, T. et al., 2003. Spontaneously emerging cortical representations of visual attributes. *Nature*, 425(6961), 954-956.

Khazipov, R. et al., 2004. Early motor activity drives spindle bursts in the developing somatosensory cortex. *Nature*, 432(7018), 758-761.

Kittelberger, J.M. & Mooney, R., 1999. Lesions of an avian forebrain nucleus that disrupt song development alter synaptic connectivity and transmission in the vocal premotor pathway. *J Neurosci*, 19(21), 9385-9398.

Knörnschild, M., Behr, O. & von Helversen, O., 2006. Babbling behavior in the sac-winged bat (Saccopteryx bilineata). *Die Naturwissenschaften*, 93(9), 451-454.

Kondratiev, D. & Yershova, L., 2001. TE coolers computer simulation: incremental upgrading of rate equations approach. *Proceedings of the Sixth European Workshop on Thermoelectricity of the European Thermoelectric Society*.

Leonardo, A. & Fee, M.S., 2005. Ensemble coding of vocal control in birdsong. *J Neurosci*, 25(3), 652-661.

Levelt, W.J.M., 1993. *Speaking: from intention to articulation*, MIT Press.

Lilliefors, H.W., 1969. On the Kolmogorov-Smirnov Test for the Exponential Distribution with Mean Unknown. *J American Stat Assoc*, 64(325), 387-389.

Liu, W., Gardner, T.J. & Nottebohm, F., 2004. Juvenile zebra finches can use multiple strategies to learn the same song. *Proc Natl Acad Sci*, 101(52), 18177-18182.

Liu, W., Wada, K. & Nottebohm, F., 2009. Variable food begging calls are harbingers of vocal learning. *PloS One*, 4(6), e5929.

Lomber, S.G., Payne, B.R. & Horel, J.A., 1999. The cryoloop: an adaptable reversible cooling deactivation method for behavioral or electrophysiological assessment of neural function. *J Neurosci Methods*, 86(2), 179-194.

Long, M.A. & Fee, M.S., 2008. Using temperature to analyse temporal dynamics in the

songbird motor pathway. *Nature*, 456(7219), 189-194.

Major, G. & Tank, D., 2004. Persistent neural activity: prevalence and mechanisms. *Curr Opin Neurobiol*, 14(6), 675-684.

Marder, E. & Bucher, D., 2007. Understanding Circuit Dynamics Using the Stomatogastric Nervous System of Lobsters and Crabs. *Annu Rev Physiol*, 69(1), 291-316.

Marler, P., 1970. Birdsong and speech development: could there be parallels? *Am Sci*, 58(6), 669-673.

Marler, P., 1997. Three models of song learning: evidence from behavior. *J Neurobiol*, 33(5), 501-516.

Milh, M. et al., 2007. Rapid cortical oscillations and early motor activity in premature human neonate. *Cereb Cortex*, 17(7), 1582-1594.

Miller, G.F., 1997. Protean primates: the evolution of adaptive unpredictability in competition and courtship. In A. Whiten & R. W. Byrne, eds. *Machiavellian intelligence II*. Cambridge University Press, pp. 312-340.

Mooney, R., 1992. Synaptic basis for developmental plasticity in a birdsong nucleus. *J Neurosci*, 12(7), 2464-2477.

Mooney, R. & Rao, M., 1994. Waiting periods versus early innervation: the development of axonal connections in the zebra finch song system. *J Neurosci*, 14(11 Pt 1), 6532-6543.

Nottebohm, F., Kelley, D.B. & Paton, J.A., 1982. Connections of vocal control nuclei in the canary telencephalon. *J Comp Neurol*, 207(4), 344-357.

Nottebohm, F., Stokes, T.M. & Leonard, C.M., 1976. Central control of song in the canary, Serinus canarius. *J Comp Neurol*, 165(4), 457-486.

Nottebohm, F., 1976. Assymetries in neural control of vocalizations in the canary. In S. Harnad et al., eds. *Lateralization in the Nervous System*. New York: Academic Press, pp. 23-44.

Nudo, R.J. et al., 1996. Neural substrates for the effects of rehabilitative training on motor recovery after ischemic infarct. *Science*, 272(5269), 1791-1794.

Okanoya, K., 2004. The Bengalese finch: a window on the behavioral neurobiology of birdsong syntax. *Ann N Y Acad Sci*, 1016, 724-735.

Oller, D.K. et al., 1976. Infant Babbling and Speech. *J Child Lang*, 3(01), 1-11.

Ölveczky, B.P., Andalman, A.S. & Fee, M.S., 2005. Vocal experimentation in the juvenile songbird requires a basal ganglia circuit. *PLoS Biol*, 3(5), e153.

Pastalkova, E. et al., 2008. Internally generated cell assembly sequences in the rat hippocampus. *Science*, 321(5894), 1322-1327.

Pepperberg, I.M., Brese, K.J. & Harris, B.J., 2008. Solitary sound play during acquisition of English vocalizations by an African Grey parrot (Psittacus erithacus): Possible parallels with children's monologue speech. *Appl Psycholinguist*, 12(02), 151.

Perkel, D.J. et al., 2002. Electrophysiological analysis of a songbird basal ganglia circuit essential for vocal plasticity. *Brain Res Bull*, 57(3-4), 529-532.

Petersson, P. et al., 2003. Spontaneous muscle twitches during sleep guide spinal self-organization. *Nature*, 424(6944), 72-75.

Petitto, L.A. & Marentette, P.F., 1991. Babbling in the manual mode: evidence for the ontogeny of language. *Science*, 251(5000), 1493-1496.

Pires, A. & Hoy, R.R., 1992. Temperature coupling in cricket acoustic communication. II. Localization of temperature effects on song production and recognition networks in Gryllus firmus. *J Comp Physiol A*, 171(1), 79-92.

Prechtl, H., 2001. General movement assessment as a method of developmental neurology: new paradigms and their consequences. The 1999 Ronnie MacKeith lecture. *Dev Med Child Neurol*, 43(12), 836-842.

Prechtl, H.F.R., 1997. The importance of fetal movements. In K. J. Connolly & H. Forssberg, eds. *Neurophysiology & neuropsychology of motor development.* Cambridge University Press, pp. 42-53.

Rall, W., 1962. Theory of physiological properties of dendrites. *Ann N Y Acad Sci*, 96, 1071-1092.

Reiner, A. et al., 2004. Revised nomenclature for avian telencephalon and some related brainstem nuclei. *J Comp Neurol*, 473(3), 377-414.

Reiss, D. & McCowan, B., 1993. Spontaneous vocal mimicry and production by bottlenose dolphins (Tursiops truncatus): evidence for vocal learning. *J Comp Psych*, 107(3), 301-312.

Robinson, S.R. et al., 2000. Spontaneous motor activity in fetal and infant rats is organized into discrete multilimb bouts. *Behav Neurosci*, 114(2), 328-336.

Ronacher, B., 1989. Stridulation of acridid grasshoppers after hemisection of thoracic

ganglia: evidence for hemiganglionic oscillators. *J Comp Physiol B*, 164(6), 723.

Rowe, D.M., 1995. *CRC handbook of thermoelectrics*, CRC Press.

Saar, S. & Mitra, P.P., 2008. A technique for characterizing the development of rhythms in bird song. *PloS One*, 3(1), e1461.

Scharff, C. & Nottebohm, F., 1991. A comparative study of the behavioral deficits following lesions of various parts of the zebra finch song system: implications for vocal learning. *J Neurosci*, 11(9), 2896-2913.

Seung, H.S., 2003. Learning in spiking neural networks by reinforcement of stochastic synaptic transmission. *Neuron*, 40(6), 1063-1073.

Simpson, H.B. & Vicario, D.S., 1990. Brain pathways for learned and unlearned vocalizations differ in zebra finches. *J Neurosci*, 10(5), 1541-1556.

Smeets, W.J., Marín, O. & González, A., 2000. Evolution of the basal ganglia: new perspectives through a comparative approach. *J Anat*, 196 (Pt 4), 501-517.

Snowdon, C., 2001. Social processes in communication and cognition in callitrichid monkeys: a review. *Anim Cogn*, 4(3), 247-257.

Sokolowski, M.B., 2010. Social Interactions in "Simple" Model Systems. *Neuron*, 65(6), 780-794.

Sporns, O. & Edelman, G.M., 1993. Solving Bernstein's problem: a proposal for the development of coordinated movement by selection. *Child Dev*, 64(4), 960-981.

Stark, L.L. & Perkel, D.J., 1999. Two-stage, input-specific synaptic maturation in a nucleus essential for vocal production in the zebra finch. *J Neurosci*, 19(20), 9107-9116.

Stent, G.S. et al., 1978. Neuronal generation of the leech swimming movement. *Science*, 200(4348), 1348-1357.

Stewart, M. & Fox, S.E., 1990. Do septal neurons pace the hippocampal theta rhythm? *Trends Neurosci*, 13(5), 163-168.

Sutton, R.S. & Barto, A.G., 1998. Reinforcement learning: an introduction. *IEEE Transactions on Neural Networks / a Publication of the IEEE Neural Networks Council*, 9(5), 1054.

Tchernichovski, O. et al., 2004. Studying the song development process: rationale and methods. *Ann N Y Acad Sci*, 1016, 348-363.

Tchernichovski, O. et al., 2001. Dynamics of the vocal imitation process: how a zebra finch learns its song. *Science*, 291(5513), 2564-2569.

Tchernichovski, O. et al., 2000. A procedure for an automated measurement of song similarity. *Anim Behav*, 59(6), 1167-1176.

Thompson, J.A. & Johnson, F., 2007. HVC microlesions do not destabilize the vocal patterns of adult male zebra finches with prior ablation of LMAN. *Dev Neurobiol*, 67(2), 205-218.

Thompson, S.M., Masukawa, L.M. & Prince, D.A., 1985. Temperature dependence of intrinsic membrane properties and synaptic potentials in hippocampal CA1 neurons in vitro. *J Neurosci*, 5(3), 817-824.

Troyer, T.W. & Bottjer, S.W., 2001. Birdsong: models and mechanisms. *Curr Opin Neurobiol*, 11(6), 721-726.

Vates, G.E., Vicario, D.S. & Nottebohm, F., 1997. Reafferent thalamo- "cortical" loops in the song system of oscine songbirds. *J Comp Neurol*, 380(2), 275-290.

Vogels, T.P., Rajan, K. & Abbott, L.F., 2005. Neural network dynamics. *Annu Rev Neurosci*, 28, 357-376.

Volgushev, M. et al., 2000a. Synaptic transmission in the neocortex during reversible cooling. *Neuroscience*, 98(1), 9-22.

Volgushev, M. et al., 2000b. Membrane properties and spike generation in rat visual cortical cells during reversible cooling. *J Physiol*, 522 Pt 1, 59-76.

van Vreeswijk, C. & Sompolinsky, H., 1998. Chaotic balanced state in a model of cortical circuits. *Neural Comput*, 10(6), 1321-1371.

Wallace, P.S. & Whishaw, I.Q., 2003. Independent digit movements and precision grip patterns in 1-5-month-old human infants: hand-babbling, including vacuous then self-directed hand and digit movements, precedes targeted reaching. *Neuropsychologia*, 41(14), 1912-1918.

Whishaw, I.Q., Haun, F. & Kolb, B., 1999. Analysis of Behavior in Laboratory Rodents. In U. Windhorst & H. Johansson, eds. *Modern Techniques in Neuroscience Research*. Springer, pp. 1243-1275.

Wild, J.M., 2004. Functional Neuroanatomy of the Sensorimotor Control of Singing. *Ann N Y Acad Sci*, 1016(Behavioral Neurobiology of Birdsong), 438-462.

Williams, H. & McKibben, J.R., 1992. Changes in stereotyped central motor patterns controlling vocalization are induced by peripheral nerve injury. *Behav Neural*

Biol, 57(1), 67-78.

Williams, H., 2004. Birdsong and singing behavior. *Ann N Y Acad Sci*, 1016, 1-30.

Wilson, D.M., 1961. The Central Nervous Control of Flight in a Locust. *J Exp Biol*, 38(2), 471-490.

Wilson, H.R., 1999. *Spikes, decisions, and actions*, Oxford University Press.

Yamaguchi, A. et al., 2008. Temperature-Dependent Regulation of Vocal Pattern Generator. *J Neurophysiol*, 100(6), 3134-3143.

Yang, J.F., Stephens, M.J. & Vishram, R., 1998. Infant stepping: a method to study the sensory control of human walking. *J Physiol*, 507(3), 927-937.

Yu, A.C. & Margoliash, D., 1996. Temporal hierarchical control of singing in birds. *Science*, 273(5283), 1871-1875.

Zann, R.A., 1996. *The zebra finch*, Oxford University Press.

Zhang, J.X., Ni, H. & Harper, R.M., 1986. A miniaturized cryoprobe for functional neuronal blockade in freely moving animals. *J Neurosci Methods*, 16(1), 79-87.